AD-A179 727 FUNDAMENTAL STUDIES ON HIGH TEMPERATURE DEFORMATION 1/2
RECRYSTALLIZATION AND (U) MARYLAND UNIV COLLEGE PARK
DEPT OF CHEMICAL AND NUCLEAR ENGIN S ANKEM ET AL
UNCLASSIFIED 18 FEB 87 AFOSR-TR-87-0458 AFOSR-85-0367 F/G 11/6 1 NL

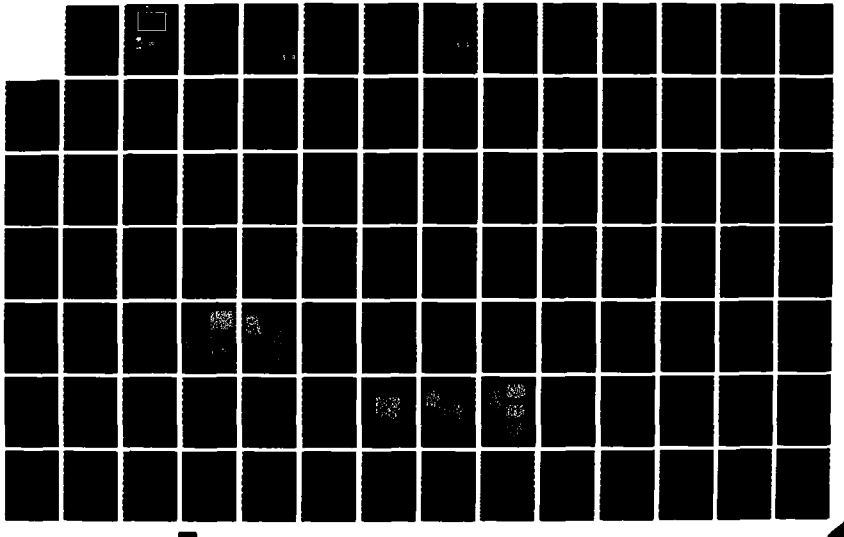

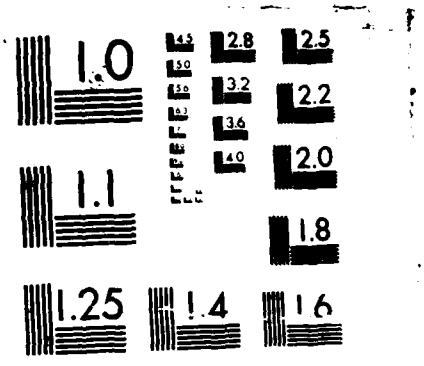

AFOSR-TR- 87-0458

Rosenstein

(2)

Report

AD-A179 727

FUNDAMENTAL STUDIES ON HIGH TEMPERATURE DEFORMATION, RECRYSTALLIZATION, AND GRAIN GROWTH OF TWO-PHASE MATERIALS

BY

S. ANKEM, G. GREWAL, and J.G. SHYUE

Department of
Chemical and Nuclear Engineering

Chemical Engineering Program

College of Engineering
University of Maryland
College Park

DISCLAIMER NOTICE

THIS DOCUMENT IS BEST QUALITY PRACTICABLE. THE COPY FURNISHED TO DTIC CONTAINED A SIGNIFICANT NUMBER OF PAGES WHICH DO NOT REPRODUCE LEGIBLY.

INTERIM TECHNICAL REPORT

(Annual)

(2)

FUNDAMENTAL STUDIES ON
HIGH TEMPERATURE DEFORMATION,
RECRYSTALLIZATION,AND GRAIN GROWTH

OF TWO—PHASE MATERIALS

BY

S.ANKEM,G.GREWAL,and J.G. SHYUE

SUBMITTED TO

AIR FORCE OFFICE OF SCIENTIFIC RESEARCH

ELECTRONIC AND SOLID STATE SCIENCES

BOLLING AIR FORCE BASE

WASHINGTON,DC 20332

FOR THE PERIOD

SEPTEMBER 1,1985—NOVEMBER 30,1986

AFOSR — 85— 0367

FEBURARY 1987

SECURITY CLASSIFICATION OF THIS PAGE

AD-A179 727

REPORT DOCUMENTATION PAGE

1a. REPORT SECURITY CLASSIFICATION: Unclassified	1b. RESTRICTIVE MARKINGS
2a. SECURITY CLASSIFICATION AUTHORITY	3. DISTRIBUTION / AVAILABILITY OF REPORT: Unlimited
2b. DECLASSIFICATION / DOWNGRADING SCHEDULE	
4. PERFORMING ORGANIZATION REPORT NUMBER(S)	5. MONITORING ORGANIZATION REPORT NUMBER(S): AFOSR-TR- 87-0458
6a. NAME OF PERFORMING ORGANIZATION: University of Maryland; 6b. OFFICE SYMBOL (If applicable)	7a. NAME OF MONITORING ORGANIZATION: AFOSR/NE
6c. ADDRESS (City, State, and ZIP Code): Dept. of Chemical & Nuclear Engineering, University of Maryland, College Park, MD 20742-2111	7b. ADDRESS (City, State, and ZIP Code): Bldg. u10, Bolling Air Force Base, Washington, D.C. 20332-6448
8a. NAME OF FUNDING / SPONSORING ORGANIZATION: AFOSR/NE; 8b. OFFICE SYMBOL (If applicable)	9. PROCUREMENT INSTRUMENT IDENTIFICATION NUMBER: AFOSR-85-0367A
8c. ADDRESS (City, State, and ZIP Code): Same as 7b	10. SOURCE OF FUNDING NUMBERS: PROGRAM ELEMENT NO. 61102F; PROJECT NO. 2306; TASK NO. A1; WORK UNIT ACCESSION NO.

11. TITLE (Include Security Classification)
Fundamental Studies on High Temperature Deformation, Recrystallization and Grain Growth of Two-Phase Materials

12. PERSONAL AUTHOR(S)
S. Ankem, G. Grewal and J.G. Shyue

13a. TYPE OF REPORT	13b. TIME COVERED	14. DATE OF REPORT (Year, Month, Day)	15. PAGE COUNT
Interim	FROM 9/1/85 TO 11/30/86	Feb. 18, 1987	93

16. SUPPLEMENTARY NOTATION

17. COSATI CODES			18. SUBJECT TERMS (Continue on reverse if necessary and identify by block number)
FIELD	GROUP	SUB-GROUP	

19. ABSTRACT (Continue on reverse if necessary and identify by block number)

An investigation has been initiated to study the basic factors which control the high temperature deformation, recrystallization, and grain growth of two phase Ti alloys. It was found that the particle growth kinetics of the α_{ALPHA} and the β_{BETA} phases, in titanium alloys, could be represented by simple algebraic equations in terms of time and volume percents of the phases. The observation of the various growth constants in these equations indicated that under identical conditions, the growth of alpha particles in a beta matrix was faster than the growth of beta in an alpha matrix. This was attributed to the higher diffusivities in the beta phase. Furthermore the results of the investigation strongly suggest that one must consider the self diffusivity of the matrix in predicting the growth kinetics, if the self diffusivity is lower than that of the solute.

20. DISTRIBUTION / AVAILABILITY OF ABSTRACT: ☒ UNCLASSIFIED/UNLIMITED ☐ SAME AS RPT. ☐ DTIC USERS	21. ABSTRACT SECURITY CLASSIFICATION: UNCLASSIFIED
22a. NAME OF RESPONSIBLE INDIVIDUAL: Rosenstein	22b. TELEPHONE (Include Area Code): 767-4931; 22c. OFFICE SYMBOL

DD FORM 1473, 84 MAR — 83 APR edition may be used until exhausted. All other editions are obsolete.

SECURITY CLASSIFICATION OF THIS PAGE

A

Cont

This is in contrast to the present particle coarsening theories which only consider the diffusivity of the solute. It was also found that for identical conditions (vol frac., temp) particle sizes of the Ti-V system were slightly smaller than the Ti-Mn system. This was attributed to the slightly smaller diffusivity of vanadium in comparison to the self diffusivity of titanium.

The high temperature deformation studies showed that strain softening which occurs in β-titanium alloys, can also occur in α-β Ti alloys. The strain softening increased with the volume percent of the Beta phase. In addition, it was shown that the law of mixtures rule cannot predict the high temperature stress-strain behavior of two phase alloys. This is due to the fact that interaction stresses develop as a result of the cooperative deformation of the phases. The nature of the interactions depended on the strain rate and volume fraction of the phases. It is of interest to note that at low strain rates, the high temperature flow stress of an α-β alloy with 55 volume percent beta phase is the same as that of the alpha phase. Based on the simple law of mixtures rule, the strength of this alloy should have been much higher because the beta phase is stronger than the alpha phase. This was attributed to a possible phenomenon of interface sliding occuring at these temperatures and strain rates.

TABLE OF CONTENTS

I. INTRODUCTION

Two-phase materials are technologically important. In some of the two-phase materials both the phases can deform and these include α-β titanium alloys which are extensively used in aerospace applications. However, there is a lack of understanding in the areas of high temperature deformation, recrystallization and grain growth behaviors of two-phase alloys in terms of the properites of component phases.

The lack of understanding stems from the complex deformation behavior of two-phase materials. Whenever a material consisting of two or more phases is subjected to strain, the component phases deform differently and hence result in inhomogeneous strain (1-18) and stress (12, 13, 16, 17, 18) distributions. In addition, "interaction stresses" develop as a result of interactions between deforming phases. For these reasons, the deformation behavior of two-phase materials cannot be explained by the "law of mixture rule." This is due to the fact that the law of mixture rule always assumes either constant stress or constant strain, and, as mentioned before, this never happens in reality.

It is known that recrystallization is a nucleation and growth process and this process is promoted by increased cold work and high temperature. Therefore, the recrystallization process in single phase materials is somewhat straightforward. However, in two-phase alloys, where both the phases can deform, the recrystallization behavior is not easy to understand. In these materials, the softer phase deforms more than the harder

phase (18) and therefore one can argue that the recrystallization process is much faster in the softer phase than in the harder phase. However, the process is also temperature dependent meaning that diffusion plays an important role. Therefore, if the diffusivity in the harder phase is higher, then it is difficult to predict which phase recrystallizes faster. This is particularly true in the case of some α-β titanium alloys where the β phase is harder (17) but its diffusivities are higher than that of α phase (19). To further complicate this matter, the nature and magnitude of strain inhomogeneity also depends on volume percent of phases (18). To date, there is no model or mechanism which explains the recrystallization of two-ductile phase alloys in terms of the volume percent of phases, strain inhomogeneities, and diffusivities of the component phases.

For many single phase materials, isothermal grain growth data can be represented by the empirical equation of the form

$$D = Kt^n \tag{1}$$

where D is the mean grain diameter, t is the time, K is the constant of proportionality and n is the grain growth exponent. It is also known that impurity atoms in solid solution and impurities in the form of inclusions or second phase particles retard grain growth. Furthermore, in two-phase materials, size and volume fraction of the second phase is also known to affect the grain growth (21-25). However, there is no significant information as to the empirical relationships which can predict grain growth behavior in two-phase materials, up until recently

(26). Ankem and Margolin (26) derived empirical relationships for grain growth of two-phase alloys in terms of the volume fraction of phases. Their derivations are based on the experimental results on α-β titanium alloys. They found that, under identical conditions, α phase retards grain growth of β phase much more effectively than vice versa. Reasons were suggested for this behavior, but never proven. In addition, no atomistic or any other physical model was suggested for the grain growth of two-phase materials.

The aim of this program is to systematically study the high temperature deformation, recrystallization and grain growth behavior of two-phase materials. While this study will be focussed on two-phase materials where both the phases can deform, it is expected that the information and the mechanisms to be developed can be applied to any two-phase material system. It is hoped that the outcome of this study will be useful in improving processing (forging, rolling, superplastic forming, etc.) methods, obtaining optimal microstructures for improved mechanical properties and increasing the high temperature capability of two-phase materials. Such a fundamental knowledge will be of great importance in developing new titanium alloys for high temperature applications.

II. OBJECTIVES OF THE PROGRAM

1. Determine the high temperature (923 - 1023^{o}K) deformation behavior of two-phase titanium-manganese and titanium-vanadium alloys. The factors to be studied include a determination of the effect of volume percent and nature of second phase (strength, diffusivity), temperature and strain rate.
2. Determine the high temperature deformation mechanisms in the two-phase titanium alloys: slip, interface sliding, etc.
3. Study the recrystallization behavior of these two-phase titanium alloys by taking into account the inhomogeneous strain distributions and diffusivity differences between the component phases.
4. Study the grain growth mechanisms and develop grain-growth relationships for two-phase alloys in terms of the volume fraction of phases, diffusivities, temperature, etc.
5. Predict the stress-strain curves and stress and strain distributions in various two-phase materials.
6. Based on this information, propose models for high temperature deformation, recrystallization and grain growth of two-phase materials.

III. RESEARCH PROGRESS

In this report, research progress made during the first period of the program, September 1, 1985-November 30, 1986, is presented. During this period, all the required materials have been obtained and high temperature deformation studies and grain growth studies have been started. The results of these studies have been presented separately.

A. MATERIALS

The materials required for this program have been obtained from the RMI Company, Niles, Ohio. Six Ti-Mn alloys and six Ti-V alloys have been selected for this study. The aim alloy compositions of Ti-Mn and Ti-V alloys are indicated in Figs. 1 and 2 respectively. The alloys were melted as 13.6 kg (30-lb) ingots. The actual chemistry of the ingots is given in Tables 1 and 2. Note that the actual chemical compositions of the ingots are close to the aim compositions in most of the cases. The ingots were processed to 1.74 cm diameter bars according to the procedure given in Fig. 3. It is to be noted that in the last step all the alloys were processed in the $\alpha + \beta$ field from 973^{o}K (700^{o}C). The amount of work given in this step (60% reduction in area) was found to be sufficient to recrystallize all the alloys within 12 hours at 973^{o}K.

B. EXPERIMENTAL

a. Heat Treatments

For grain growth studies, all the twelve alloys were heat treated for 25, 50, 100, 200 and 400 hours at 973 K followed by

water quenching. These treatments were carried out in vacuum encapsulated quartz tubes. For high temperature deformation studies, the tensile specimens were heat treated in a vacuum furnace (10^{-6} mm of Hg) at 700°C for 200 hours followed by water quenching.

b. Optical Metallography

Standard polishing and etching techniques were used. The Ti-Mn alloys were etched with A-etch for about 10 sec followed by etching with R-etch for about 10 sec. This two-step etching was found to be beneficial for α-β microstructures. The composition of A-etch and R-etch are given below:

A-etch: 25 ml HF 50%
25 ml HNO_3 conc.
50 ml Glycerine

R-etch: 18.5 gm (17 ml) Benzalkonium Chloride (50%)
35 ml Ethanol

The Ti-V alloys were etched with the following ethant for about 10 sec.

4% HNO_3
2% HF
Bal. H_2O

c. High Temperature Tensile Tests

Special 1.625 inch gauge length specimen, shown in Fig. 4, was used for the high temperature tensile tests. A unique arrangement, shown in Figs. 5 and 6 was used to conduct the high temperature tensile tests. The grips were fabricated inhouse

from the high temperature material Udimet-720. All the tests were carried out in vacuum (10^{-5} - 10^{-6} mm Hg.) at 973°K in a special vacuum chamber shown in Fig. 6. The temperature of the specimen was controlled by a set of two thermocouples, spot welded onto the specimen at the two respective gauge section ends. The maximum temperature variations between the two thermocouples was controlled to within $\pm$ 3°K. All the Ti-Mn alloys were tested at four different engineering strain rates of 2.6 X 10^{-2}/sec, 2.6 X 10^{-3}/sec, 2.6 X 10^{-4}/sec, and 1.1 X 10^{-4}/sec. After testing, the specimen were fast cooled with compressed air. The load elongation curves were digitized on an APPOLO minicomputer, to obtain the true stress-strain plots, and various mechanical parameters were determined.

C. RESULTS AND DISCUSSION

a. Grain Growth Studies

Though it is known that the size and the volume fractions of the second phase affects the growth in two-phase alloys (21, 25), up until recently there was no significant empirical information available on the growth relationships in these alloys (26). Ankem and Margolin (26) derived empirical relationships for grain growth of the two-phase alloys in terms of the volume fractions of the phases. Their derivations which are based on experimental work on two-phase α-β titanium alloys, showed that under identical conditions, α retards grain growth of β phase much more effectively than vice-versa. Though reasons based on diffusivity considerations were given, they were not proven. In addition, because of the fact that only one alloy system based on Ti-Mn was

used to investigate the growth processes, the mechanisms controlling the grain growth, and consequently the rate controlling steps in these mechanisms could not be identified. It was to this effect that a study was undertaken on two model systems. In addition to the Ti-Mn system used by Ankem and Margolin (26) a α-β alloy system based on titanium-vanadium was chosen. The reason for choosing a vanadium based system was the singular fact that the diffusivity of vanadium is at least an order of magnitude lower than the corresponding diffusivity of manganese in titanium. The diffusivity of V in titanium is slightly lower than the self diffusivity of Ti. It was thus conjectured that if the rate controlling step in the growth of the phases in a two-phase alloy is the diffusion of the solute, then the particle sizes obtained, under identical conditions of heat treatment would be significantly higher in the Ti-Mn system when compared to the Ti-V system. It was further hoped that such observed significant differences would be clearly brought out in the regression equations developed to fit these growth characteristics. On the other hand, if the rate controlling step was not the diffusion of the solute, but was, as is more reasonable to expect, the slowest diffusing species in the respective systems, then one would expect the particle sizes of the Ti-V system to be slightly smaller than the corresponding particle sizes in the Ti-Mn system for identical conditions. The actual size difference depends on the rate controlling step in the growth mechanism.

1. Theoretical Considerations

As mentioned earlier, for single phase materials, all isothermal grain-growth data can be represented by empirical

equations of the form

$$D = Kt^n \qquad (1)$$

The theoretical framework behind the single phase kinetic expression (1) has been extensively investigated. In this framework, single phase grain growth is known to occur by thermally activated motion of grain boundary interfaces (29). The interfaces move by random jumping of atoms from grain to grain, the driving force for the process being the reduction of free energy associated with the grain boundaries. No long range diffusion is involved in the process and the self diffusion of the matrix does not come into the picture. Based on this framework an Arrenhius type rate expression is written for the velocity of an interface as

$$V = Ke^{\frac{-\Delta G^a}{RT}} \cdot \frac{\Delta G}{V_m} \qquad (2)$$

where V is the velocity of interface

K is constant

ΔG^a is thermal activation barrier across a grain boundary

V_m is molar volume of atomic species

ΔG is chemical potential differential across the interface

$$\Delta G = \frac{2\gamma^c V_m}{r}$$

where γ= surface energy

V_m = molar volume

r = radius of equivalent volume sphere enclosing a grain

The rate expression (2) is then coupled with statistical and grain contiguity considerations to generate an expression of type (1). Extensive theory of single phase grain growth has been developed in the classic papers of Hillert (30) and Feltham (31).

The two-phase systems which have been theoretically investigated are the typical Ostwaldian type of systems. A typical Ostwaldian system is a two-phase system constituting a solute lean matrix dispersed with solute rich particles. A statistical dispersion of particles in a matrix is thermodynamically unstable due to the excess free energy associated with their interfacial surface area and thus the system tends to decrease this free energy by the process of particle coarsening. The solubility or the dissolution of these particles depends on their radii of curvature and is described by the Gibbs-Thompson relation (3).

$$C_r = C_\infty \left(1 + \frac{2\gamma V_m}{RT} \quad \frac{1}{r}\right) \qquad (3)$$

where

C_r = concentration in matrix of solute near a particle of size r

γ = surface free energy

V_m = molar volume

R,T = gas constant and temperature respectively

The fundamental theory of particle coarsening in a supersaturated solid solution decomposing by diffusion has been developed by Lifshitz and Slyosov (32) and independently by Wagner (33), and is referred to as the LSW theory. The basic growth mechanism of the LSW theory is assumed to be a long range concentration gradient driven diffusion of solute through the matrix, between the second phase particles. The concentration gradients are created locally in the matrix near the particle-matrix boundaries as a result of the dependence of the equilibrium solute concentration, C(r) on the radius of the particles.

The LSW theory was derived for the limiting case of the second phase tending to zero (32, 34) and is thus generally not valid for finite volume fractions of the second phase.

To bring real, finite second phase volume fraction systems into the framework of the LSW theory, modifications were made by Ardell (34). This modified LSW theory, known as the MLSW theory predicts that while the basic $t^{1/3}$ kinetics of the LSW theory are maintained, the coarsening rate increases with increasing volume fractions. This result is valid as even very small values of the volume fraction of the second phase (34).

The Ardellian modification is based on the assumption that the diffusion of the solute to a growing particle will depend on a distance characteristic of the spatial distribution of particles in the matrix. In addition, the assumption of steady state diffusion under conditions of steady state symmetry are assumed (34). A somewhat different approach than that used by Ardell (34) was used by Davies, et al., (35) to incorporate the

effect of finite volume fraction second phases into the framework of LSW theory. The rationale of the Davies (35) modification is the observation that the Ardellian approach predicts a strong volume fraction dependent growth kinetics which are generally not experimentally observed. The central idea of the Davies approach is that of "encounters" between growing particles. A growing particle encounters another growing particle, and a strong diffusion interaction results as a consequence of which the particles spontaneously coalesce to become a single particle. This theory, as modified by Davies, et al. is referred to as the LSEM theory (35). A more recent work by Brailsford, et al. (36) developed a theory of particle coarsening, which assumes that the growth rate of particles of one size class is a function of the entire size distribution and the existing concentration gradients around the particle. The growth rate predicted by this theory is more sensitive to volume fraction of the second phase than the theory proposed by Davies but is less sensitive to the theory proposed by Ardell.

Apart from the above theories, various models have been developed to explain the shape of the particle size distributions curves observed in real finite volume Ostwaldian type of systems. These models essentially use different geometrical approaches to obtain expressions for the radius of the influence sphere. The expression for the influence sphere is then substituted into the standard LSW theoretical formulation and the kinetic expression is evaluated by solving the resulting equation. An excellent paper which develops six such models is that of Tsumuraya, et al.

(37).

In contrast to the single phase and the Ostwaldian second phase dispersed systems discussed above, the two-phase alloy systems are unique. Grain growth in the two phase systems involves the simultaneous growth of both the phases. An $\alpha-\beta$ titanium alloy system contains $\alpha-\alpha$, $\beta-\beta$ and $\alpha-\beta$ boundaries. Growth in the $\alpha-\beta$ system occurs by the motion of all these three types of boundaries. The $\alpha-\alpha$, and the $\beta-\beta$ boundaries migrate by thermally activated processes akin to the process occurring in single phase materials, with the atoms jumping across these boundaries by random thermal vibrations. The driving force for the migration of these "like-like" boundaries being the excess chemical potential differential existing for each of the constituent components across the boundary as a result of the presence of finite surfaces around the grains. The $\alpha-\beta$ boundaries on the other hand can only move by the process of long range diffusion of both the constituent species (assuming a two component system). Thus diffusion processes in both the phases are involved. Details of the growth processes of the two-phase alloys are presented below.

2. Results

The volume percents of alpha, for the $\alpha-\beta$ Ti-Mn alloy system, varied from 10% for alloy no. 5 to 79% for alloy no. 2. The volume percents of alpha for the $\alpha-\beta$ Ti-V alloy system varied from 7% for alloy no. 11 to 70% for alloy no. 7. It is pertinent to note that though the volume fractions of the alloys studied are different, the chemical composition of the alpha and

the beta phases is the same in all the alloys in each of the two systems studied. The chemical composition of the phases, in the two systems studied, is shown by the ends of the tie lines drawn for 973°K, in Figs. 1 and 2, respectively.

The heat treatments resulted in equiaxed alpha + beta microstructures. Typical equiaxed alpha + beta microstructures of Ti-Mn and the Ti-V alloys heat treated at 973°K for 200 hours are shown in Figs. 7 and 8 respectively.

As expected, the alpha and the beta sizes increased as a function of time. The microstructural data for Ti-Mn and Ti-V system is given in Tables 3 to 6 and 8 to 12, respectively. The particle sizes of the alpha and beta phases plotted as a function of time for alloys 2, 3, 4 and 5 of the Ti-Mn system and for alloy nos. 7, 8, 9, 10 and 11 of the Ti-V system are shown in Figs. 9 to 17.

It was found that in the Ti-Mn system, particle growth of the alpha and the beta phases could be written by equations of the form

$$D_{\alpha}^{\alpha-\beta} = K_{\alpha}^{\alpha-\beta} \; t^{n\alpha} \tag{11}$$

$$D_{\beta}^{\alpha-\beta} = K_{\beta}^{\alpha-\beta} \; t^{n\beta} \tag{12}$$

It can be seen that the growth parameters, $K_{\alpha}^{\alpha-\beta}$, and $K_{\beta}^{\alpha-\beta}$depended on the volume percents of the respective phases. The growth exponents n_{α} and n_{β} gave a constant value of approximately .28 for all the alloys studied. The numerical data for $K_{\alpha}^{\alpha-\beta}$, and $K_{\beta}^{\alpha-\beta}$

as a function of the respective other phase volume percents is shown in Table 7. It was found that the growth constants could be represented by equations of the form

$$K_{\beta}^{\alpha-\beta} = \frac{K_{\beta}}{V_{\alpha}^{m\alpha}} \tag{13}$$

$$K_{\alpha}^{\alpha-\beta} = \frac{K_{\alpha}}{V_{\beta}^{m\beta}} \tag{14}$$

where m_{β}, and m_{α} are known as retardation exponents as per the terminology introduced by Ankem and Margolin (26). The growth constants $K_{\alpha}^{\alpha-\beta}$ was plotted as a function of the volume percent of the beta phase (V_{β}), and $K_{\beta}^{\alpha-\beta}$ was plotted as a function of alpha phase (V_{α}). The numerical forms of equations (13) and (14), also shown in Table 7, are

$$K_{\beta}^{\alpha-\beta} = \frac{105.19}{V_{\alpha}^{1.146}} \tag{15}$$

and

$$K_{\alpha}^{\alpha-\beta} = \frac{22.90}{V_{\beta}^{.7385}} \tag{16}$$

A plot of $K_{\alpha}^{\alpha-\beta}$ versus V_{β} and $K_{\beta}^{\alpha-\beta}$ versus V_{α} is shown in Fig. 18.

The microstructural growth data for the Ti-V systems is shown in Tables 8 to 12.

It was found that equations identical to 11 and 12 could be written for the Ti-V system, with only the constants having different values. The numerical form of the equations is presented below.

$$D_{\alpha}^{\alpha-\beta} = K_{\alpha}^{\alpha-\beta} \; t^{.25} \tag{17}$$

$$D_{\alpha}^{\alpha-\beta} = K_{\beta}^{\alpha-\beta} \; t^{.25} \tag{18}$$

The individual values of $K_{\alpha}^{\alpha-\beta}$, and $K_{\alpha}^{\alpha-\beta}$ for various alloys are presented in Tables 8 to 12.

Table 13 shows the data for $K_{\alpha}^{\alpha-\beta}$ and $K_{\beta}^{\alpha-\beta}$ as a function of the respective other phase. It was found that equations $K_{\alpha}^{\alpha-\beta}$ as a function of V_{β}, and $K_{\beta}^{\alpha-\beta}$ as a function of V_{α} had the form of equations 13 and 14. The exact numerical forms of equations (13) and (14) for the Ti-V system are

$$K_{\beta}^{\alpha-\beta} = \frac{88.866}{V_{\alpha}^{1.1206}} \tag{19}$$

and

$$K_{\alpha}^{\alpha-\beta} = \frac{22.125}{V_{\alpha}^{.7578}} \tag{20}$$

Plots of $K_{\alpha}^{\alpha-\beta}$ versus V_{β} and $K_{\beta}^{\alpha-\beta}$ versus V_{α} are shown in Fig. 19.

3. Discussions

Comparison of equa[illegible] 15 and 16 show two differences. The first difference pertains to the numerator K_{β} and K_{α} in equations 15 and 16 respectively. The K_{β} value which is larger than K_{α} by a factor of almost 4.5 is obviously related in some manner to the diffusivities ratios of the slower diffusing species in beta and alpha. It is to be noted that K_{β} and K_{α} become the dominant factors when V_{α}, and V_{β} respectively are small. Thus K_{β} and K_{α}

are the measures of the growth parameters in the respective matrix phases.

The second difference is in the exponents m^{α}, and m^{β}. We note that m^{α} is larger than m^{β}. To analyze and correlate this difference we must first note that the retardation exponents become significant when V_{α} and V_{β} are very high. This of course corresponds to the β and the α phase distributed as particles in the corresponding other matrices. The mechanism of diffusion in such a case is that of α growth by diffusional exchange through matrix β and the particulate β growing by diffusional exchange through matrix alpha. Now since diffusivities of the slowest diffusing species is higher in β than in α, we expect the α particles to grow at a faster rate than β particles. In other words for the same amounts of matrix α and β, the corresponding sizes of particulate α in matrix β will be higher than vice versa, at any given time under identical conditions. (This can clearly be observed from the right hand sides of Figs 18 and 19). This implies that m^{α} be higher than m^{β}. This, in fact, is the actual observation made. It may well be that m^{β} and m^{α} can be related to the diffusivities of the slowest diffusing species in the respective phases, but no direct relationship was apparent in the data obtained.

The expressions for $K_{\beta}^{\alpha-\beta}$ and $K_{\alpha}^{\alpha-\beta}$ for the Ti-V are given by equations (19) and (20). Again, as observed in the Ti-Mn system, two differences are apparent. The K^{β} value is greater than the K^{α}.

The second difference in the m^{α} and m^{β} values also follows the trend observed in Ti-Mn system namely that the M^{α} value is larger than the m^{β} values. The individual values of m^{α} and m^{β}

are also not too different from the corresponding values in the Ti-Mn system.

The trend of the Ti-V system being similar to the Ti-Mn helps in concluding that the mechanisms operating in the Ti-V system are analogous to the mechanisms operating in the Ti-Mn system.

Figs. 25 and 26 show the time dependent evolution of alloy no. 4 of the Ti-Mn system, and alloy no. 9 of the Ti-V system respectively. These alloys have been chosen because they have comparable volume fractions of the phases.

The hypothesis that the slowest diffusing species determine the rate controlling step is confirmed by noting that the slowest diffusing species in Ti-V system, namely V is only slightly lower than the diffusivity of the slowest diffusing species in the Ti-Mn system, namely Ti, and that the differences between the equations for Ti-V and Ti-Mn systems is small.

It can be seen that the complete array of microstructures observed in the Ti-Mn and Ti-V systems discussed above can be split up into three distinctive groups.

Case 1

Small volume fractions of alpha distributed in a matrix of beta.

Figure 20a shows a small volume fraction of alpha particles or grains distributed in a matrix of beta. The alpha particles are assumed distributed at beta grain boundaries. To bring out the atomistic processes in the growth of alpha and beta we consider a two particle system in Fig. 20 b. For idealization,

spherical particles are assumed. From Figs. 1 and 2, one notices from the tie lines at 973°K in the two systems that the beta phase is solute rich and the alpha phase is solute lean. If one assumes that the growth of particle C at the expense of particle A does not involve the creation of a vacancy concentration higher than the already present equilibrium vacancy concentration, then the growth process will involve the following steps.

1. Atoms of the Ti in shrinking α particle A, jump across the α-β boundary and diffuse to the β regions near the growing α particle C.
2. Atoms of Mn in the beta matrix near the growing particle C diffuse towards α particle A and jump across the α-β boundary of particle A. As a consequence of this occurance, the α particle A shrinks with a part of it transforming to β and the α particle C grows by a part of the β matrix adjacent to it transforming to α. This results in α particle A shrinking, and α particle C growing and thus essentially two fluxes are involved.

(1) $Mn_C^{\beta} \rightarrow A$

(2) $Ti_A^{\beta} \rightarrow C$

where the superscript denotes the fact that the diffusion occurs in the β matrix.

Now the α - β interface being incoherent boundaries possesses high mobilities and accommodation factors close to 1,

one can safely neglect the boundary migration factor in our kinetic consideration and simply consider the growth occurring by the diffusion of Ti and Mn in the beta matrix. (It is assumed that the grain boundary diffusion will be small compared to bulk diffusion). This flow process can be represented as shown in Fig. 20c. A schematic showing the transformed regions is shown in Fig. 20 d. Figure 20e shows the net result as a consequence of the diffusional exchange process.

The interparticle flux rate for a two particle exchange process can now be evaluated as under: Let the atomic density of alpha be e^{α}, and the atomic density beta be e^{β}. Now, if the volume of particle A shrinks by δV, then the net number of Mn and Ti atoms migrating to or from the shrinking particle can be evaluated as below:

To start, we define the terminology used.

a. $\alpha \rightarrow \beta$: flux rate associated with α transforming to β

b. e^{α}, e^{β} : atomic densities of alpha and beta respectively.

c. X^{α}_{mn}, X^{α}_{ti} : respective component mole fractions of alpha

d. X^{β}_{mn}, X^{β}_{ti} : respective component mole fractions of beta

e. $J^{\alpha-\beta}_{\rightarrow mn}$: shows a flux J of atoms per unit vol. change, out of the region of occurence of $\alpha \rightarrow \beta$ type of event.

From simple conservation of mass considerations we have

$$(J^{\alpha\rightarrow\beta}_{\rightarrow Ti})\,\delta v = (X^{\alpha}_{Ti}\, e^{\alpha} - X^{\beta}_{Ti}\, e^{\beta})\,\delta v$$

$$J^{\alpha\rightarrow\beta}_{\rightarrow Ti} = X^{\alpha}_{Ti}\, e^{\alpha} - X^{\beta}_{Ti}\, e^{\beta} \qquad (4)$$

Similarly the influx of Mn is

$$J^{\alpha\to\beta}_{\leftarrow mn} = X^{\beta}_{mn}\ e^{\beta} - X^{\alpha}_{mn}\ e^{\alpha} \tag{5}$$

for a $V^{\beta} \rightarrow V^{\alpha}$ type of event, where an alpha particle grows in a beta matrix. We have

$$J^{\beta\to\alpha}_{mn} = X^{\beta}_{mn}\ e^{\beta} - X^{\alpha}_{mn}\ e^{\alpha} \tag{6}$$

and

$$J^{\beta\to\alpha}_{\leftarrow Ti} = X^{\alpha}_{Ti}\ e^{\alpha} - X^{\beta}_{Ti}\ e^{\beta} \tag{7}$$

from (4), (5), (6), and (7) one can see that

$$J^{\alpha\to\beta}_{\rightarrow Ti} = J^{\beta\to\alpha}_{\leftarrow Ti} = J_{Ti}$$

and

$$J^{\alpha\to\beta}_{\leftarrow Mn} = J^{\beta\to\alpha}_{\rightarrow Mn} = J_{mn}$$

The rate of growth of a spherical particle can now be related to the flux rates by the expression

$$\min\left(\frac{1}{J_{\rightarrow Mn}}\ \frac{dn^{mn}}{dt},\ \frac{1}{J_{\leftarrow Ti}}\ \frac{dn^{Ti}}{lt}\right) = \frac{dv}{d^{r}}\frac{dr}{dt} = 4\pi r^{2}\ \frac{dr}{dt} \tag{8}$$

where

$$\frac{dn^{Mn}}{dt}$$

and $$\frac{dn^{Ti}}{dt}$$

are the respective flux rates of Mn and Ti.

The transport of Mn from the beta matrix near the growing alpha particle to the beta matrix regions near the shrinking alpha particle and the reverse transfer of titanium can possibly be attributed to the "excess concentrations" near the interfaces.

Figure 21 brings out in a qualitative fashion the existence of such excess concentrations. In Figure 21, molar free energies of the beta matrix, the shrinking α particle A and the growing particles C, are shown as a function of mole fractions of Ti.

It can be seen that a higher concentration of Ti in the beta phase is in equilibrium with the α particle A of the smaller radii than vice versa. There will consequently be a reverse gradient for Mn. Thus, qualitatively, one can see that a driving force in the form of concentration gradients exists in the matrix to drive the components in the right direction for growth.

Case 2:

Small volume fractions of beta distributed in a matrix of alpha.

The case 2, microstructural morphology, is shown schematically in Fig. 22a. The associated two particle exchange process occurring in such a microstructure is shown in Fig. 22b. The net flow, in a manner equivalent to case 1 is shown in Fig. 22c. In a manner similar to the previous case discussed, the mechanism of growth will involve the following steps.

1. Mn atoms from the smaller β particle A jump across the α-β interface and diffuse to α matrix regions adjacent to the growing β particle C.
2. Ti from the α matrix regions near the growing β particle C diffuse to the shrinking particle A and jump across the α - β interface. As a consequence region of particle A transforms to α and the matrix adjacent to particle C transforms to β (Fig. 22d and 22e).

In a manner similar to the case 1, the kinetics of the boundary transfer across the shrinking particle are expected to be quite fast compared to the long range diffusion through the matrix. Thus the kinetics will be governed by the diffusion of the slower diffusing species in the α matrix.

In a manner similar to the previous case discussed, the number of Mn and Ti atoms required to cause unit changes in volume of the growing and shrinking particles can be worked out. The diffusion of Mn from the smaller particle to the larger particle of β, and the reverse diffusion of Ti are driven by excess local concentrations created by the excess free energies associated with the particle surfaces. A qualitative existence of such excess concentrations is shown in Fig. 23. This figure shows the molar Gibbs free energy plots of matrix α , the shrinking β particle A, and the growing β particle C, as a function of mole fractions of Mn. One notices from the common tangent construction that the equilibrium concentration of Mn in alpha is higher near the particle of the smaller radii, and consequently a reverse gradient exists for Ti.

Case 3:

Nearly equivalent volume fractions of the beta and the alpha phase.

The typical microstructures considered under case 3 are shown in Fig. 24. In such a microstructure diffusion processes will operate in both the alpha and the beta phases. Thus there will be matter transmitted to the α-β interfaces from both the sides. In such a situation it is expected that the evolution of the microstructure will be controlled by the matrix with the lower diffusivity.

At this point one notices the point of departure in two-phase materials in contrast to the cases discussed under the general framework of Ostwald ripening. All Ostwaldian type of systems treat the flow process as occurring by the diffusion of a single species, namely the solute. Thus the kinetic expression is determined by the diffusivity of the solute in the matrix. In contrast, in two-phase materials diffusion of solute as well as the solvent need to be considered. If one assumes that the driving force for both the species, Ti and Mn are the same, then the rate controlling steps which will control the growth of particles will be the diffusivity of the slowest diffusing species in the matrix. Thus it may happen that the solvent is the slowest diffusing species and is, consequently, the rate controlling step. Thus in a two component system, two-phase system (based on say, titanium--our case), the solute or the second component only becomes the rate controlling factor if and only if its diffusivity is lower than that of the solvent (in our case, titanium).

In the Ti-Mn system the diffusivity of Ti is lower than that of Mn. Thus the flow of the solvent controls the rate of growth of microstructure.

In the Ti-V system, the diffusivity of V is slightly lower than titanium, thus the flow of solute will be controlling the rate of the microstructural coarsening.

This is an important point to note because normally it is believed that an alloy which has a faster diffusing solute will have higher growth kinetics, but as shown here this is true only if the solvent, in our case Ti, has a higher self diffusivity than either of the solutes.

In other words the above discussion indicates that different alloys with solutes elements with different diffusivities may have the same growth kinetics if the diffusivities of the solutes are higher than the self diffusivities of titanium.

The grain growth studies on Ti-V and Ti-mn alloys will be continued. The alloys will be annealed at other temperatures and the results obtained will be analyzed to check if the equations of the form developed for 973^{o} K are applicable. In addition, attempts will be made to incorporate the effect of temperature into the growth equations.

High Temperature Tensile Tests

1. Results and Discussion

Figures 27 to 32 show true stress-true strain plots of alloys 1 to 6 respectively. The four plots shown in each figure represent the curves obtained by testing at four different strain rates of 1.1×10^{-4}/sec, 2.6×10^{-4}/sec, 2.6×10^{-3}/sec, and 2.6

X 10^{-2}/sec. It can be seen from figures 27 to 32 that for each of the alloys tested, the flow stress increased as the strain rate was increased, as expected, and the plastic region of curve shifted up. Alloy no. 1 (near α), shown in figure 27, exhibits strain hardening in the initial stage of deformation. It can be seen that the strain hardening increased as the strain rate was increased from 1.1 X 10^{-4}/sec to 2.6 X 10^{-2}/sec.

In contrast to the true stress-true strain curves for alloy 1 (α phase), the true stress-true strain curves for the β-phase (alloy no. 6) shown in figure 32, show strain softening. The strain softening increases as the strain rate increases from 1.1 X 10^{-4}/sec to 2.6 X 10^{-2}/sec. This strain softening might be due to the process of **sub-grain formation** occuring during the deformation process (38) but this needs to be confirmed. An important fact which can be seen from figure 32, is that the Beta alloy starts exhibiting strain softening at extremely low plastic strains (< .002).

Since the α phase (alloy 1) exhibits strain hardening, while the β phase (alloy 6) exhibits strain softening, one wonders as to what may be the behavior of an alloy containing both the α and the β phases at high temperature. True stress-true strain curves for various α-β Ti-Mn alloys are presented in figures 33 to 36. It can be seen that as the volume percent of the β phase increased the strain softening increased. At this point it is of interest to know how well the experimental curves for the α-β Ti-Mn alloys compare with the theoretical true stress-true strain curves based on an isostrain or an isostress model. Figure 37, shows a calculated true stress-true strain curve (dashed lines)

based on an isostrain model. The experimental curve is shown by solid lines. Similarly the experimental and the calculated true stress-true strain curves for strain rates of 1.1×10^{-4}/sec to 2.6×10^{-2}/sec are plotted in figures 38 through 41 respectively. It can be seen that though the calculated curve coincides with the experimental curve for some alloys (see figure 38 for alloy 3), it is not generally the case. It can be similarly demonstrated that the isostress model will also not predict the actual behavior of two phase Ti-Mn alloys, in general. This is due to the fact that the isostrain and isostress model assumes constant strain or stress, respectively, in the two phases which is not a valid assumption.

The stresses and strains in the two phases are not constant as a result of interaction stresses arising at the α-β interfaces due to the co-operative deformation of the two phases. The phenomena of non-constant stresses and strains in the α and the β phases is not surprising, as it was recently demonstrated by Ankem and Margolin [13,16-18] that interaction stresses develop in the α-β alloys as a result of deformation at room temperature. While such interaction would also occur at high temperatures, their nature might be quite different. For example, interface sliding, which is a temperature dependent activation process can occur much more readily at high temperature than at ambient temperatures.

The fact that the law of mixture cannot predict the flow stresses at high temperatures of deformation is also demonstrated in figures 42 to 47. In these plots, various flow stresses are

plotted as a function of volume percent β (V_β), at different strain rates. It can be clearly seen that the flow stress does not vary linearily with the volume percent . In fact, at the two lower strain rates of testing, the plots show a dip in the 50-60% V_β range in which the flow stress is nearly equal to the flow stress of the pure α (alloy 1). This dip is relevant for the process of forming and is relevant to the Ti fabrication industry as it presents an ideal formability window for the metal forming because of low stresses needed.

The nature of flow stress curves as function of volume percent β (V_β) suggests that interaction stresses between the α and the β phases, which develop as result of the interface compatibility requirements, need to be considered. These interaction stresses are a function of various parameters including the amount of total strain. A detailed study of the interaction stresses and also the affect of high temperature on the stress-strain behavior is the subject of the next period of this project.

Deformation studies will be continued to include testing of the six Ti-Mn alloys, at different strain rates (1.1×10^{-4} - 2.6×10^{-2}/sec), for two additional temperatures. Similar tests will also be carried out on the Ti-V system. From these results the effect of strain rate, temperature, and volume fractions on the high temperature deformation will be determined. Furthermore, attempts will be made to apply the finite element analysis to predict the high temperature deformation behavior of two phase titanium alloys.

IV. TECHNICAL PRESENTATIONS

1. Grain Growth Relationships in Two Phase Titanium Alloys - S. Ankem, G. Grewal and R.J. Arsenault; presented at 1986 Fall TMS AIME meeting at Orlando.

V. KEY PERSONNEL FOR THE FIRST PERIOD

Dr. S. Ankem - Principal Investigator

Dr. R.J. Arsenault - Faculty Participant

G. Grewal - Ph.D. Candidate

J.G. Shyue - M.S. Candidate

References

1. H. Unkel: J. Inst. of Metals, 1937, Vol. 61, p. 171.

2. R.W.K. Honeycombe and W. Boas: Aust. J. Sci. Res., 1948, Vol. A1, p. 70.

3. L.M. Clarebrough: Aust. J. Sci. Res., 1950, Vol. 3A, p. 72.

4. L.M. Clarebrough and G.R. Perger: Aust. J. Sci. Res., 1952, Vol. A5, p. 114.

5. M.F. Ashby: Phil. Mag., 1970, Vol. 21, p. 399.

6. I. Tamura, Y. Tomota, A. Akao, Y. Yamaoka, M. Ozawa, and S. Kanatoni: Trazans. Iron & Steel Inst., Japan, 1973, Vol. 13 (4), p. 283.

7. B. Karlsson and B.O. Sandstrom: Mat. Sci. & Eng., 1974, Vol. 16, p. 161.

8. Y. Tomota, K. Kuroki, and I. Tamura: J. Iron & Steel Inst., Japan, 1975, Vol. 61, p. 107.

9. T. Nakamura and K. Wakasa: Trans. Iron & Steel Inst., Japan, 1976, Vol. 16, p. 134.

10. H. Fischmeister and B. Karlsson: Z. Metallk, 1977, Vol. 68 (5), p. 311.

11. T. Inoue and S. Kinostita: Trans. Iron & Steel Inst., Japan, 1977, Vol. 17 (5), p. 245.

12. R.E. Smelser, J.L. Swedlow, and J.C. Williams: Unpublished Research, Carnegie Mellon University, Pittsburgh, PA, 1977.

13. J. Jinoch, S. Ankem, and H. Margolin: Mat. Sci. & Engr., 1978, Vol. 34, p. 203.

14. J.J. Petrovic and A.K. Vasudevan: Mat. Sci. & Eng., 1978, Vol. 34, p. 39.

15. G. Liden: Mat. Sci. & Engr., 1979, Vol. 40, p. 5.

16. S. Ankem and H. Margolin: Metall. Trans. A, 1980, Vol. 11A, p. 963.

17. S. Ankem and H. Margolin: Metall., Trans., 1982, Vol. 13A, p. 595.

18. S. Ankem and H. Margolin: Metall., Trans., 1982, Vol. 13A, p. 603.

19. F. Dyment: "Titanium '80, Science and Technology," AIME, 1980, p. 520.

20. R.E. Reed-Hill: "Physical Metallurgy Principles, Second Edition," D. Van Nostrand Company, New York, 1973, p. 309.

21. D.S. Clark and W.R. Varney: "Metallurgy for Engineers, Second Edition," D. Van Nostrand Company, New York, 1962, p. 153.

22. S.G. Byrnes: "Recovery, Recrystallization and Grain Growth," MacMillan Co., 1965, p. 100.

23. C. Zener: Private Communication Cited in C.S. Smith, Trans.-AIME, 1948, Vol. 175, p. 15.

24. E. Levine, I. Greenhut, and H. Margolin: Met. Trans., 1973, Vol. 4, p. 2519.

25. S. Ankem and H. Margolin: Met. Trans. A, 1977, Vol. 8A, p. 1320.

26. S. Ankem and H. Margolin: "Grain Growth Relationships in Two-Phase Titanium Alloys," presented at the Fifth International Conference on Titanium, held at Munich, W. Germany, September 1984, to be published in the Conference Proceedings.

27. R.P. Elliott: "Constitution of Binary Alloys, First Supplement," McGraw-Hill Inc., New York, 1965, p. 617.

28. ASM Metals Handbook, 8th Edition, Metallography and Phase Diagrams, ASM, Metals Park, OH.

29. Poster and Easterling: Phase Transformations in Metals and Alloys, Van Nostrand, UK Company ltd., 198.

30. M. Hillert: Acta Met., 1965, Vol. 13, p. 227.

31. F. Feltham: Acta Met., 1957, Vol. 5, p. 97.

32. I.M. Lifshitz, and V.V. Slyosov, J. Phy. Chem. Solids, 1961, Vol. 19, p. 35.

33. C. Wagner: Z. Electrochem, 1961, Vol. 65, p. 581.

34. A.J. Ardell: Acta Met., 1972, Vol. 20, p. 61.

35. C.K.L. Davies, P. Nash, and R.N. Stevens: Acta Met., 1980, Vol. 28, p. 179.

36. A.D. Brailsford, and P. Wynblatt, Acta. Met., 1979, Vol. 27, p. 489.

37. K. Tsumuraya and Y. Miyata: Acta Met., 1983, Vol. 31, p. 437.

38. N.E. Paton and C.H. Hamilton: "Superplasticity in Titanium Alloys", Proceedings of the Fifth International Conference on Titanium, 1985, Vol. 2, p. 649.

TABLE 1: The Aim Compositions and the Actual Ingot Chemistry of Ti-Mn Alloys

Alloy No.	Compositions					
	AIM	ACTUAL COMPOSITIONS OF INGOTS				
	%Mn	Mn	Fe	O*	N	C
1	0.6	.4	0.02	0.071	0.01	0.02
2	2.7	3.0	0.01	0.086	0.01	0.02
3	4.9	4.8	0.01	0.082	0.006	0.01
4	7.1	6.0	0.01	0.083	0.008	0.01
5	9.3	9.4	0.02	0.100	0.10	0.02
6	11.5	13	0.01	0.116	0.012	0.02

* Oxygen content of final product.

TABLE 2: The Aim Composition
and the Actual Ingot Chemistry of Ti-V Alloys

Alloy No.	Compositions					
	AIM	ACTUAL COMPOSITIONS OF INGOTS				
	%V	V	Fe	O*	N	C
7	3.9	4.3	0.01	0.078	0.017	0.02
8	6.0	6.2	0.01	0.063	0.015	0.01
9	8.3	8.1	0.01	0.082	0.016	0.02
10	10.5	10.6	0.01	0.075	0.020	0.02
11	12.8	12.6	0.01	0.083	0.019	0.02
12	15.0	14.8	0.01	0.092	0.021	0.02

* Oxygen content of final product.

TABLE 3: Isothermal Growth Data for Alloy No. 2 (79% α - 21% β Ti-Mn Alloy) Annealed at 973°K, WQ

Time T (hrs)	log T	D_α (μm)	log D_α	D_β (μm)	log D_β
25	1.3979	5.767	.7609	1.561	.1934
50	1.6989	7.024	.8465	1.9018	.2791
100	2	8.5316	.9310	2.3090	.3634
200	2.3010	10.356	1.015	2.8030	.4476
400	2.6020	12.577	1.0995	3.4043	.5319

$$D_\beta^{\alpha-\beta} = .633t^{.28} \quad \bar{\gamma} = .99$$

$$D_\alpha^{\alpha-\beta} = 2.338t^{.28} \quad \bar{\gamma} = .99$$

TABLE 4: Isothermal Growth Data for Alloy No. 3 (63% α - 37% β, Ti-Mn Alloy) Annealed at 973 K, WQ

Time T (hrs)	log T	D_α (μm)	log D_α	D_β (μm)	log D_β
25	1.3979	4.0686	.60944	2.2482	.37073
50	1.6989	4.7367	.67547	2.7338	.43676
100	2	5.4439	.73591	3.1420	.49720
200	2.3010	6.5235	.81448	3.7651	.57577
400	2.6020	8.7940	.94418	5.0758	.70550

$$D_\alpha^{\alpha-\beta} = 1.654t^{.268} \quad \bar{\gamma} = .986$$

$$D_\beta^{\alpha-\beta} = .9552t^{.268} \quad \bar{\gamma} = .986$$

TABLE 5: Isothermal Growth Data for Alloy No. 4 (45% α - 55% β, Ti-Mn Alloy) Annealed at 973 K, WQ

Time T (hrs)	log T	D_α (μm)	log D_α	D_β (μm)	log D_β
25	1.3979	3.1170	.4937	3.7819	.5777
50	1.6989	3.4176	.5337	4.1456	.6175
100	2	4.4004	.6434	5.3377	.7273
200	2.3010	5.6767	.7540	6.8858	.8379
400	2.6020	6.4138	.8071	7.7800	.8909

$$D_\alpha^{\alpha-\beta} = 1.2119t^{.28} \quad \bar{\gamma} = .988$$

$$D_\beta^{\alpha-\beta} = 1.4709t^{.28} \quad \bar{\gamma} = .988$$

TABLE 6: Isothermal Growth Data for Alloy No. 5 (10% α - 90% β, Ti-Mn Alloy) Annealed at 973 K, WQ

Time T (hrs)	log T	D_α (μm)	log D_α	D_β (μm)	log D_β
25	1.3979	2.0066	.3024	17.5318	1.2438
50	1.6989	2.4843	.3952	21.7061	1.3365
100	2	2.8980	.4620	25.3230	1.4035
200	2.3010	3.726	.5712	32.5590	1.5126
400	2.6020	4.3476	.6382	37.9857	1.5796

$$D_\alpha^{\alpha-\beta} = .8147t^{.28} \quad \bar{\gamma} = .99$$

$$D_\beta^{\alpha-\beta} = 7.079t^{.28} \quad \bar{\gamma} = .99$$

TABLE 7: Isothermal Growth Parameters $K_{\alpha}^{\alpha-\beta}$ and $K_{\beta}^{\alpha-\beta}$ for the Various Ti-Mn Alloys

Alloy No.	V_{α}	log V_{α}	$K_{\beta}^{\alpha-\beta}$	log $K_{\beta}^{\alpha-\beta}$	V_{β}	log V_{β}	$K_{\alpha}^{\alpha-\beta}$	log $K_{\alpha}^{\alpha-\beta}$
2	78.673	1.895	.636	- .1992	21.32	1.3287	2.35	.3710
3	63.405	1.8021	.9552	- .0199	36.59	1.5633	1.654	.21876
4	45.180	1.6549	1.4709	.1676	54.812	1.7388	1.2119	.0835
5	10.270	1.0115	7.079	.85	89.73	1.9527	.8147	-.089

$$D_{\beta}^{\alpha-\beta} = \frac{105.394}{V_{\alpha}^{1.146}} \qquad \bar{\gamma} = .99$$

$$D_{\alpha}^{\alpha-\beta} = \frac{22.908}{V_{\beta}^{.7385}} \qquad \bar{\gamma} = .99$$

TABLE 8: Isothermal Growth Data for Alloy No. 7 (70% α - 30% β, Ti-V Alloy) Annealed at 973 K, WQ

Time T (hrs)	log T	D_α (μm)	log D_α	D_β (μm)	log D_β
25	1.3979	3.6586	.5633	1.584	.199
50	1.6989	4.291	.632	1.8580	.269
100	2	5.03	.701	2.179	.338
200	2.3010	5.902	.7709	2.555	.4073
400	2.6020	6.922	.8402	2.997	.476

$$D_\alpha^{\alpha-\beta} = 1.745t^{.23} \quad \bar{\gamma} = .99$$

$$D_\beta^{\alpha-\beta} = .7556t^{.23} \quad \bar{\gamma} = .99$$

TABLE 9: Isothermal Growth Data for Alloy No. 8 (56% α -44% β, Ti-V Alloy) Annealed at 973 K, WQ

Time T (hrs)	log T	D_α (μm)	log D_α	D_β (μm)	log D_β
25	1.3979	2.9342	.4674	2.267	.3550
50	1.6989	3.1665	.5005	2.446	.3885
100	2	3.934	.5948	3.040	.4828
200	2.3010	4.806	.6817	3.713	.5697
400	2.6020	5.833	.7658	4.5073	.6539

$$D_\alpha^{\alpha-\beta} = 1.216t^{.258} \quad \bar{\gamma} = .99$$

$$D_\beta^{\alpha-\beta} = .9397t^{.258} \quad \bar{\gamma} = .99$$

TABLE No. 10: Isothermal Growth Data for Alloy No. 9 (44% α - 56% β - Ti-V Alloy) Annealed at 973 K, WQ

Time T (hrs)	log T	D_α (μm)	log D_α	D_β (μm)	log D_β
25	1.3979	2.3407	.3693	2.9326	.4672
50	1.6989	2.8216	.4504	3.5350	.5483
100	2	3.1175	.4938	3.9058	.5917
200	2.3010	3.887	.5896	4.8708	.6876
400	2.6020	4.796	.6808	6.0108	.7789

$$D_\alpha^{\alpha-\beta} = 1.0240t^{.253} \quad \bar{\gamma} = .99$$

$$D_\beta^{\alpha-\beta} = 1.2823t^{.253} \quad \bar{\gamma} = .99$$

TABLE 11: Isothermal Growth Data for Alloy No. 10 (29% α - 71% β, Ti-V Alloy) Annealed at 973 K, WQ

Time T (hrs)	log T	D_α (μm)	log D_α	D_β (μm)	log D_β
25	1.3979	2.004	.30189	4.8604	.6866
50	1.6989	2.4118	.3823	5.8483	.7670
100	2	2.871	.4580	6.9623	.8427
200	2.3010	3.5476	.54990	8.6025	.9340
400	2.6020	4.0630	.6088	9.8540	.9936

$$D_\beta^{\alpha-\beta} = 2.1183t^{.259} \quad \bar{\gamma} = .99$$

$$D_\alpha^{\alpha-\beta} = .8731t^{.259} \quad \bar{\gamma} = .99$$

TABLE 12: Isothermal Growth Data for Alloy No. 11 (7% α - 93% β, Ti-V Alloy) Annealed at 973 K, WQ

Time T (hrs)	log T	D_α (μm)	log D_α	D_β (μm)	log D_β
50	1.6989	1.893	.277	23.01	1.3619
100	2	2.235	.3492	27.179	1.434
200	2.3010	2.6403	.4216	32.098	1.5064
400	2.6020	3.1181	.4938	37.908	1.5787

$$D_\alpha^{\alpha-\beta} = .7403t^{.24} \quad \bar{\gamma} = .99$$

$$D_\beta^{\alpha-\beta} = 9\,t^{.24} \quad \bar{\gamma} = .99$$

TABLE 13: Isothermal Growth Parameters $K_{\alpha}^{\alpha-\beta}$ and $K_{\beta}^{\alpha-\beta}$ for the Various Ti-V Alloys

Alloy No.	V_{α}	log V_{α}	$K_{\beta}^{\alpha-\beta}$	log $K_{\beta}^{\alpha-\beta}$	V_{β}	log V_{β}	$K_{\sigma}^{\alpha-\beta}$	log $K_{\alpha}^{\alpha-\beta}$
7	69.82	1.8439	.7556	- .1217	30.18	1.479	1.745	.242
8	56.412	1.7513	.9397	- .027	43.587	1.6393	1.2164	.085
9	44.388	1.6472	1.282	.108	55.612	1.7451	1.0240	.0101
10	29.198	1.4653	2.1183	.326	70.8018	1.850	.87317	-.0589
11	7.67	.8808	9	.954	92.4	1.9656	.74034	-.13058

$$D_{\beta}^{\alpha-\beta} = \frac{88.866}{V_{\alpha}^{1.1206}} \qquad \bar{\gamma} = .999$$

$$D_{\alpha}^{\alpha-\beta} = \frac{22.125}{V_{\beta}^{.7578}} \qquad \bar{\gamma} = .999$$

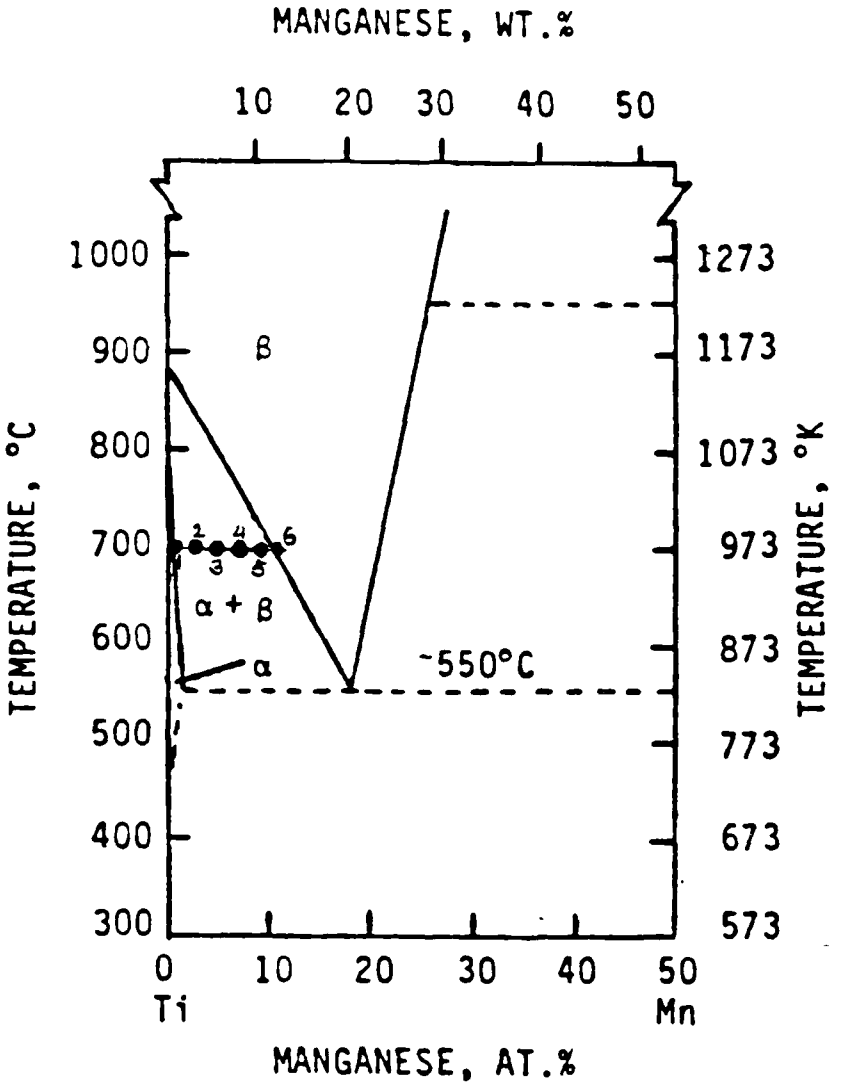

Fig. 1: Partial Ti rich end of the Ti—Mn phase diagram(27). The aim compositions of alloys 1to6 are indicated with solid circles.

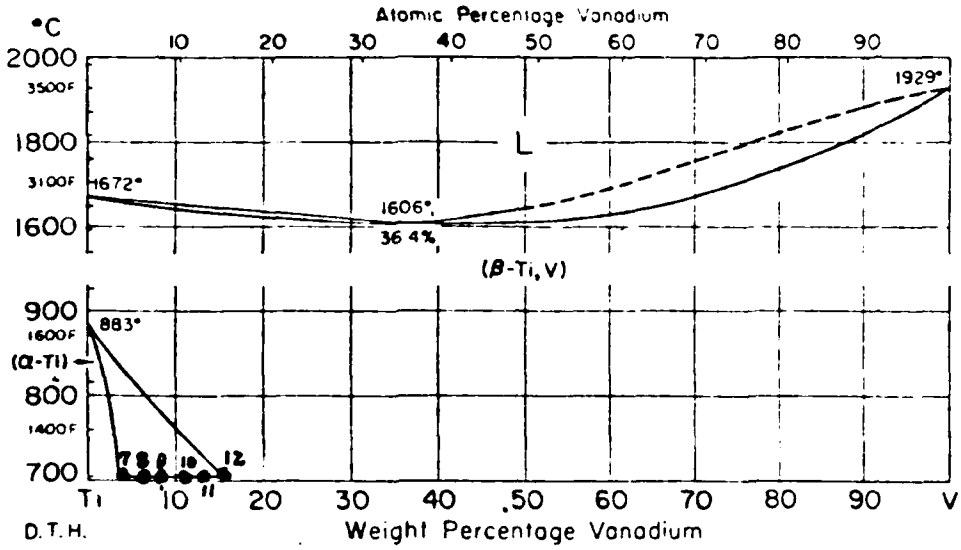

Fig. 2 : The Ti—V phase diagram(28).The aim compositions of alloys 7—12 are indicated with solid circles.

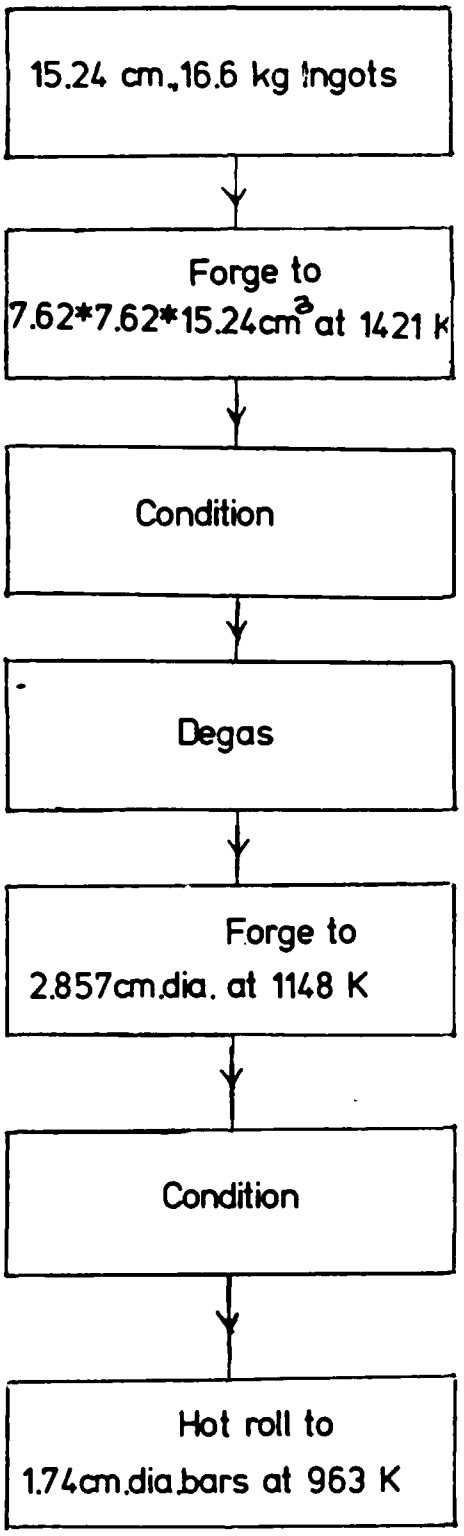

Fig. 3 : Processing sequence for Ti—Mn and Ti—V alloys listed in tables 1,and tables 2 respectively.

SPECIMEN

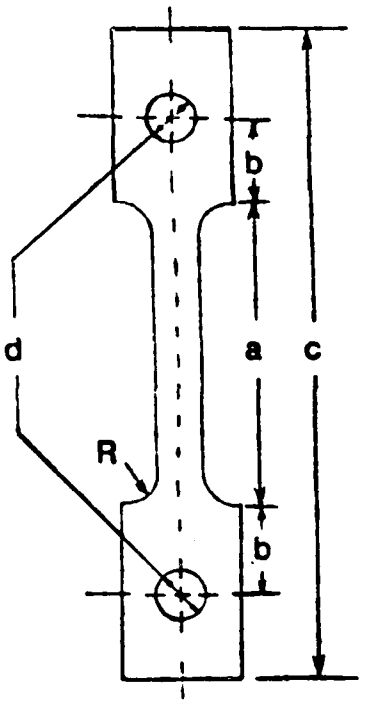

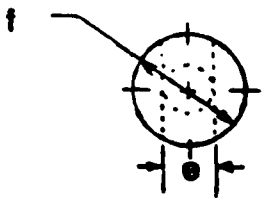

a: $1.625^{+0.005}_{-0.000}$

b: 0.400±0.002

c: sample length

d: $0.250^{+0.002}_{-0.000}$

e: 0.250±0.002

f: 0.620±0.002

R: 3/16 ±0.005

UNIT: INCH

Fig. 4 : High temperature tensile test specimen.

UDIMET GRIPS

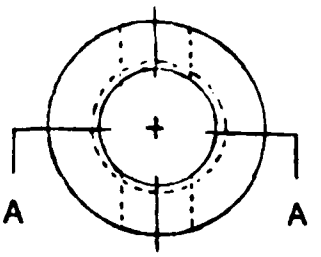

AA

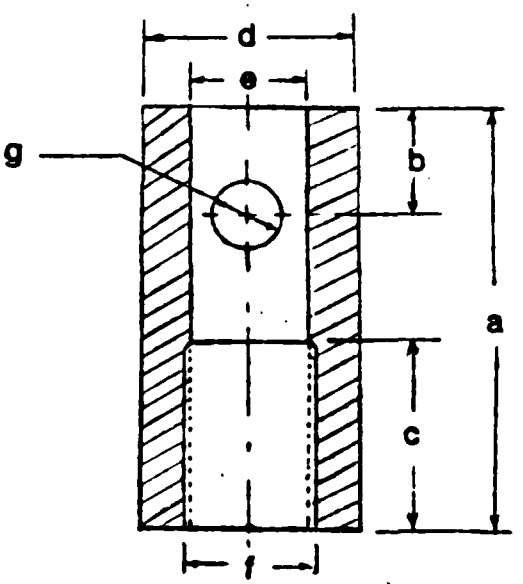

UNIT: INCH

a: 2.25

b: 0.560±0.005

c: 1.00

d: 1.125±0.005

e: 0.630±0.005

f: chase 3/4 -10

g: 3/8±0.002

Fig. 5 : High temperature grip.The grips and pins were made up of UDIMET—720.

VACUUM SYSTEM

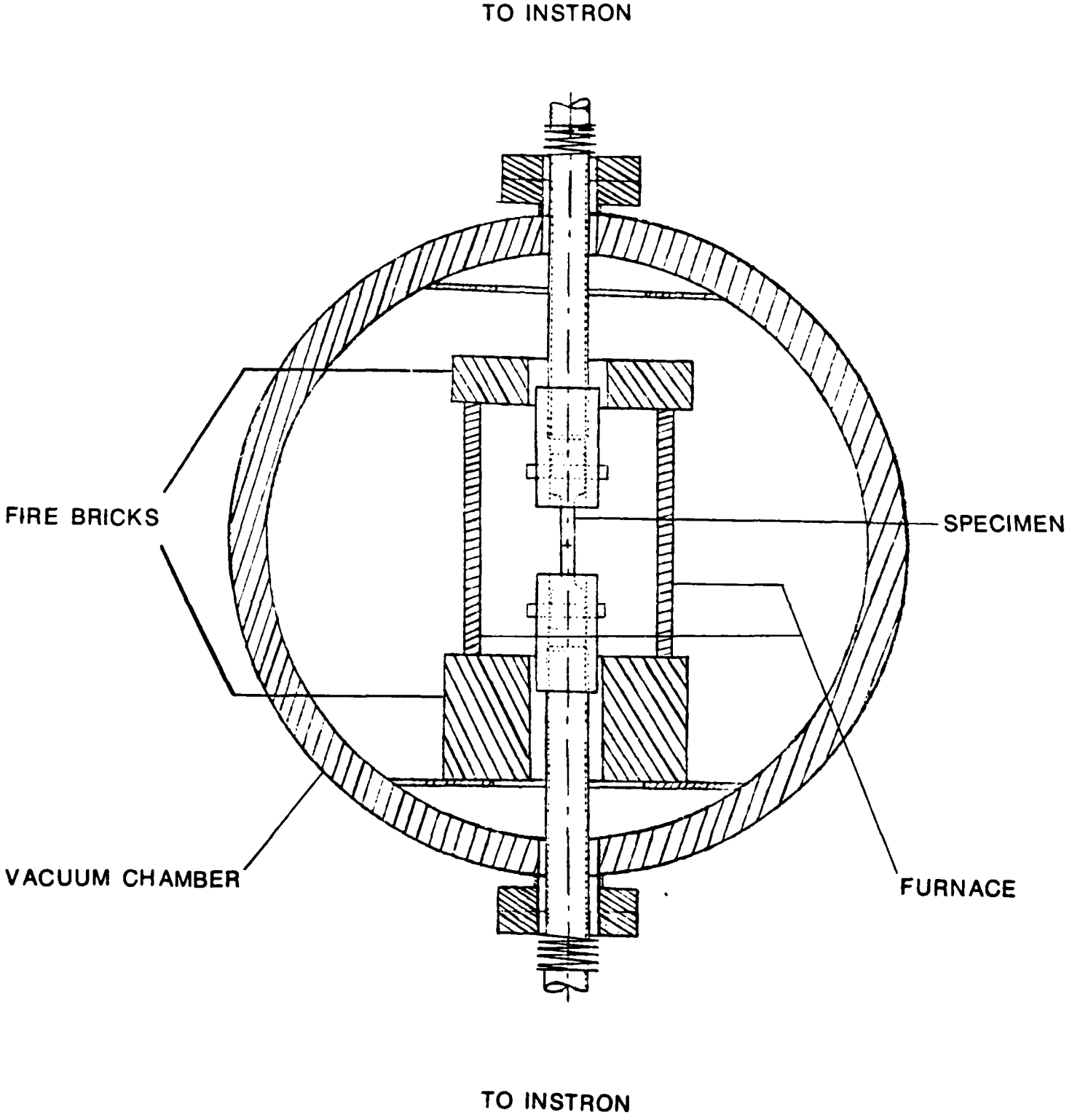

SCALE 1:2.7

Fig. 6: A schematic of the high temperature vacuum chamber used for tensile tests.

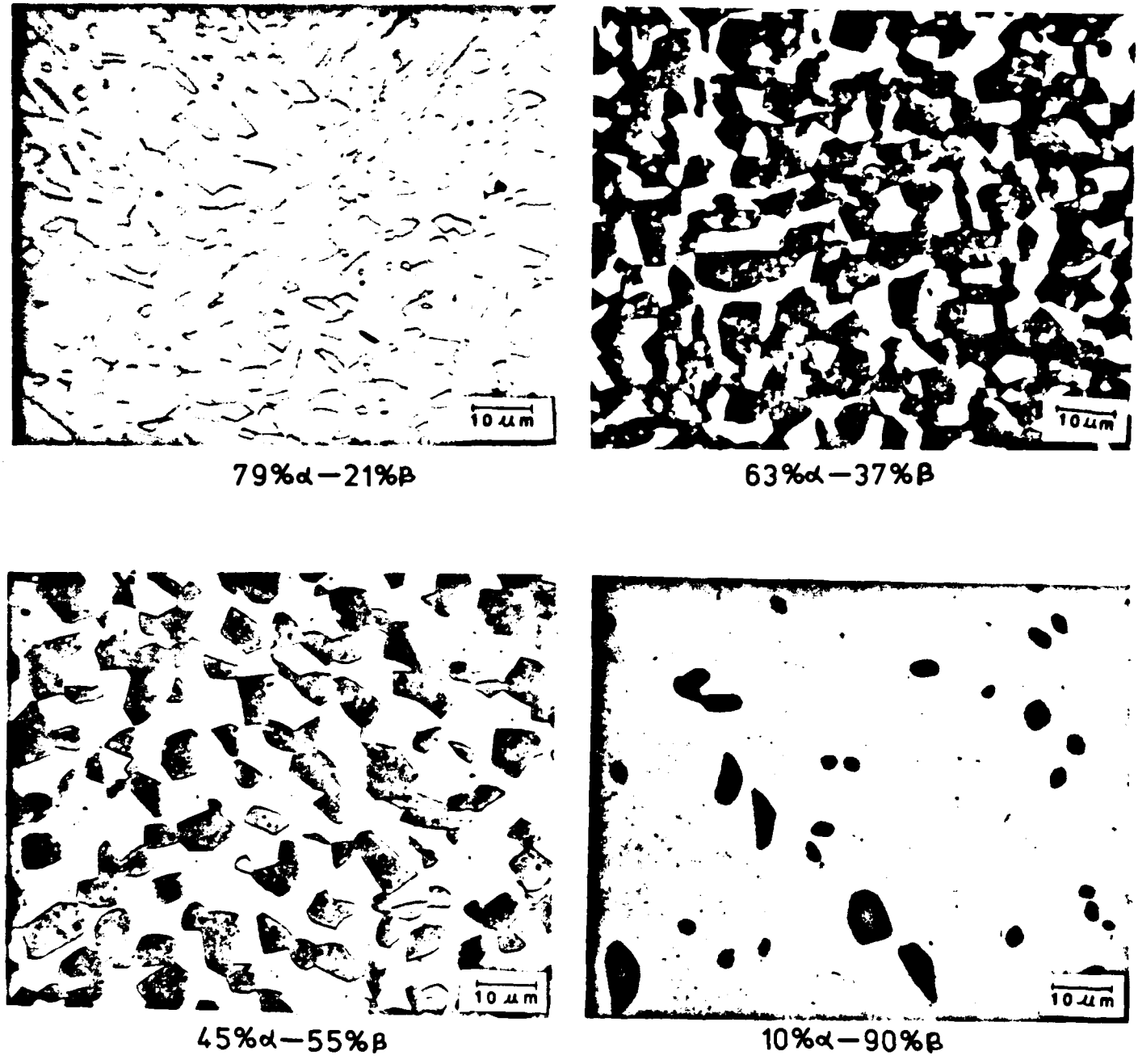

Fig. 7 : Photomicrographs of equiaxed microstructures of Ti—Mn alloys heat treated for 200 hrs. at 973 K, WQ.

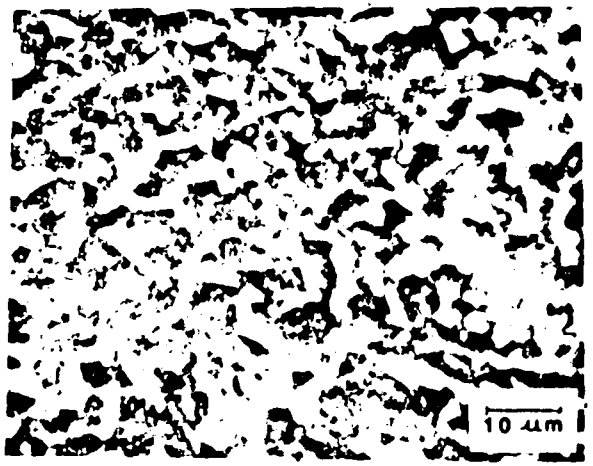

70%α–30%β

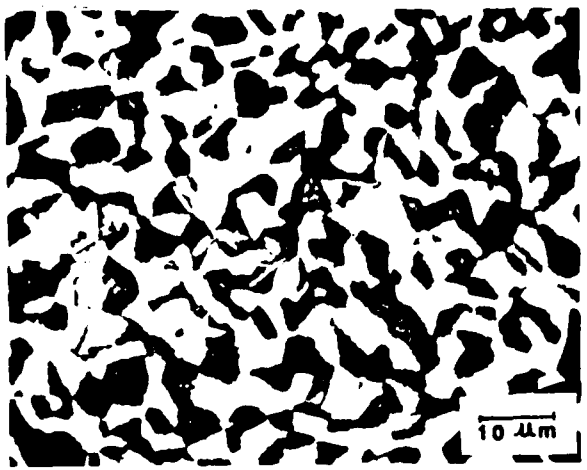

56%α–44%β

44%α–56%β

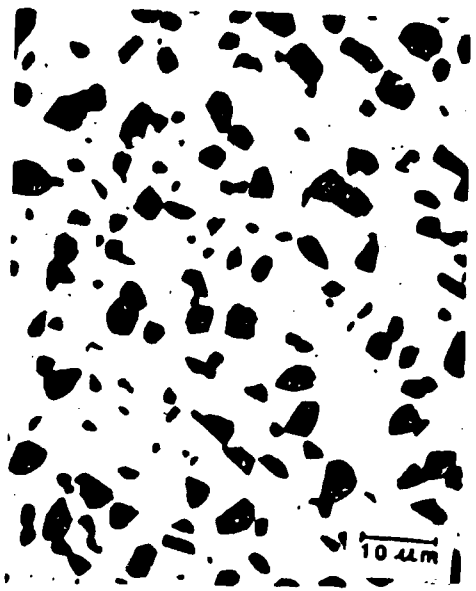

29%α–71%β

7%α–93%β

Fig. 8 : Photomicrographs of equiaxed microstructures of Ti–V alloys heat treated for 200 hrs. at 973 K,WQ.

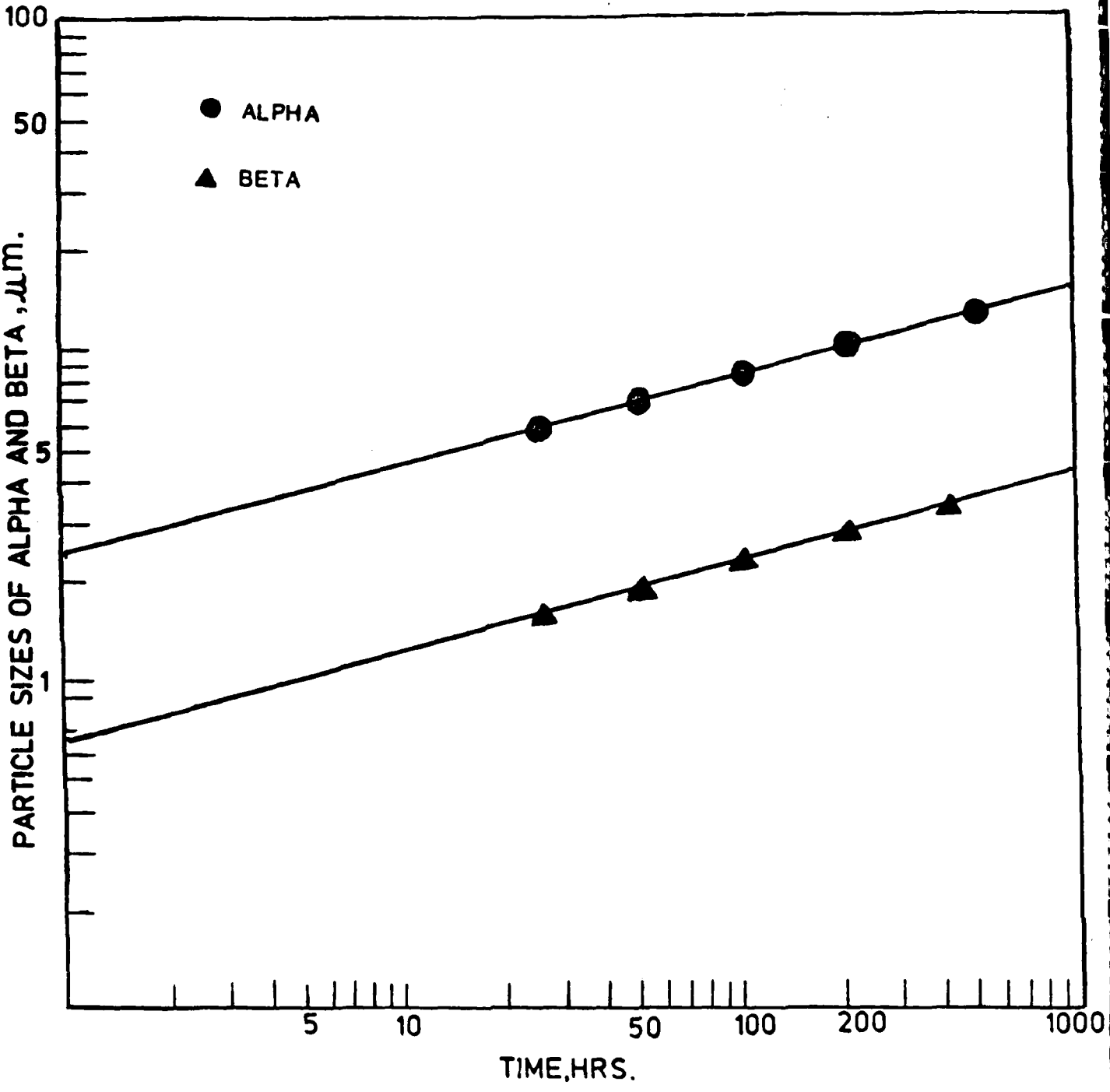

Fig. 9 : Particle sizes of alpha and beta in alloy 2(79%α—21%β,Ti—Mn alloy) .The alloy was annealed for various times at 973 K,WQ.

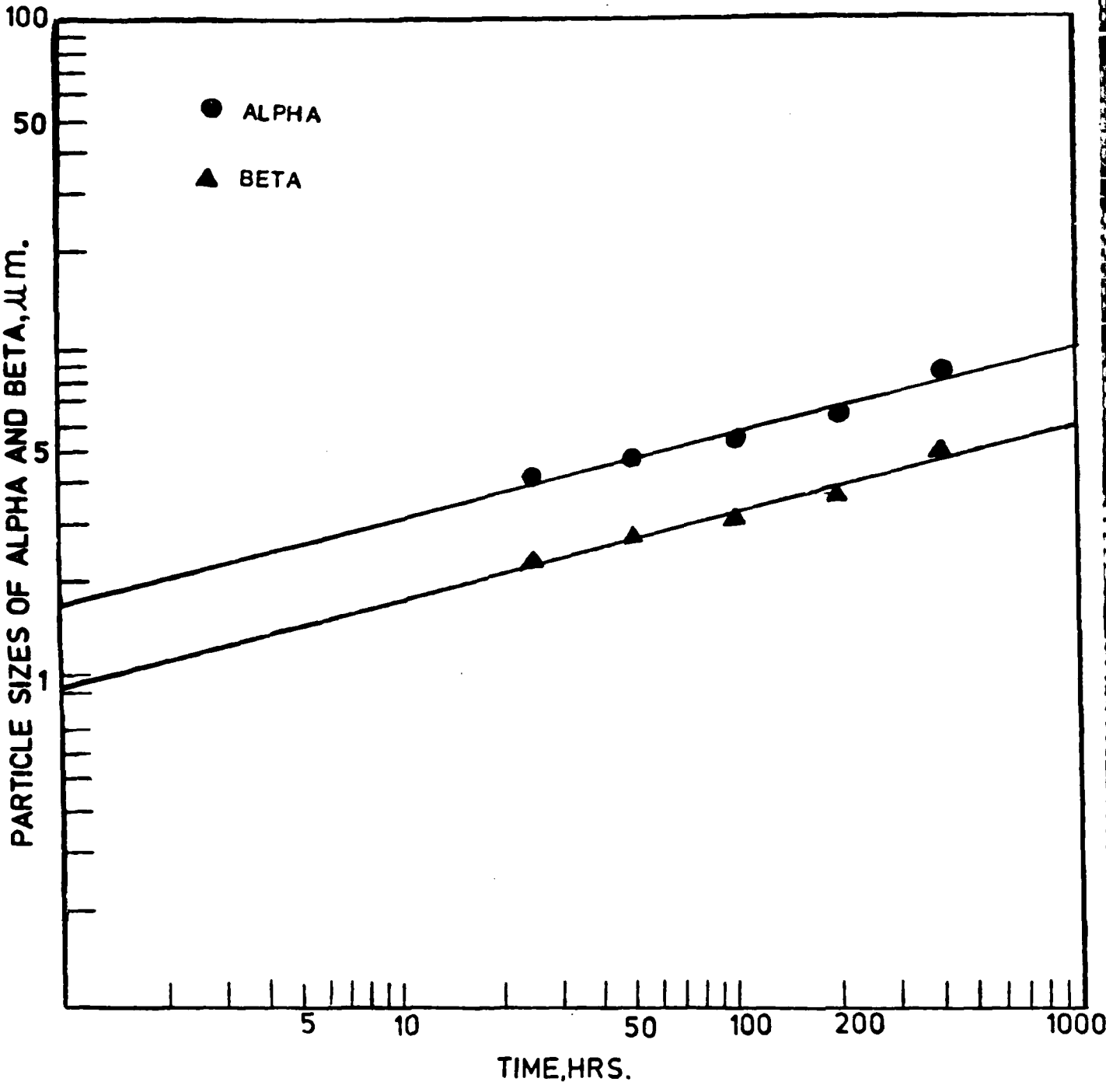

Fig. 10: Particle sizes of alpha and beta in alloy 3(63%α—37%β, Ti—Mn alloy). The alloy was annealed for various times at 973 K, WQ.

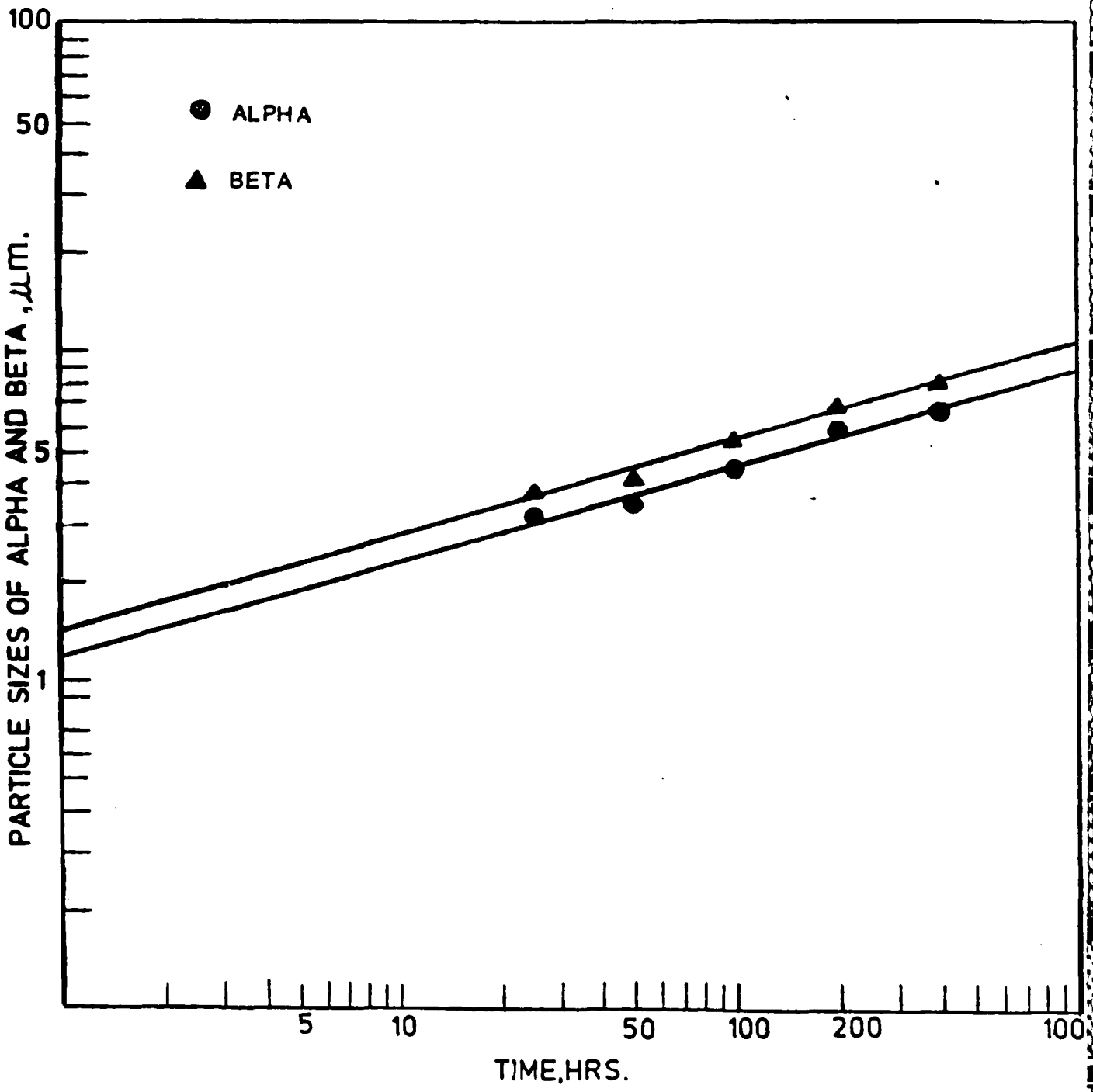

Fig. 11: Particle sizes of alpha and beta in alloy 4(45%α—55%β, Ti—Mn alloy). The alloy was annealed for various times at 973 K, WQ.

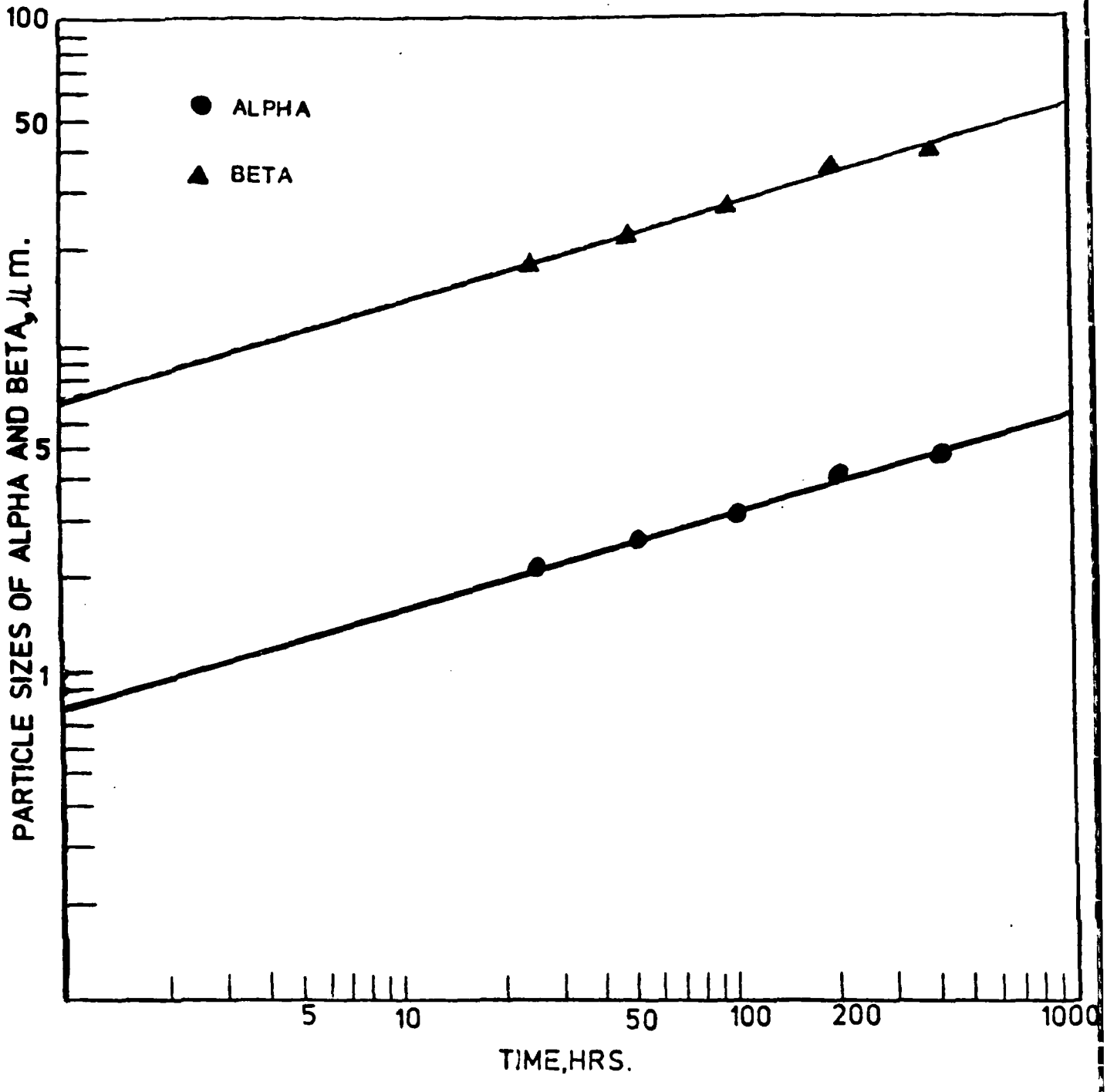

Fig. 12: Particle sizes of alpha and beta in alloy 5(10%α—90%β, Ti—Mn alloy). The alloy was annealed for various times at 973 K, WQ.

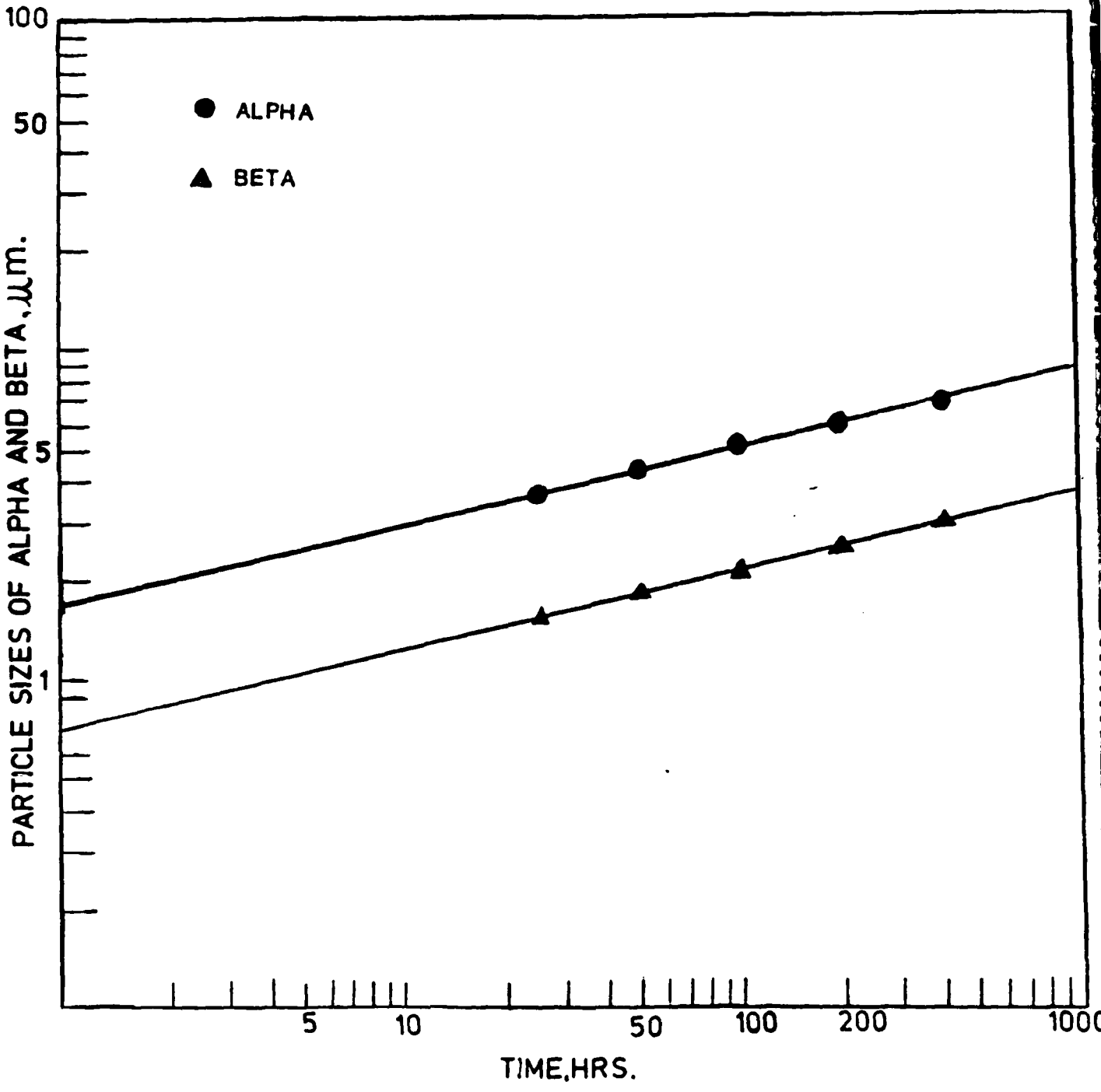

Fig. 13: Particle sizes of alpha and beta in alloy 7(70%α–30%β, Ti–V alloy). The alloy was annealed for various times at 973 K, WQ.

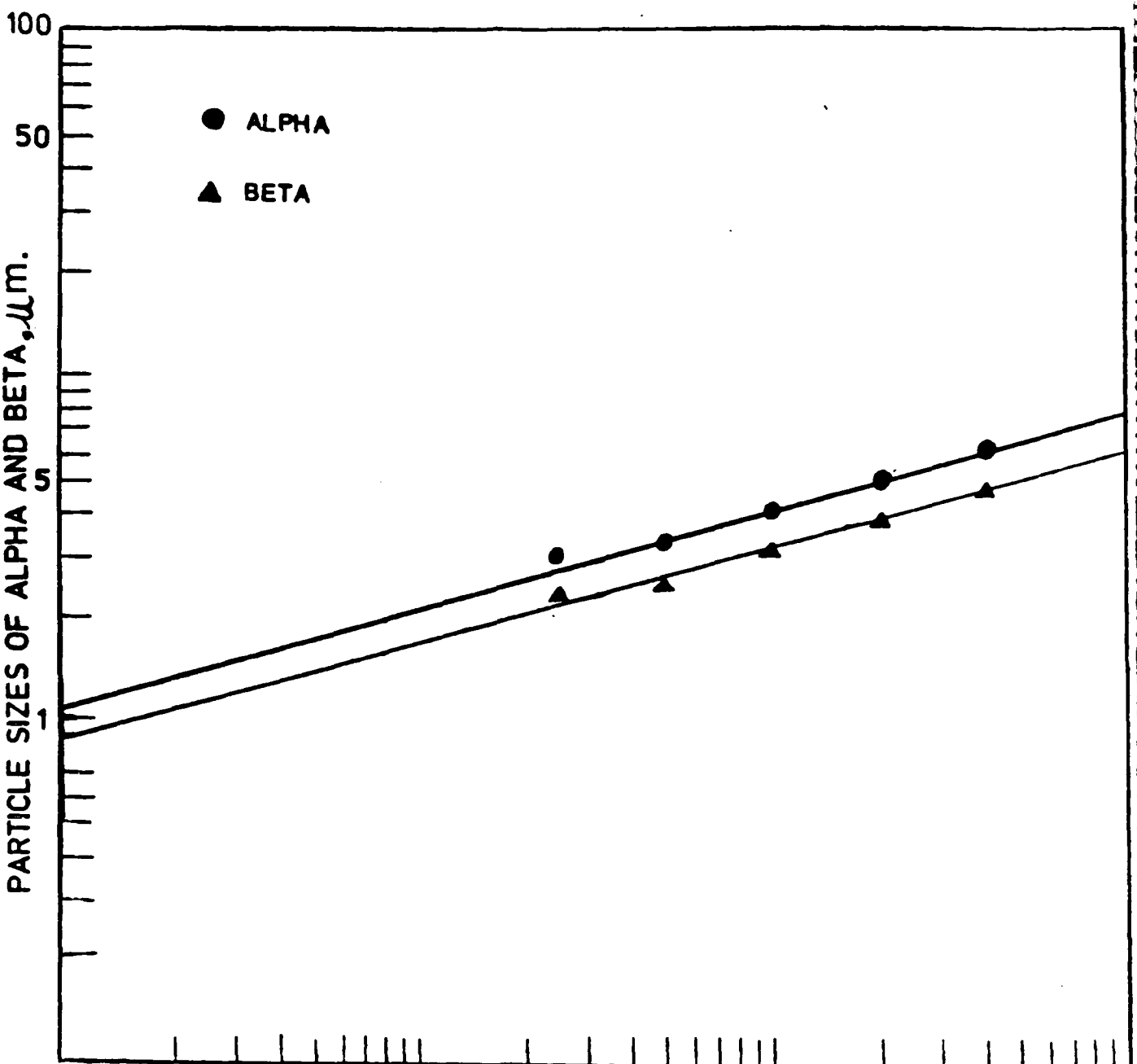

Fig. 14: Particle sizes of alpha and beta in alloy 8(56%α—44%β, Ti—V alloy). The alloy was annealed for various times at 973 K, WQ.

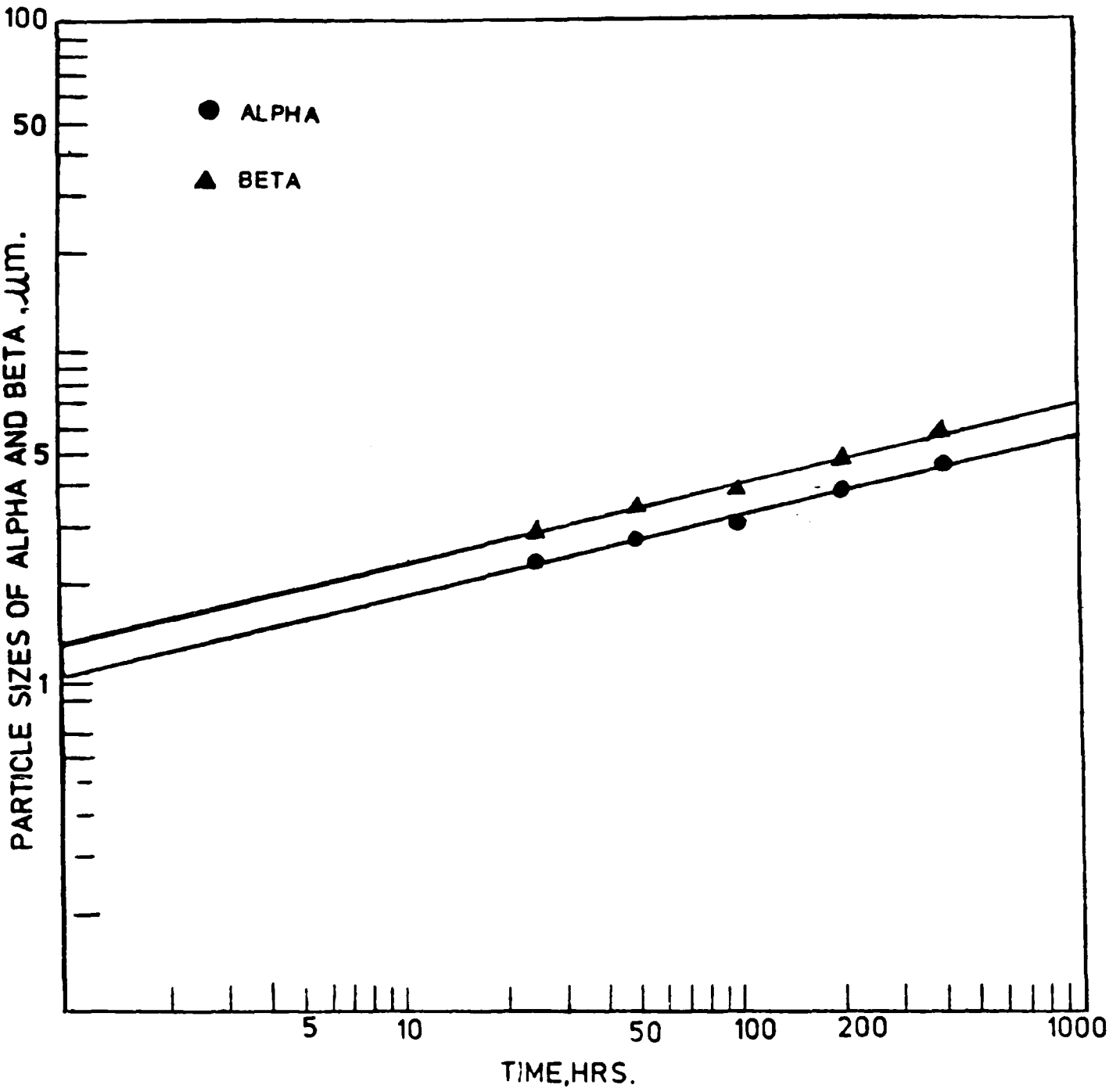

Fig. 15: Particle sizes of alpha and beta in alloy 9(44%α−56%β,Ti−V alloy). The alloy was annealed for various times at 973 K,WQ.

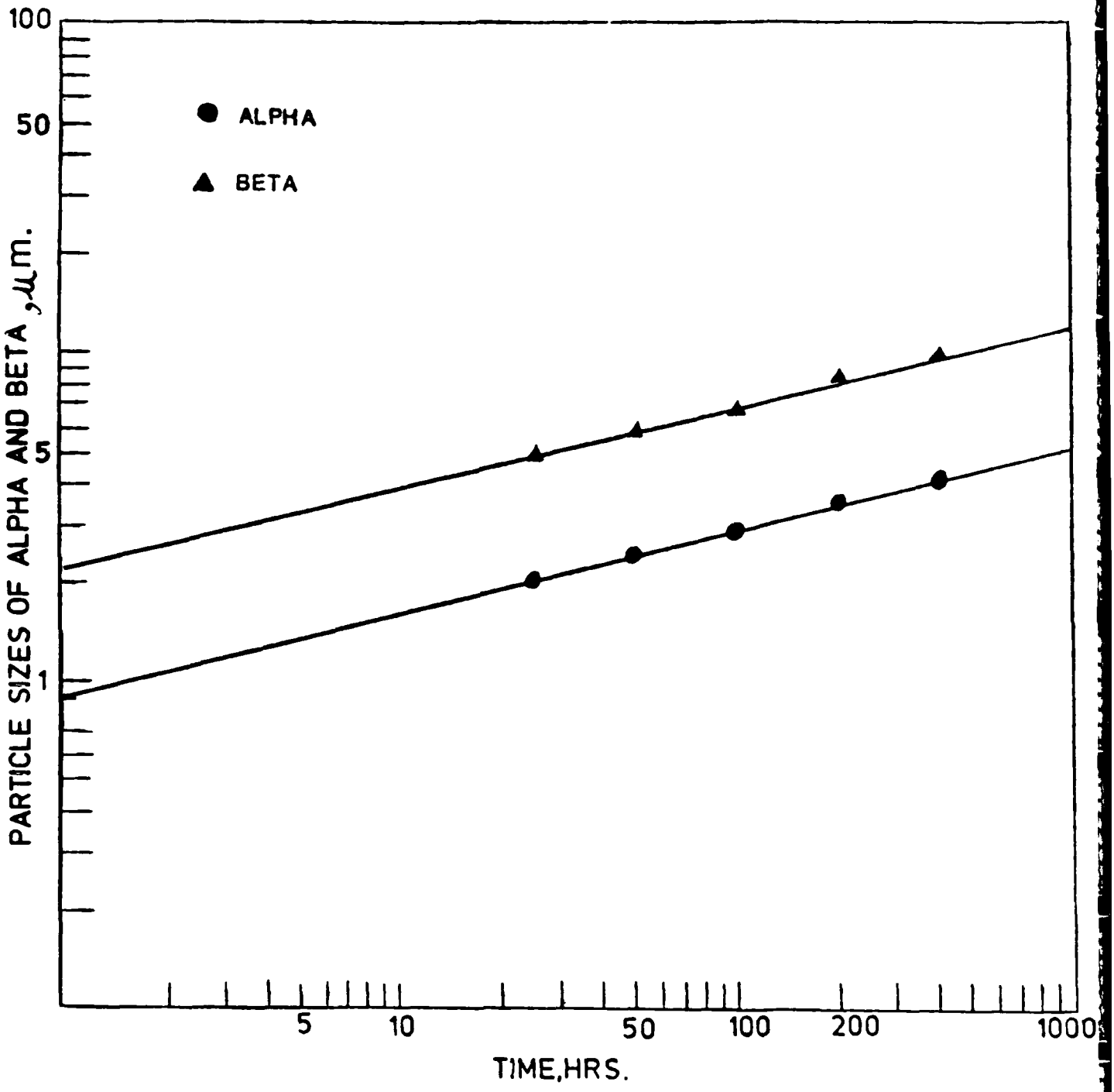

Fig. 16: Particle sizes of alpha and beta in alloy 10(29%α—71%β). The alloy was annealed for various times at 973 K,WQ.

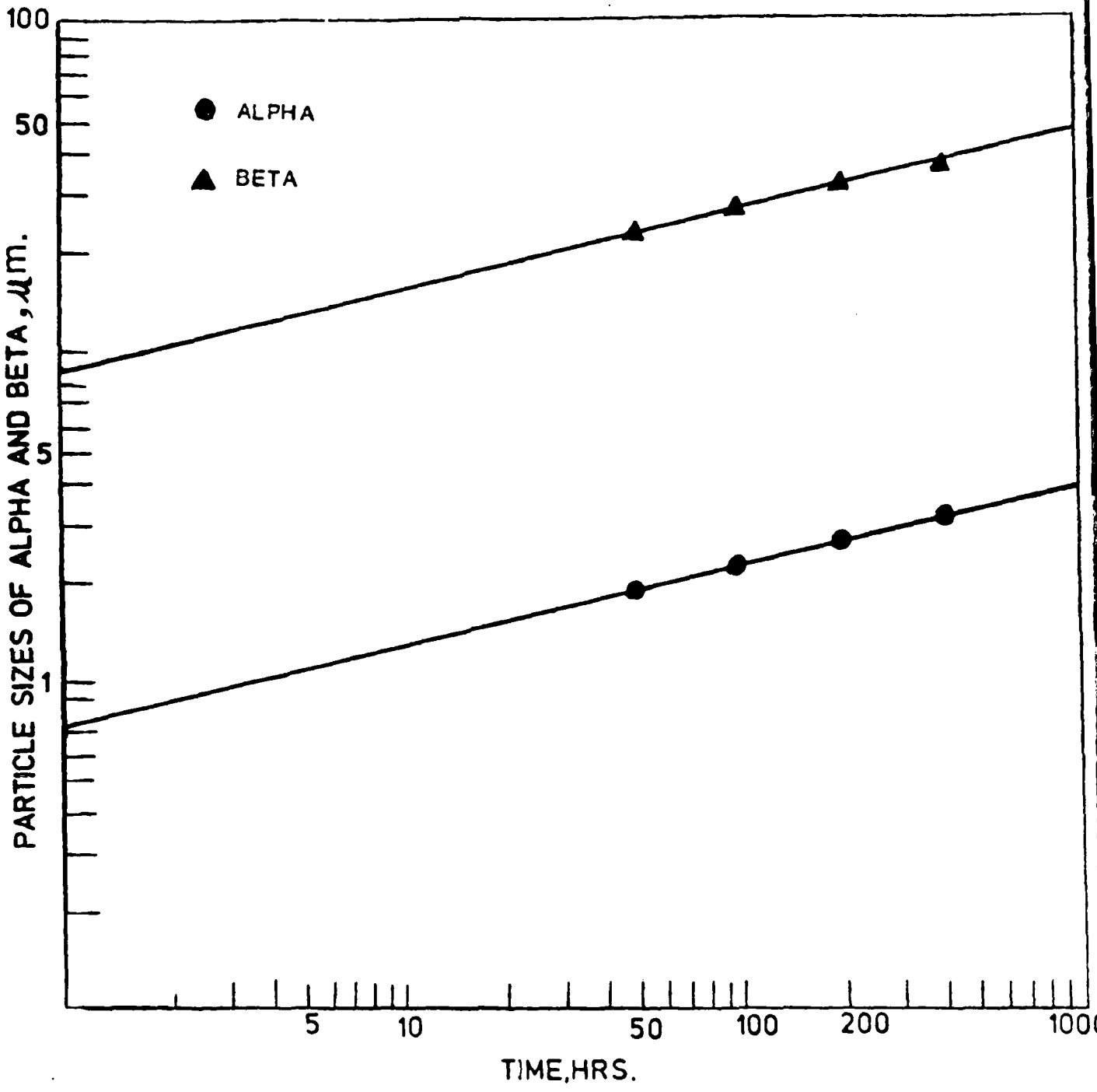

Fig. 17: Particle sizes of alpha and beta in alloy 11(7%α–93%β, Ti–V alloy). The alloy was annealed for various times at 973 K, WQ.

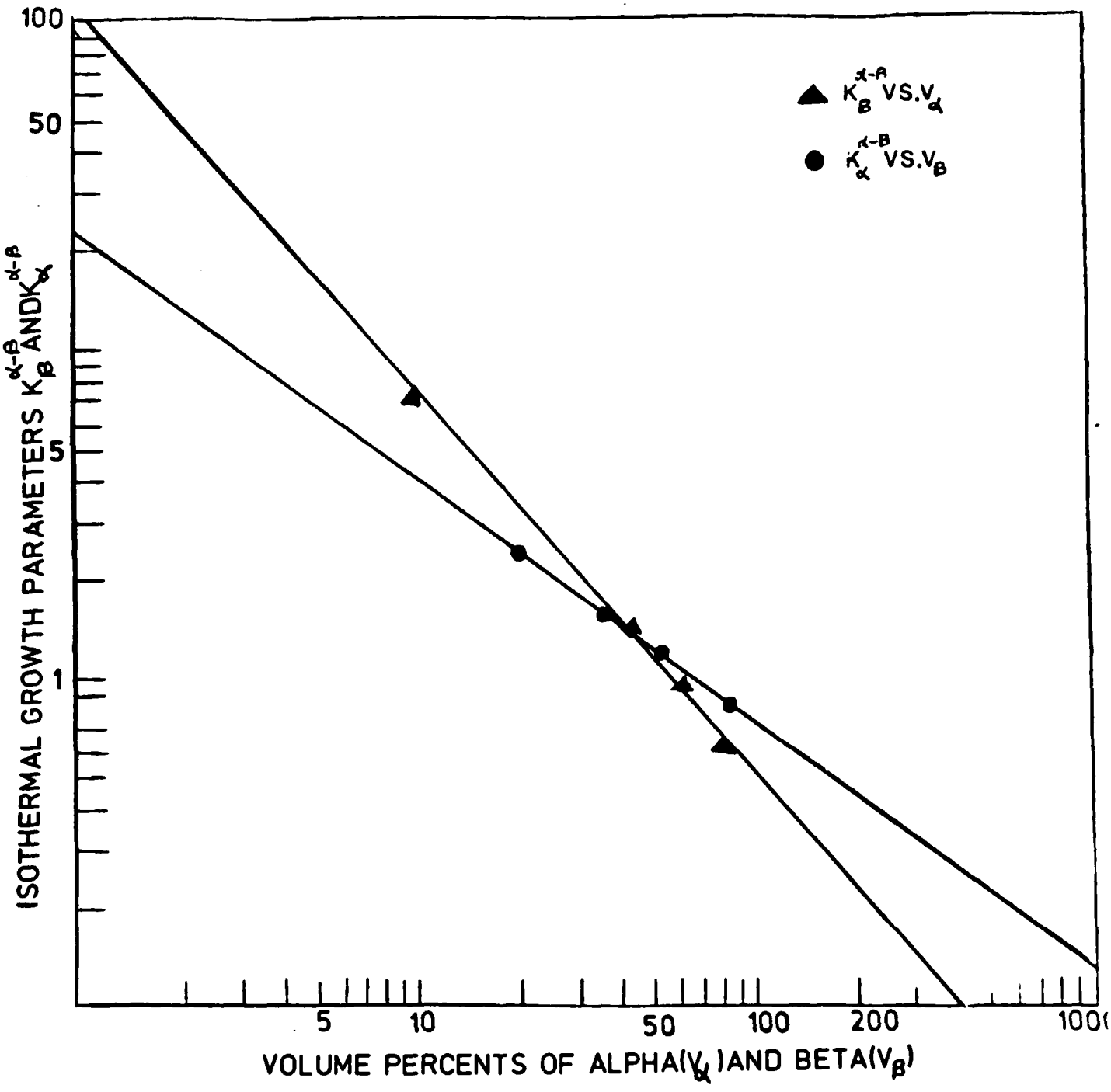

Fig. 18: Dependency of the growth parameters $K_\alpha^{\alpha-\beta}$ and $K_\beta^{\alpha-\beta}$ on volume percent of beta(V_β) and alpha(V_α), respectively, for the Ti—Mn system.

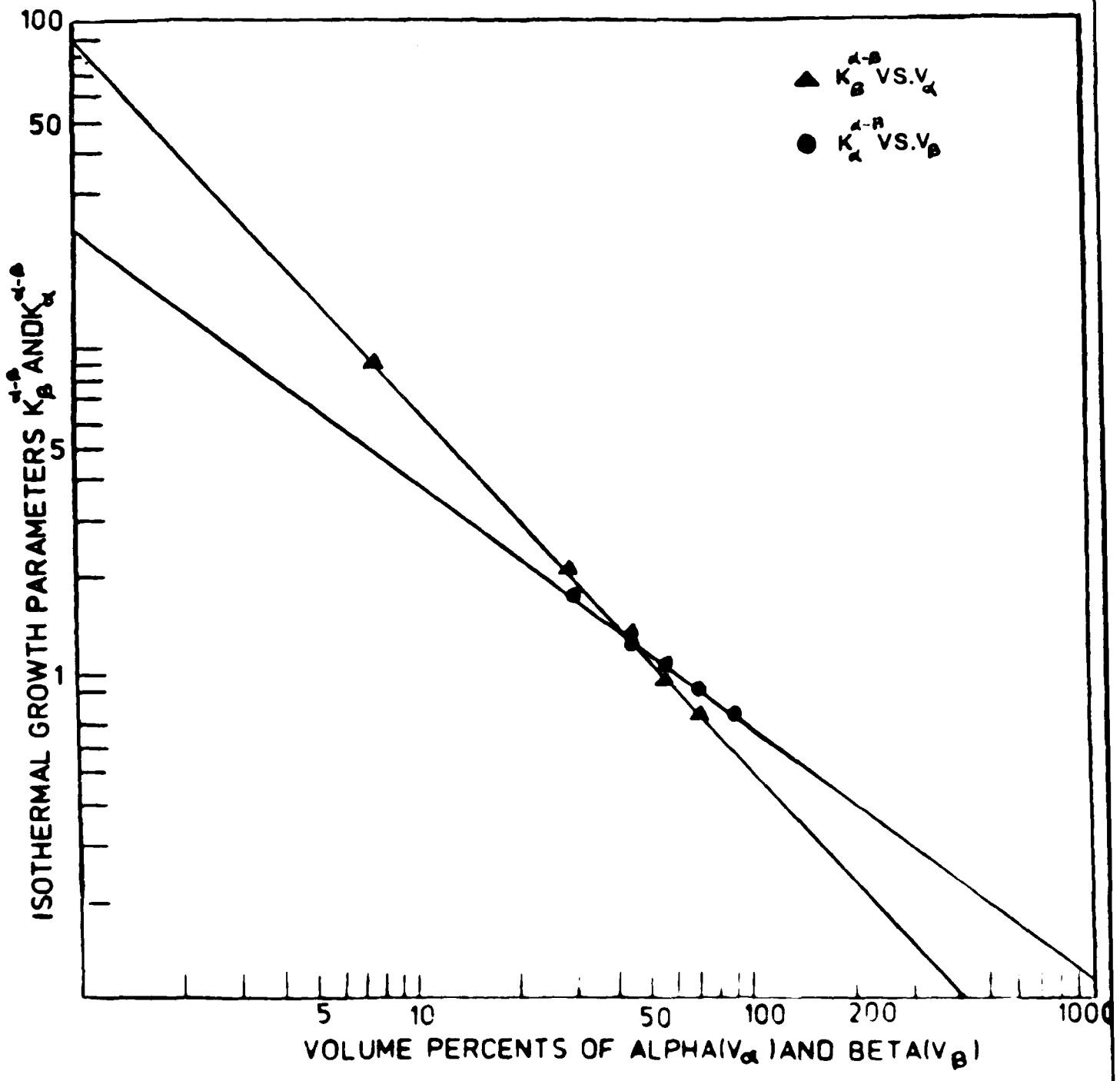

Fig. 19: Dependency of the growth parameters $K_\alpha^{\alpha-\beta}$ and $K_\beta^{\alpha-\beta}$ on volume percents of beta(V_β) and alpha(V_α) respectively, for the Ti-Al system

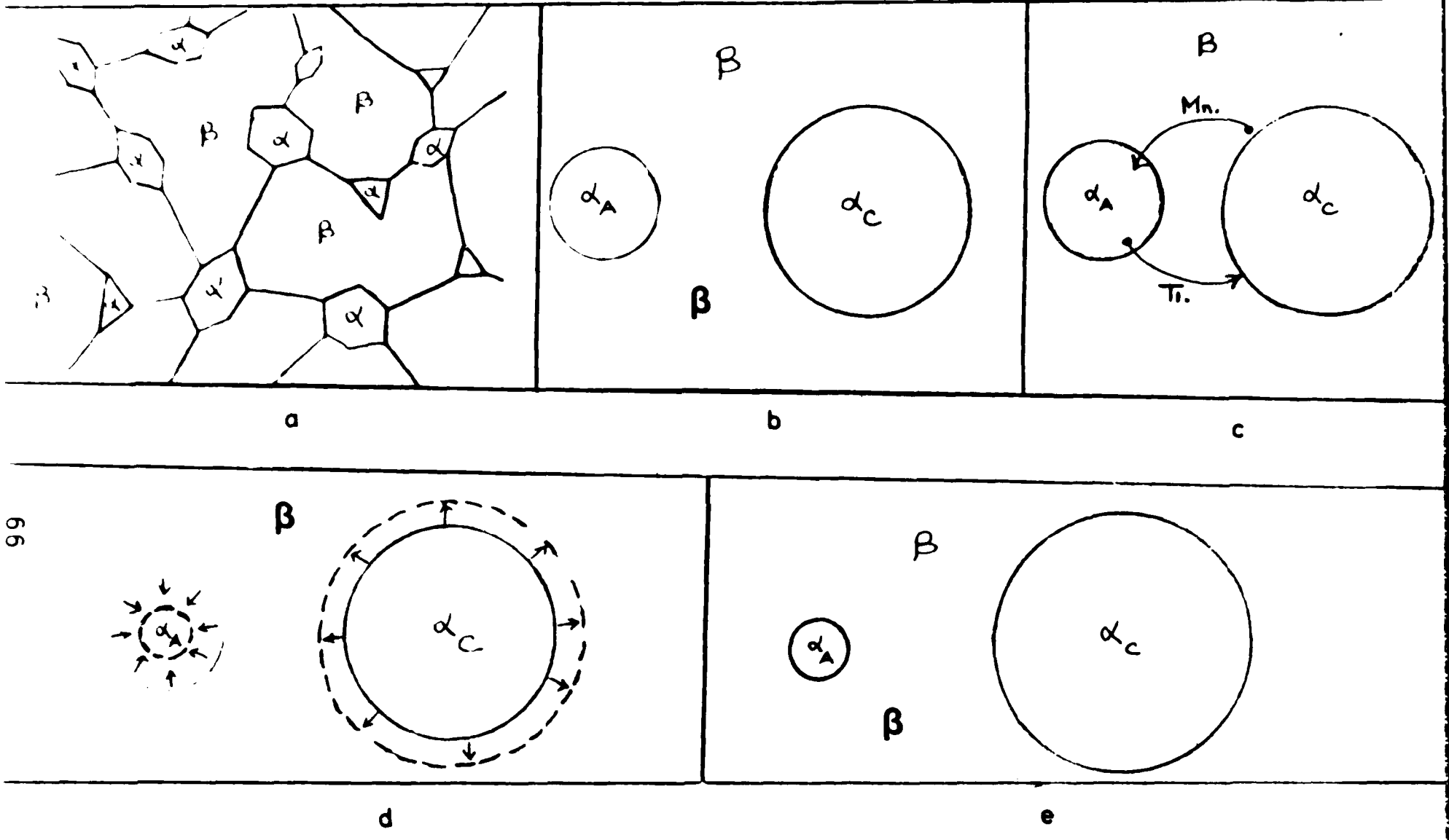

Fig. 20: A schematic of particle growth in type 1(alpha particles in beta matrix) microstructures

a).Typical microstructure b)Idealized microstructure c).Diffusion of Ti and Mn

d).Arrows indicate direction of motion of alpha—beta interfaces

e)Final idealized microstructures after a certain time.

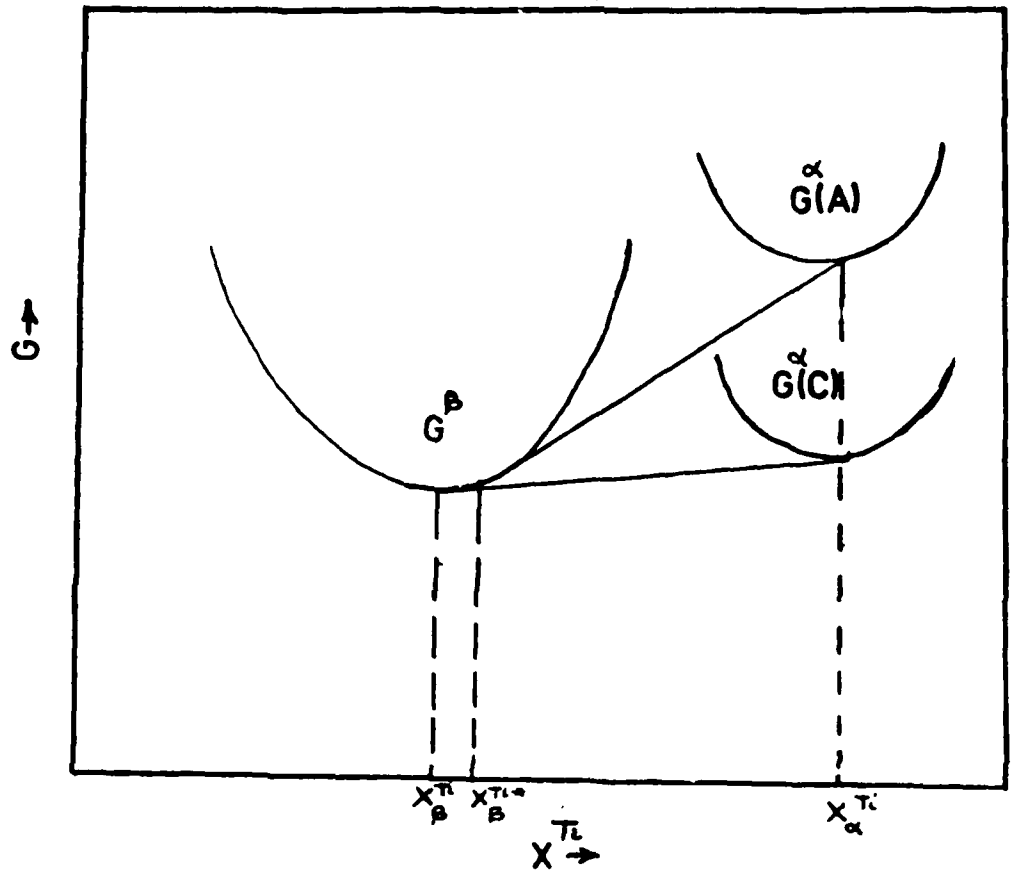

Fig. 21: Free energy diagram of the constituents of type 1 microstructure.

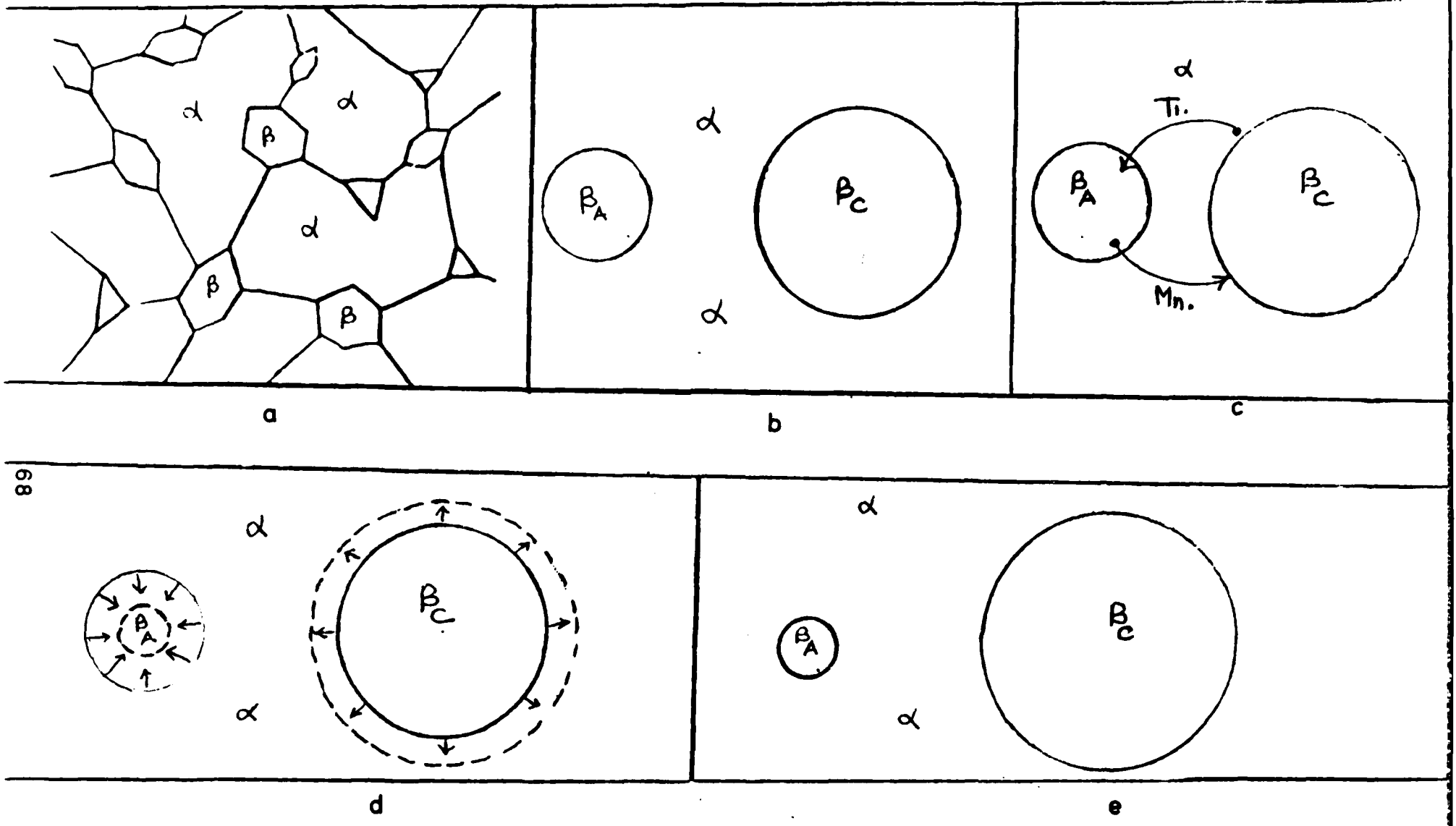

Fig. 22: A schematic of particle growth in type 2(beta particles in alpha matrix) microstructures

a).Typical microstructure b)Idealized microstructure c)Diffusion of Tiand Mn

d).Arrows indicate direction of motion of alpha—beta interfaces

e)Final idealized microstructure after a certain time

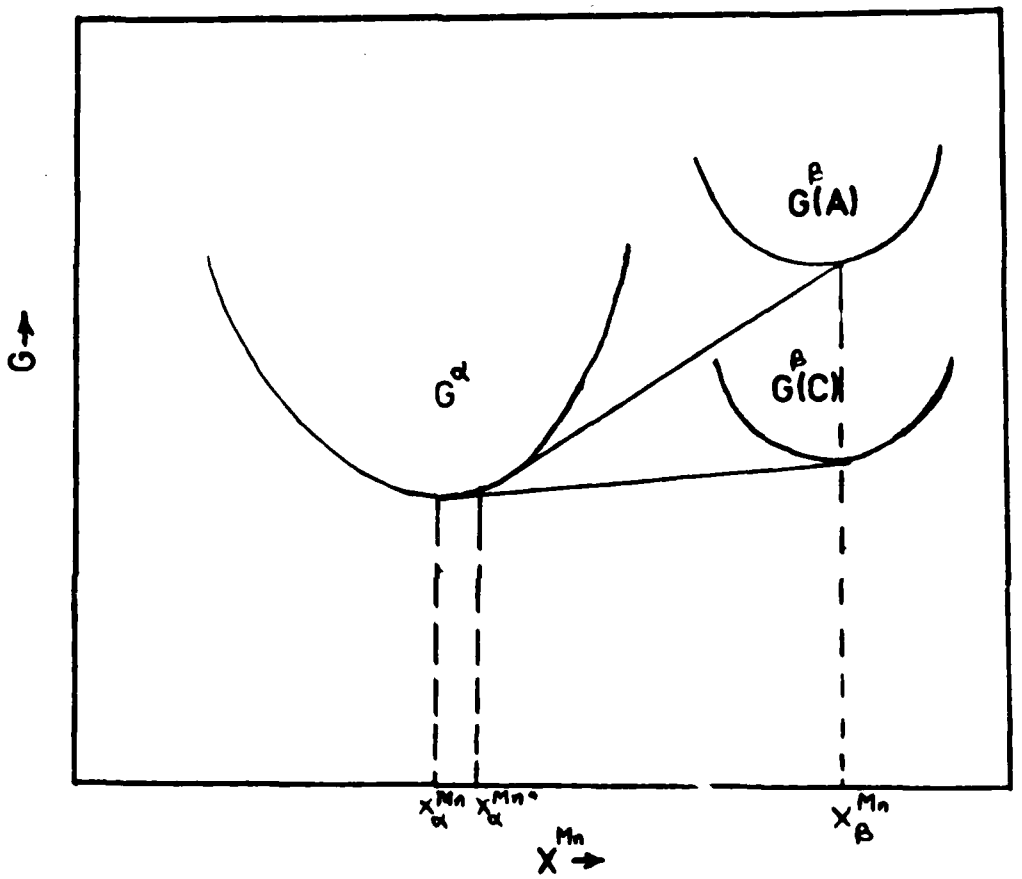

Fig. 23: Free energy diagram of the constituents of the type 2 microstructure.

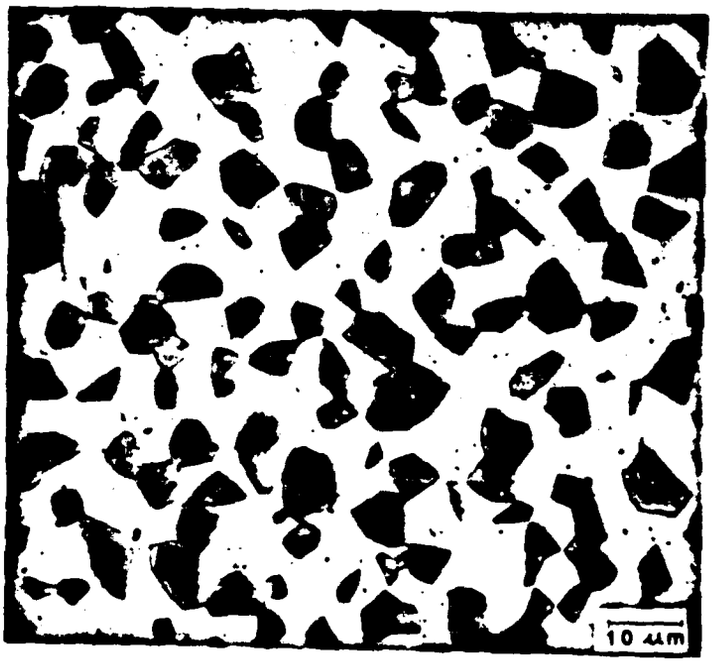

Fig. 24: Typical type 3 (nearly equivalent volume percents of alpha and beta) microstructure.

25hrs.

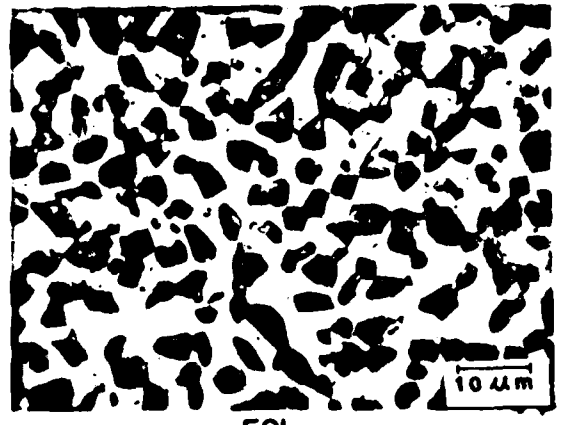

50hrs.

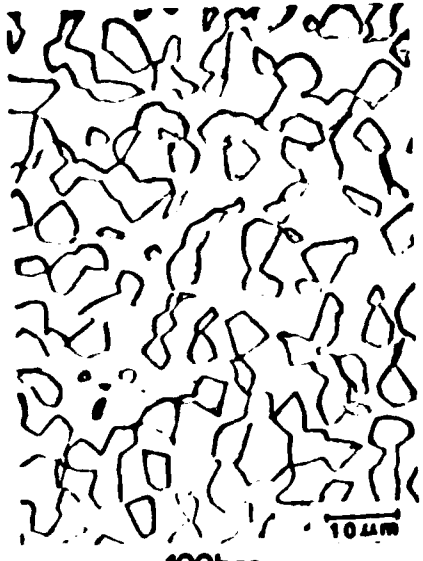

100hrs.

200hrs.

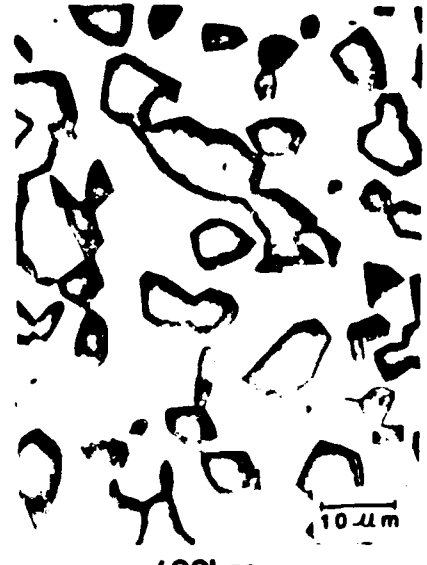

400hrs.

Fig. 25: Photomicrographs of alloy 4(45%α—55%β,Ti—Mn alloy),heat treated for various times at 973 K,WQ.

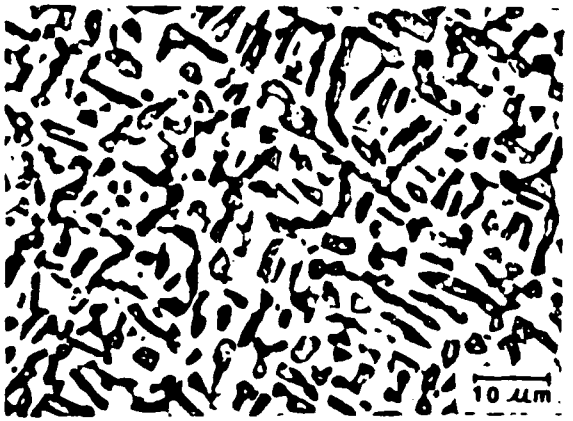

25hrs.

50hrs.

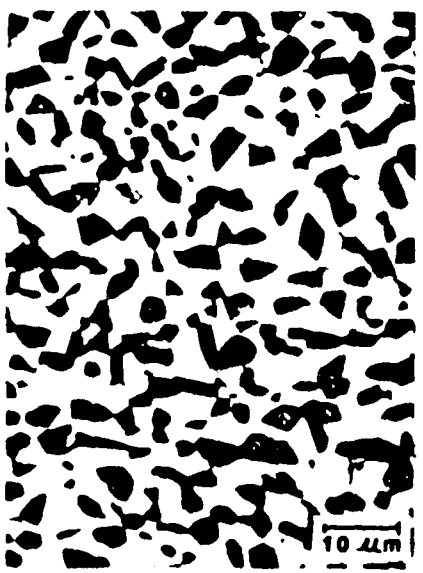

100hrs.

200hrs.

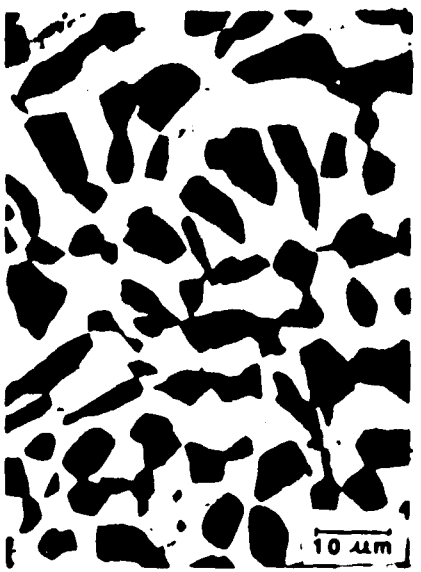

400hrs.

Fig. 26: Photomicrographsof alloy 9(44%α—56%βTi—V alloy),heat treated for various times at 973 K,WQ.

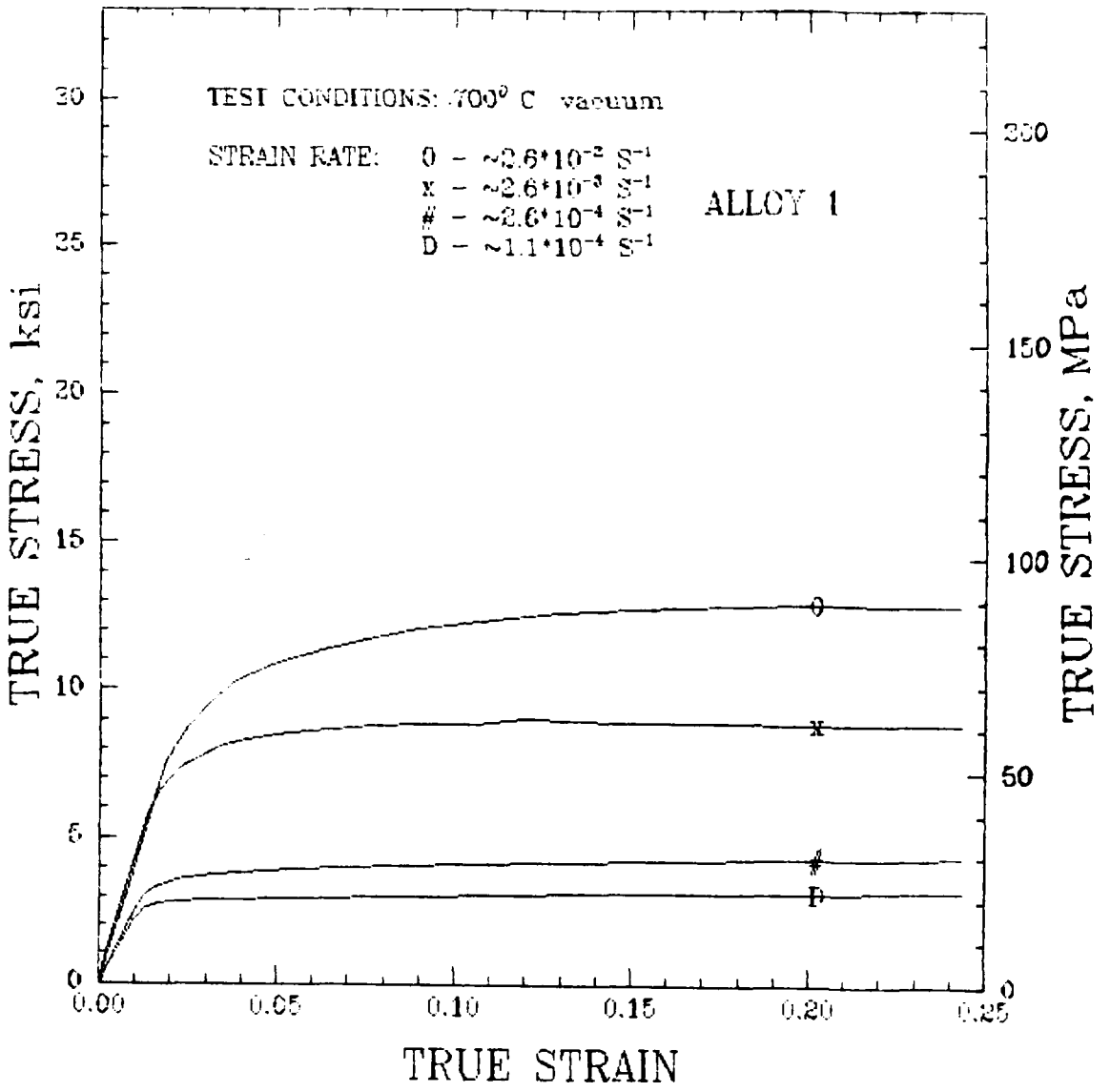

Fig. 27: True stress—True strain curves of alloy 1(100% alpha,Ti—Mn alloy) tested in vacuum at 973 K at different strain rates.

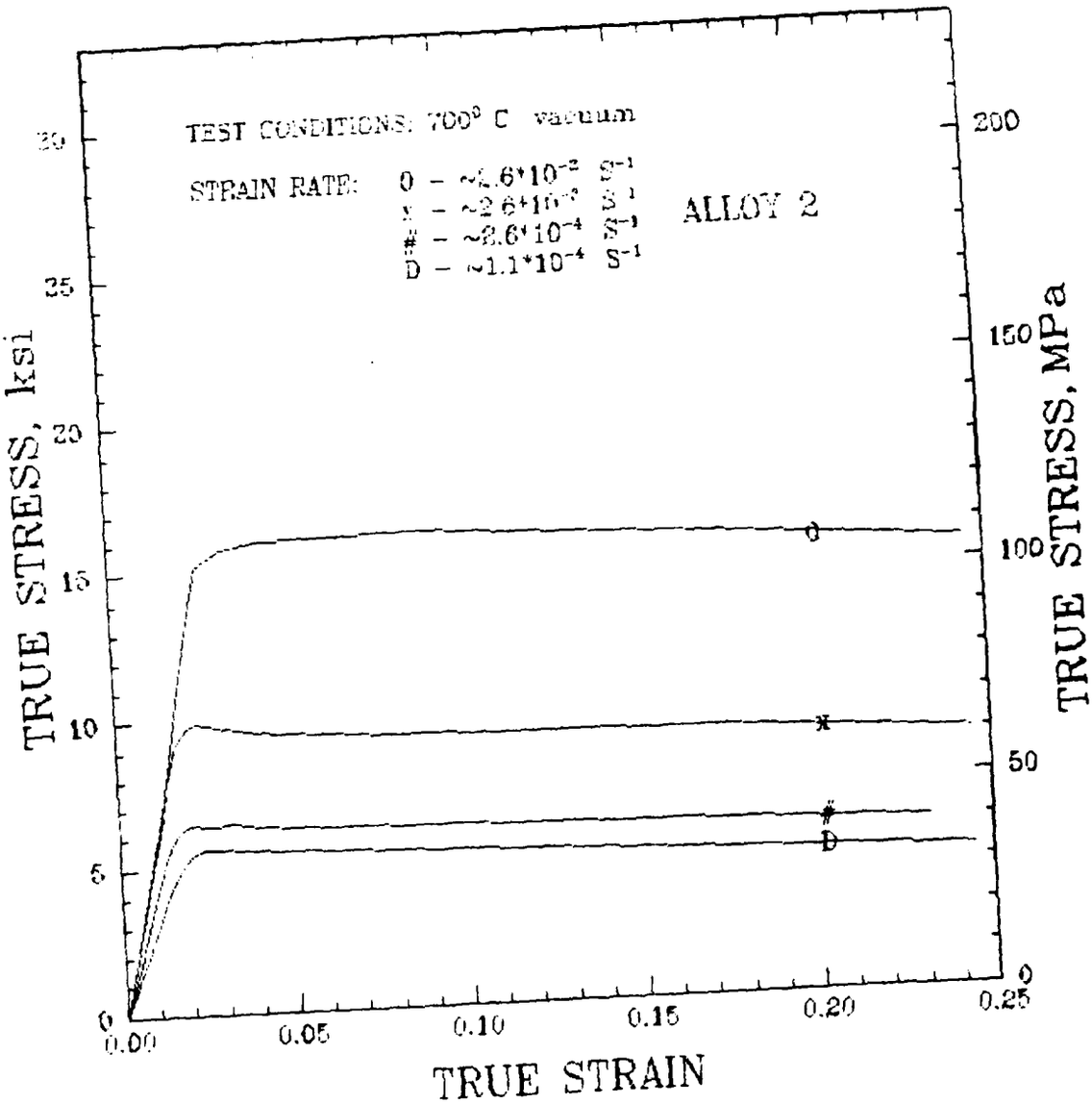

Fig. 28: True stress—True strain curves of alloy 2(79%α—21%β,Ti—Mn alloy) tested in vacuum at different strain rates.

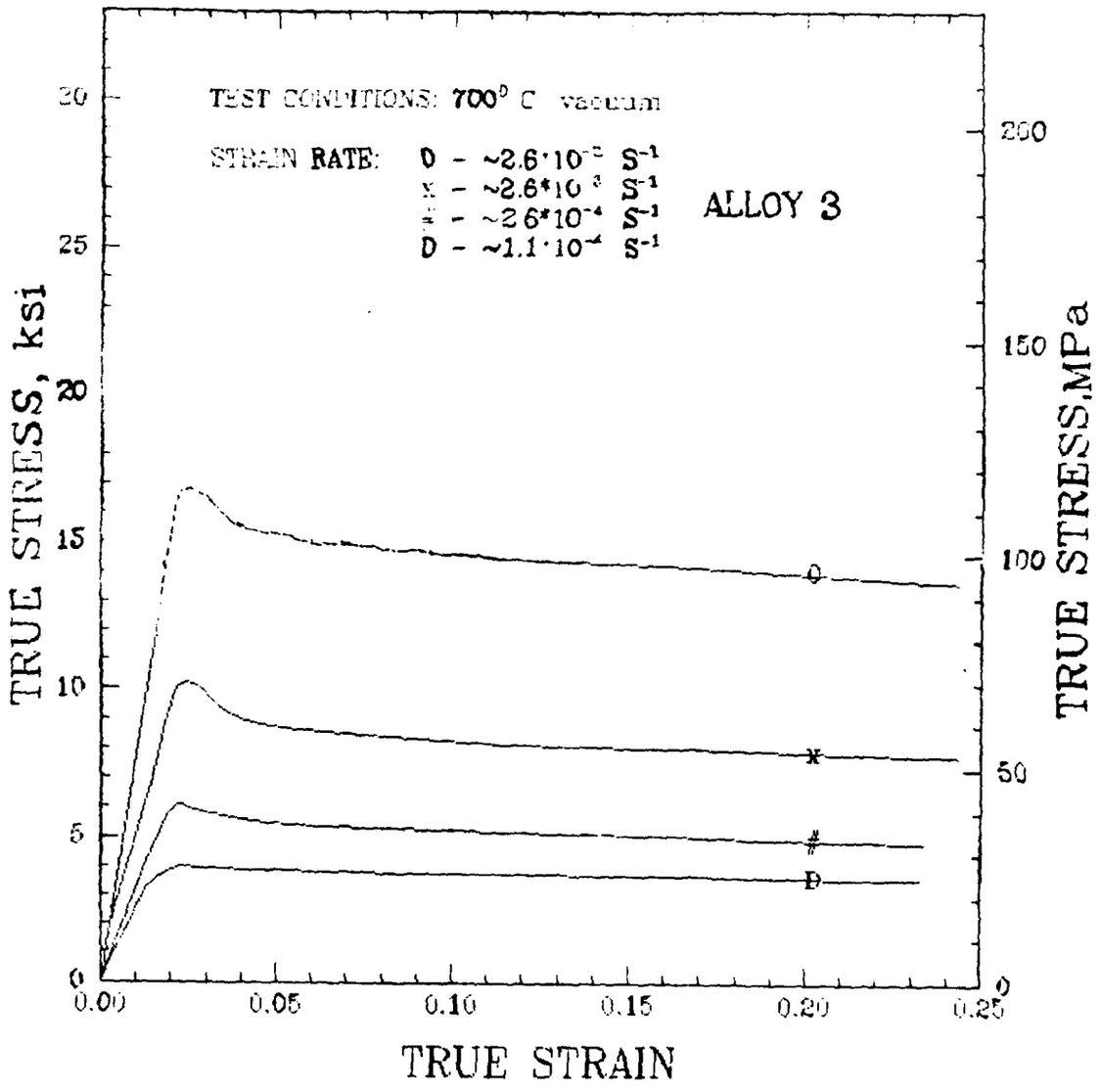

Fig. 29: True stress—True strain curves of alloy 3(63%α—37%β,Ti—Mn alloy) tested in vacuum at 973 K at different strain rates.

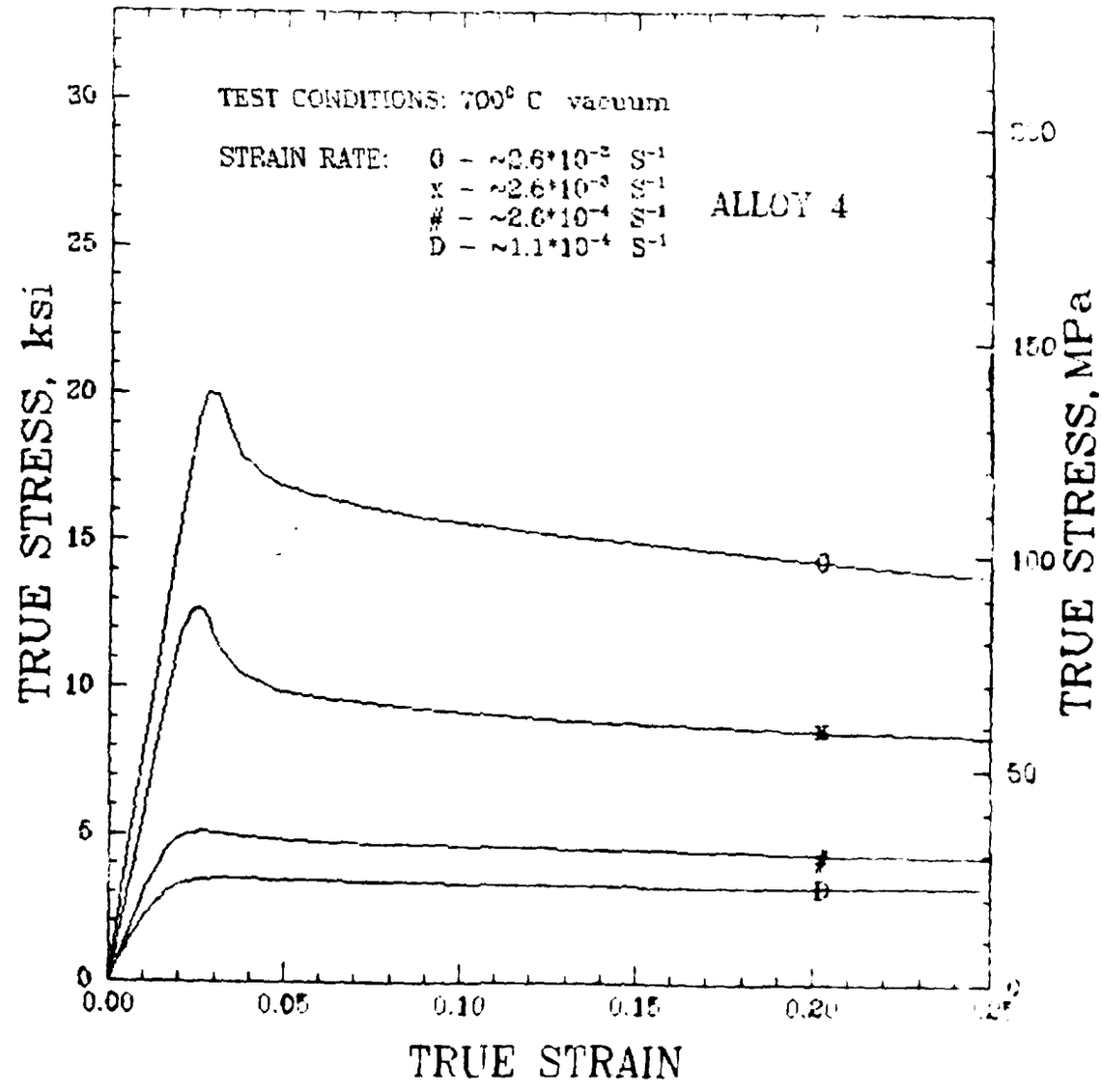

Fig. 30: True stress—True strain curves of alloy 4(45%α—55%β,Ti—Mn alloy) tested in vacuum at 973 K at different strain rates.

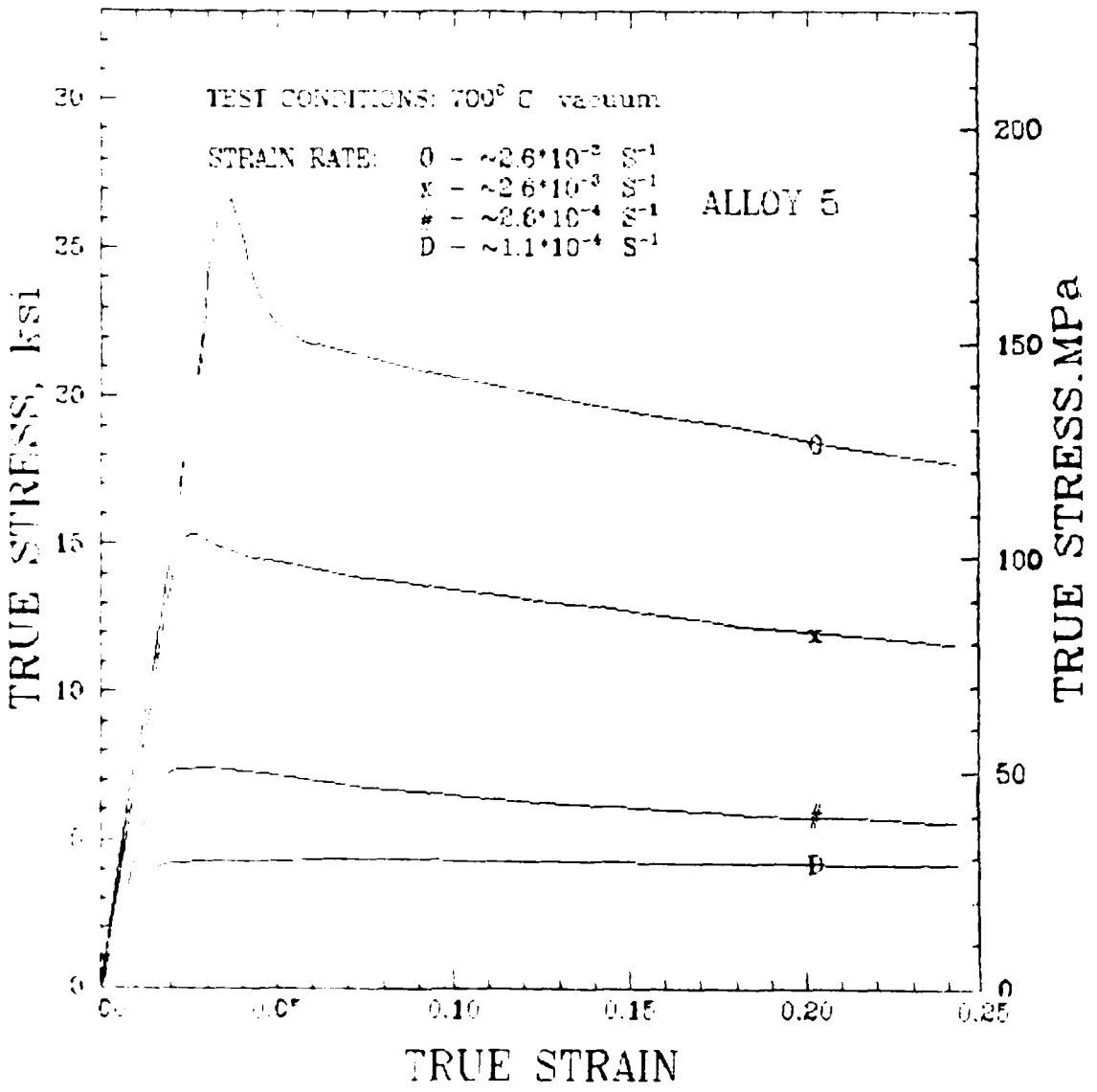

Fig. 31: True stress—True strain curves of alloy 5(10%α—90%β,Ti—Mn alloy) tested in vacuum at 973 K at different strain rates.

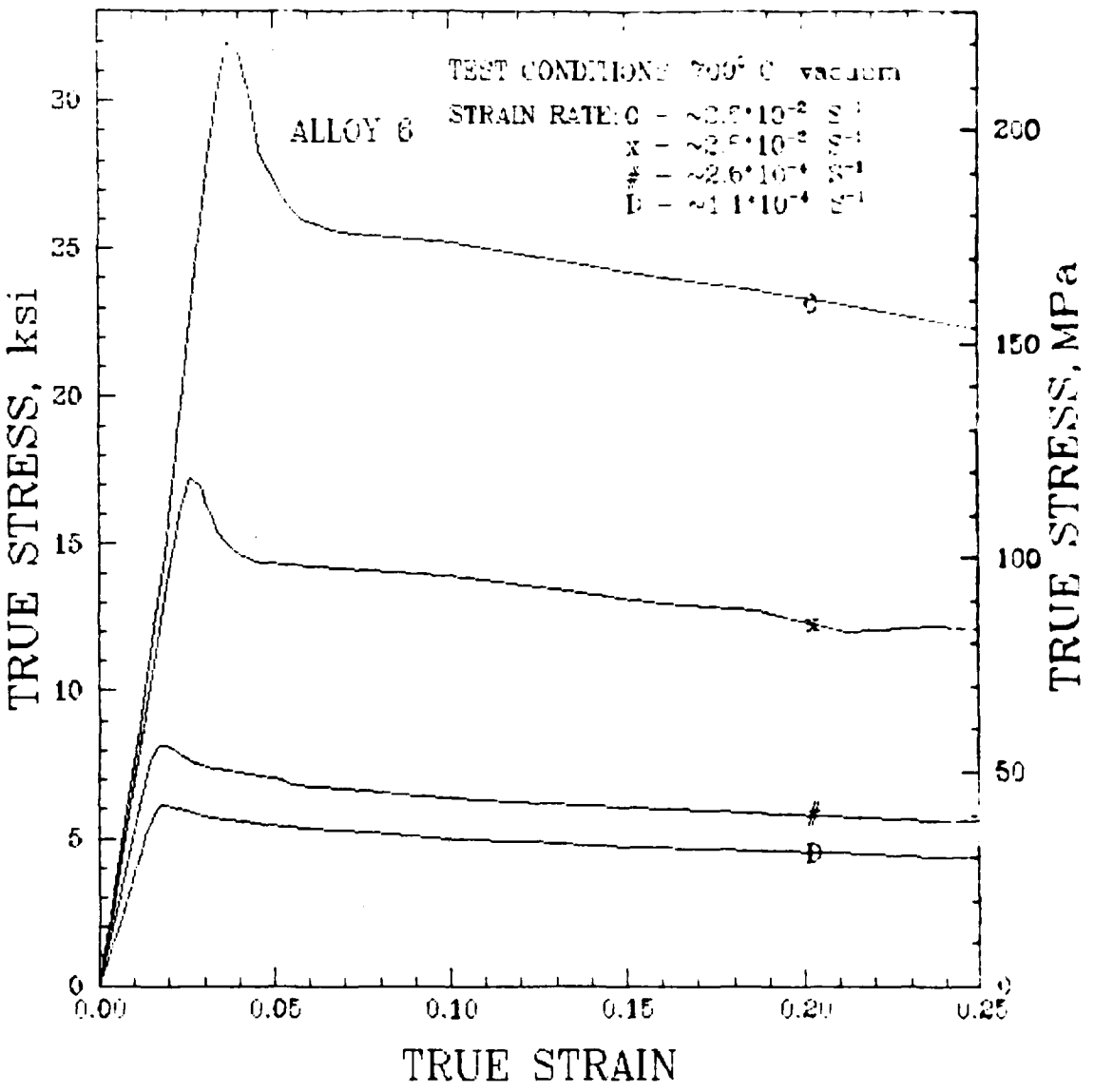

Fig. 32: True stress—True strain curves of alloy 6(100% Pl tested in vacuum at 973 K at different strain rates.

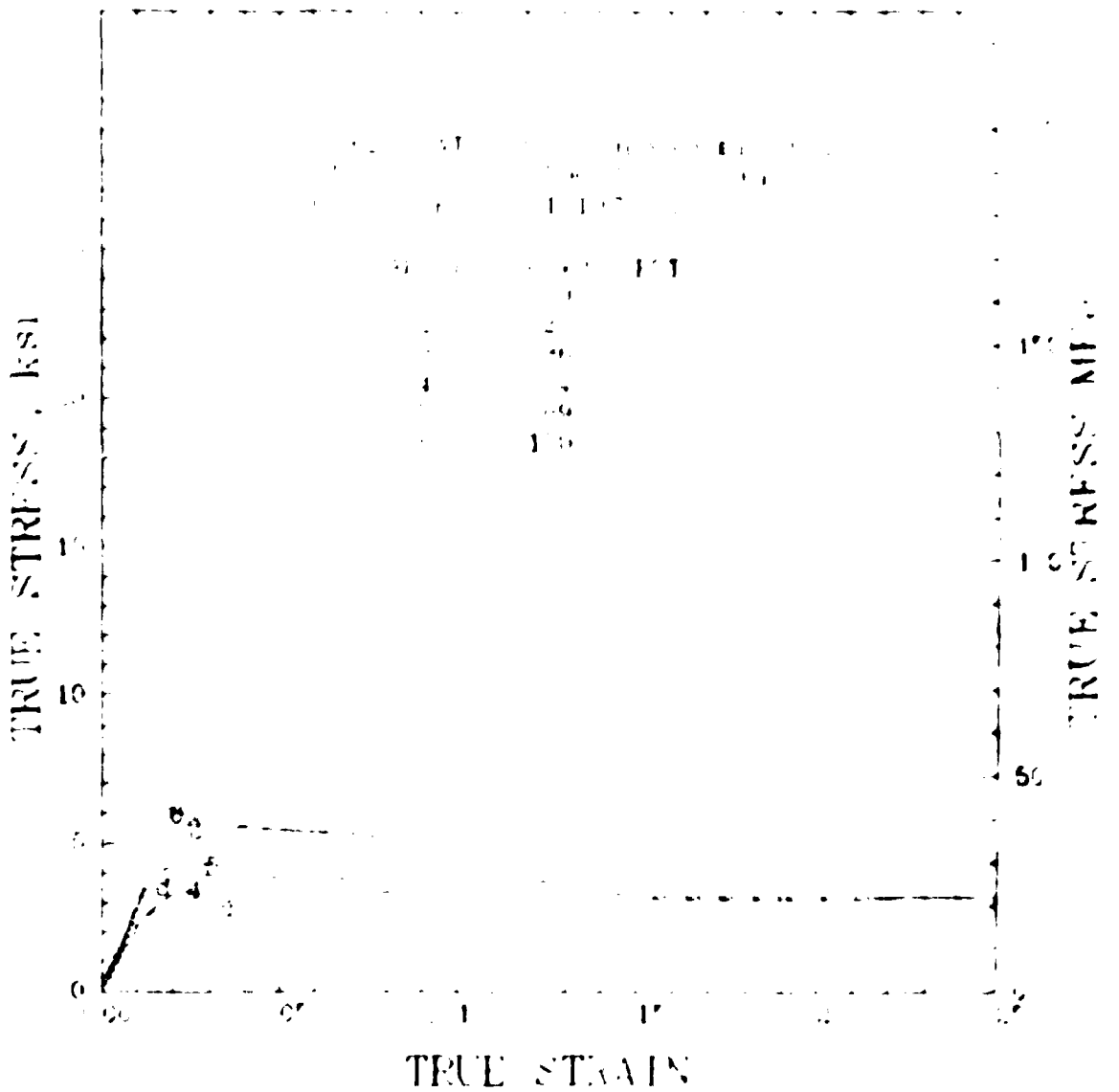

Fig. 33: True stress—True strain curves of alloys 1—6 tested at 973 K at a strain rate of $1.1*10^{-4}$/ sec.

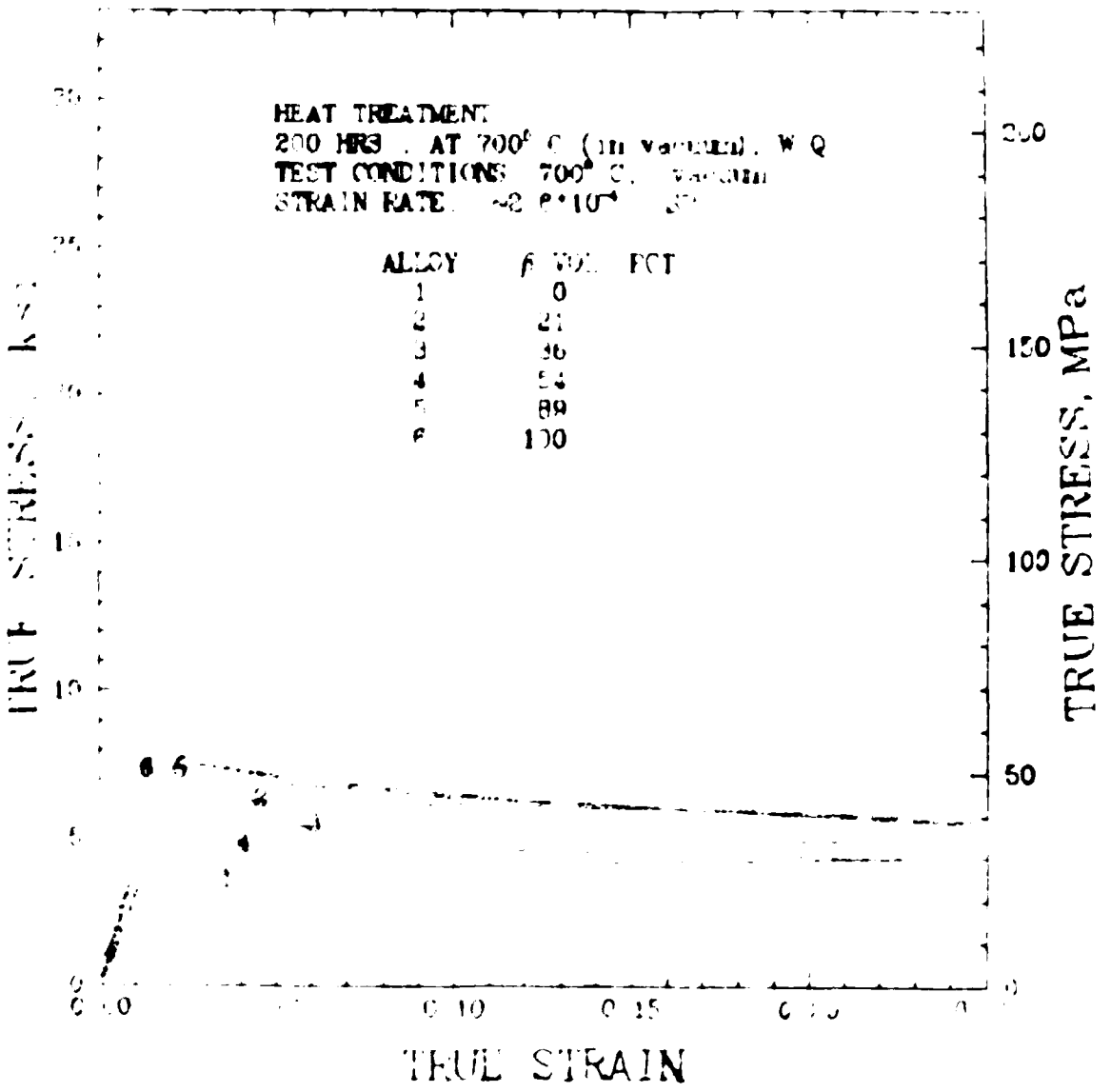

Fig. 34: True stress—true strain curves of alloys 1—6 tested at 973 K at a strain rate of $2.6*10^{-4}$/sec.

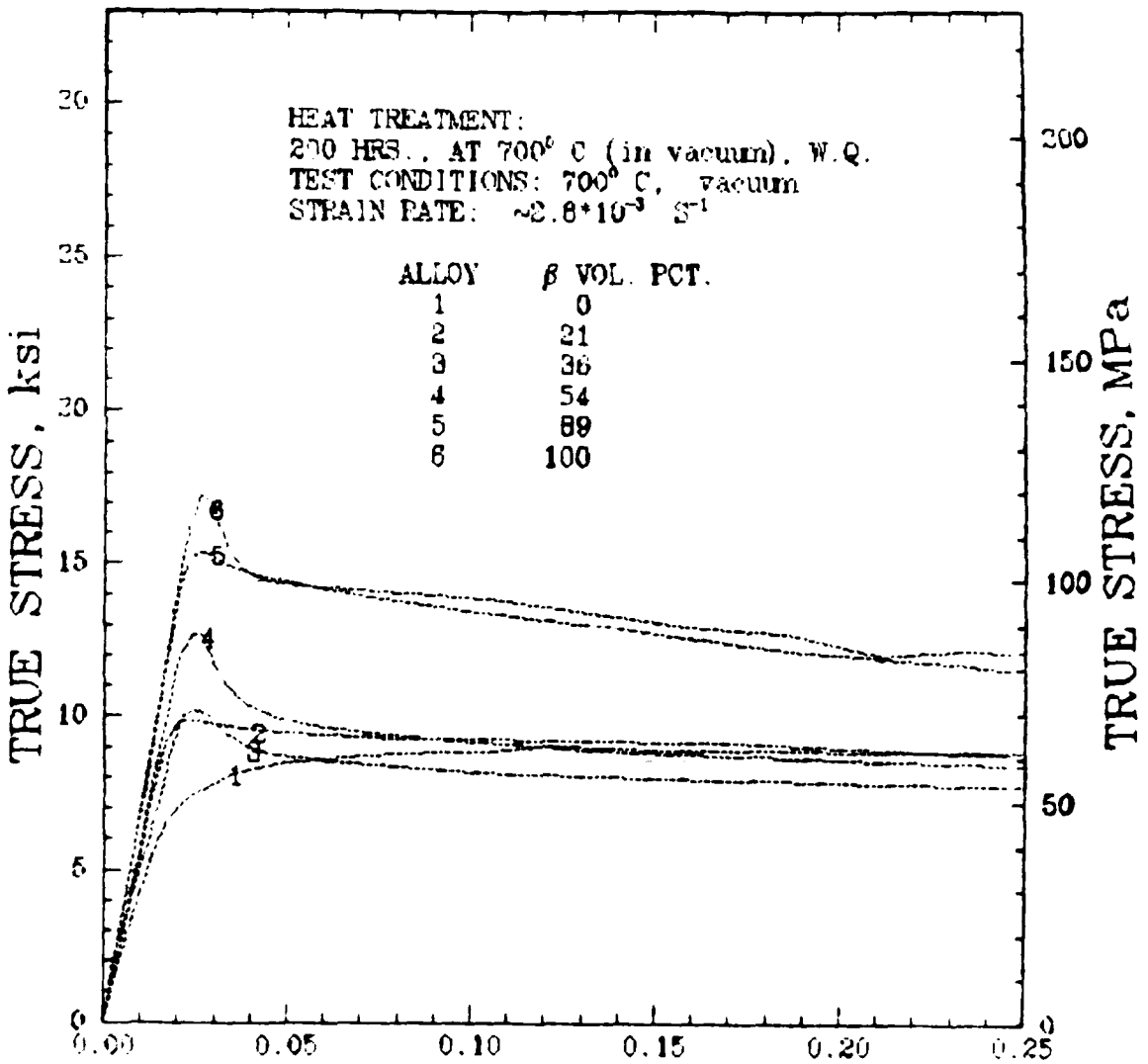

Fig. 35: True stress—true strain curves of alloys 1—6 tested at 973 K at a strain rate of $2.6*10^{-3}$/sec.

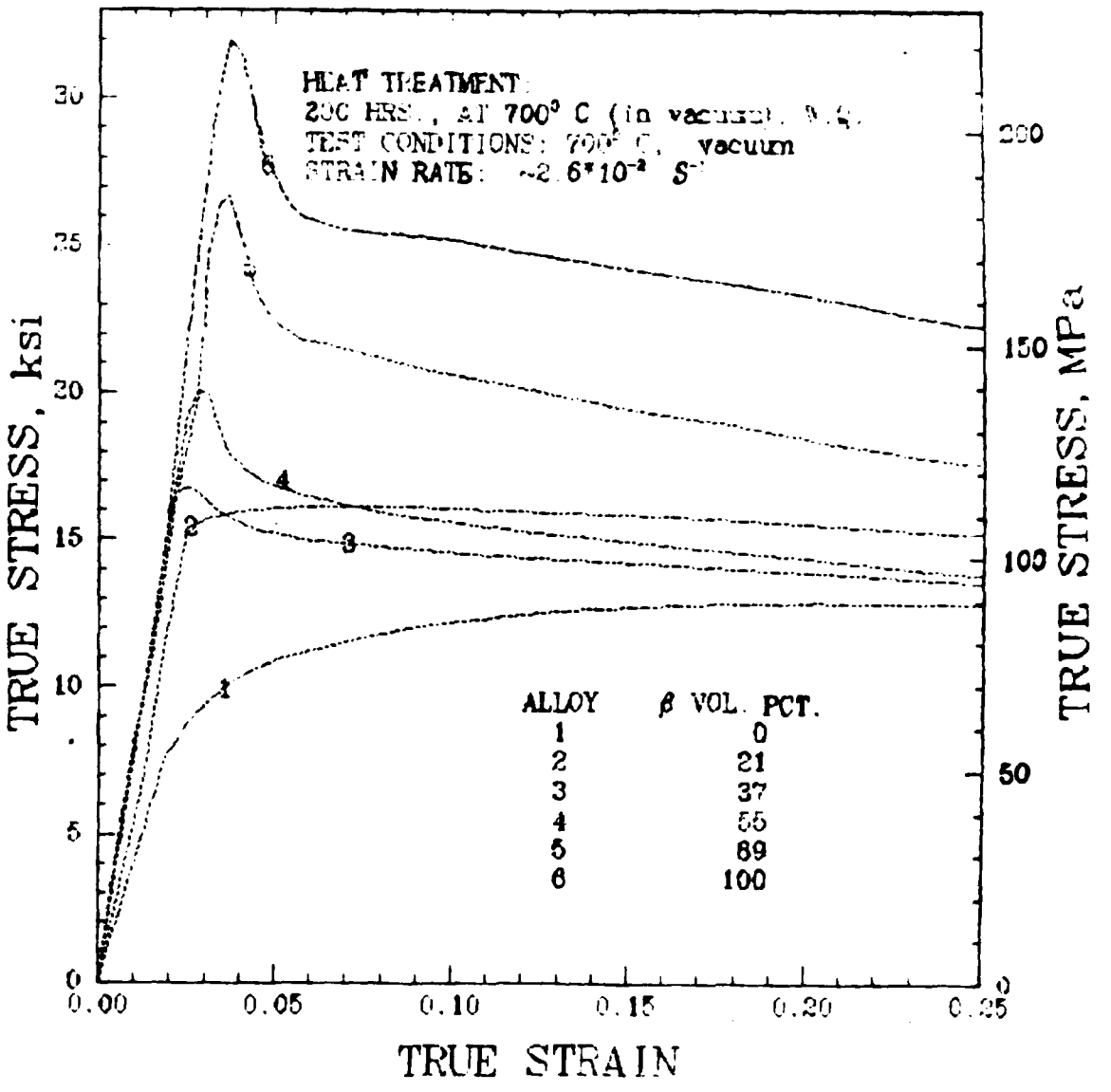

Fig. 36: True stress—true strain curves of alloys 1—6 tested at 973 K at a strain rate of $2.6*10^{-2}$/sec.

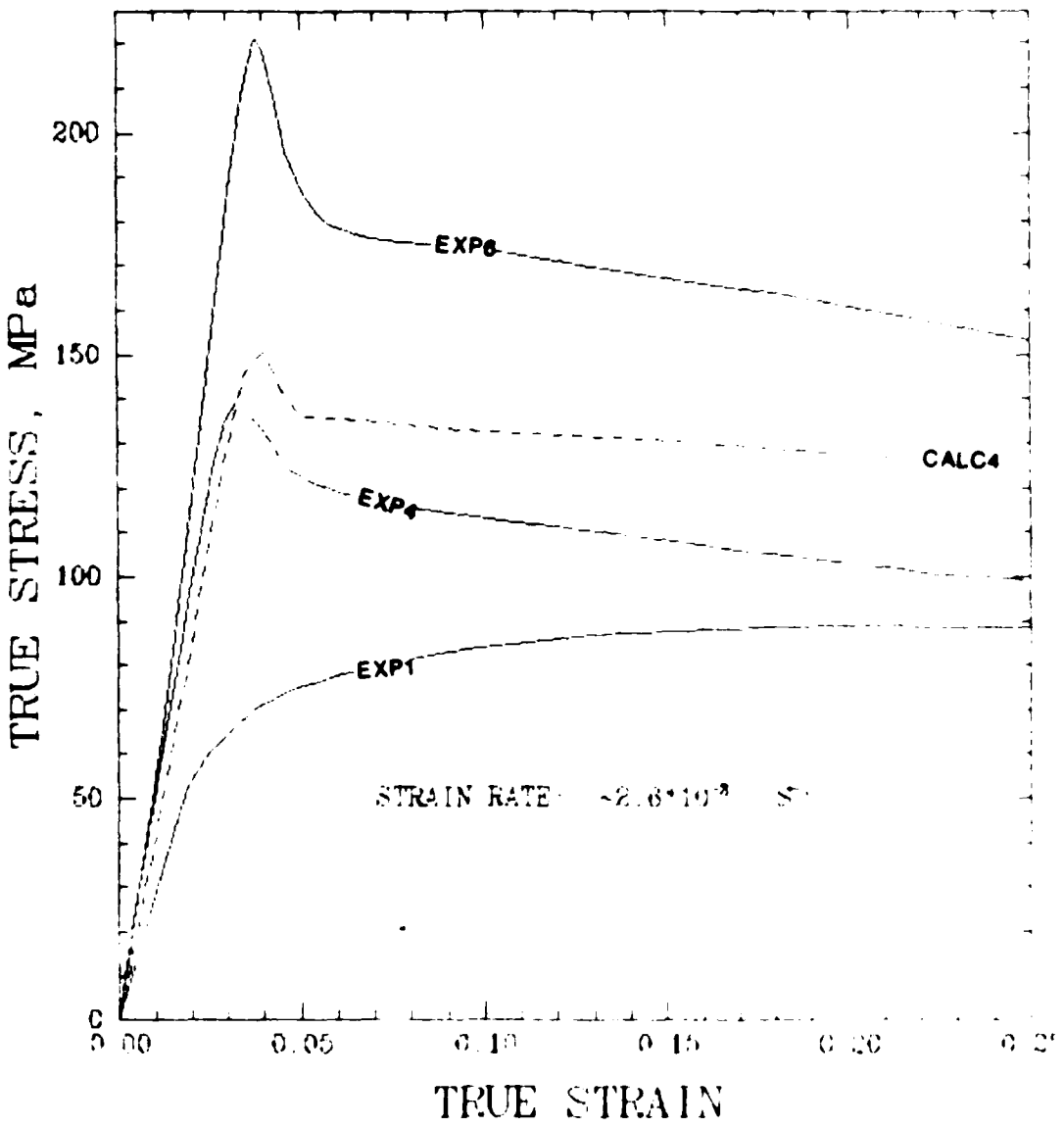

Fig.37: Calculation of true stress—true strain curves for alloy 4 (45%α—55%β)based on iso—strain model

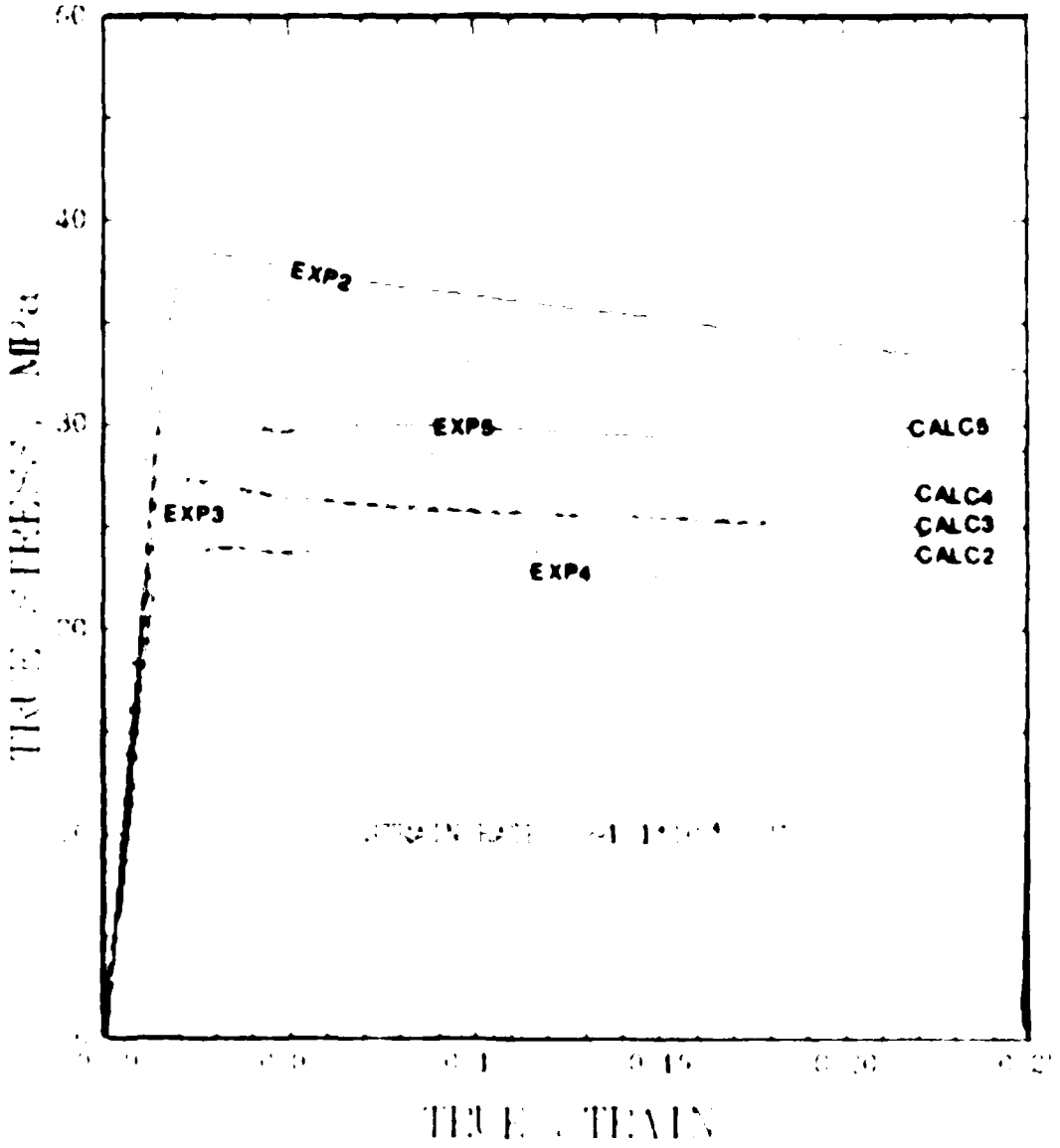

Fig. 38: Comparison of calculated (iso—strain model) and experimental curves for various α+β Ti—Mn alloys tested at a strain rate of $1.1 * 10^{-4}$/sec.

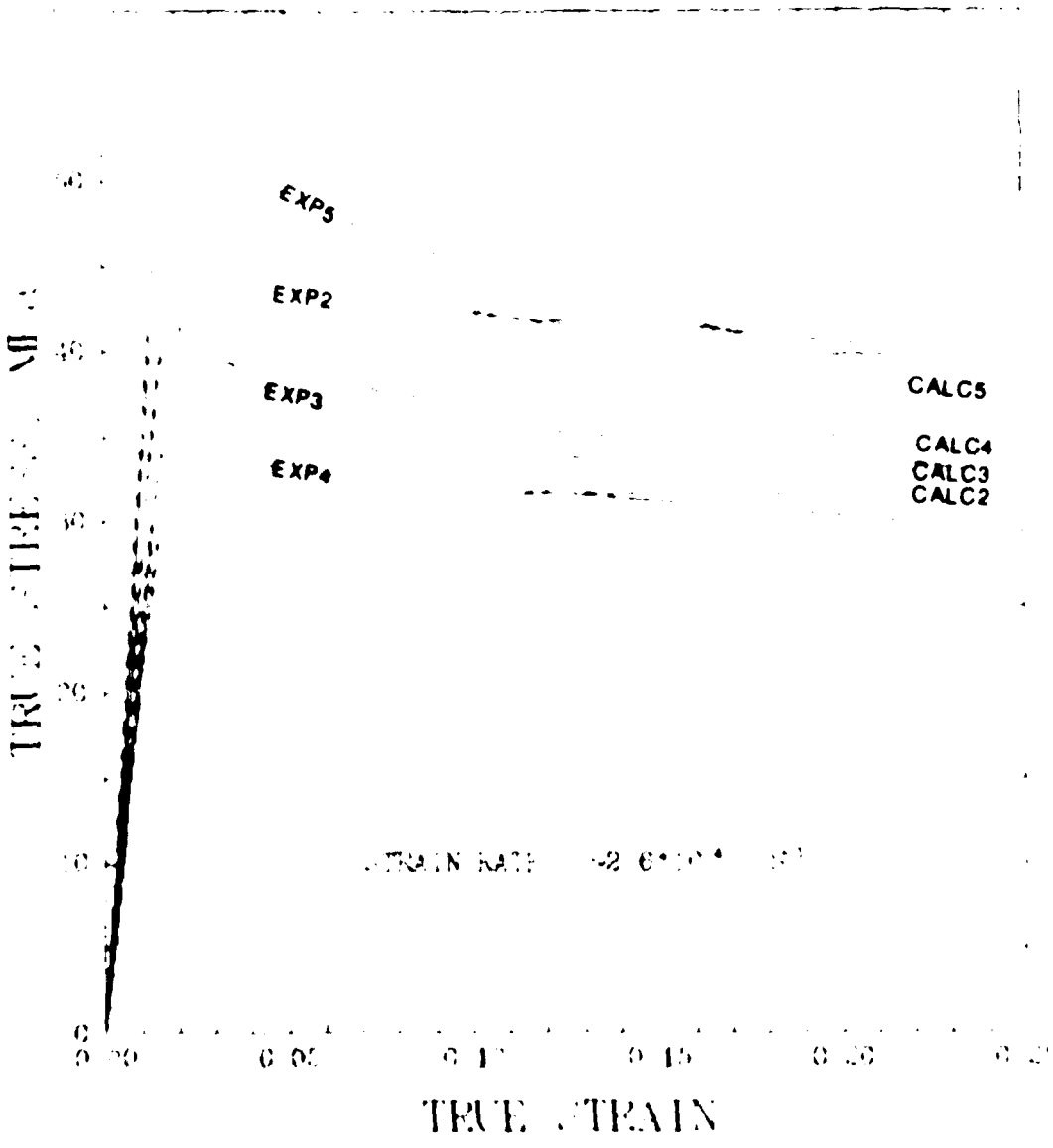

Fig.39: Comparison of calculated iso-strain model and experimental curves for various α-β Ti-Mn alloys at a strain rate of $2.6*10^{-4}$/sec.

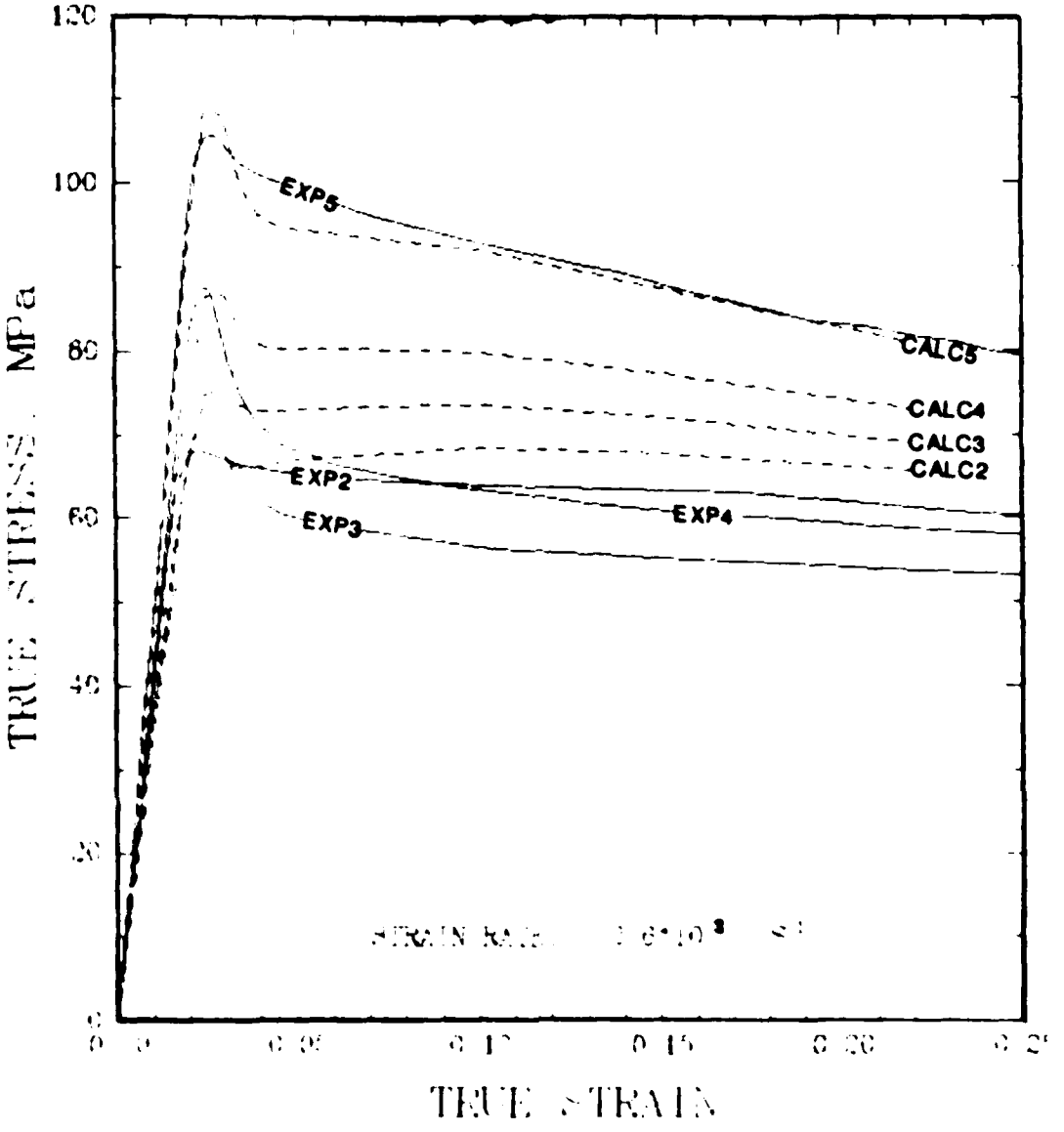

Fig.40 Comparison of calculated (iso—strain model) and experimental curves for various α - β Ti—Mn alloys at a strain rate of $2.6*10^{-3}$ /sec.

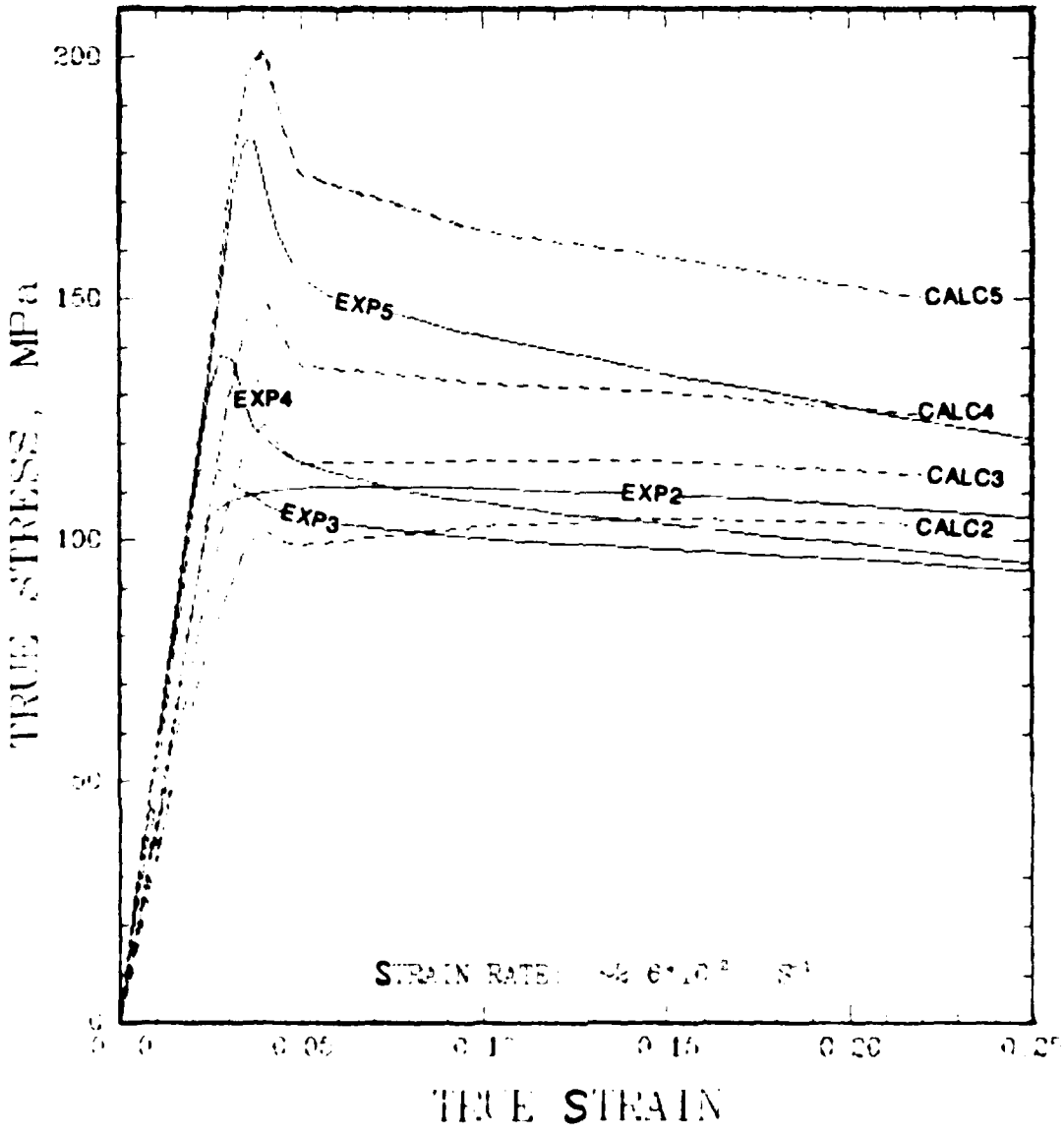

Fig.4t Comparison of calculated (iso—strain model) and experimental curves for various α-β Ti—Mn alloys at a strain rate of $2.6*10^{-2}$/sec.

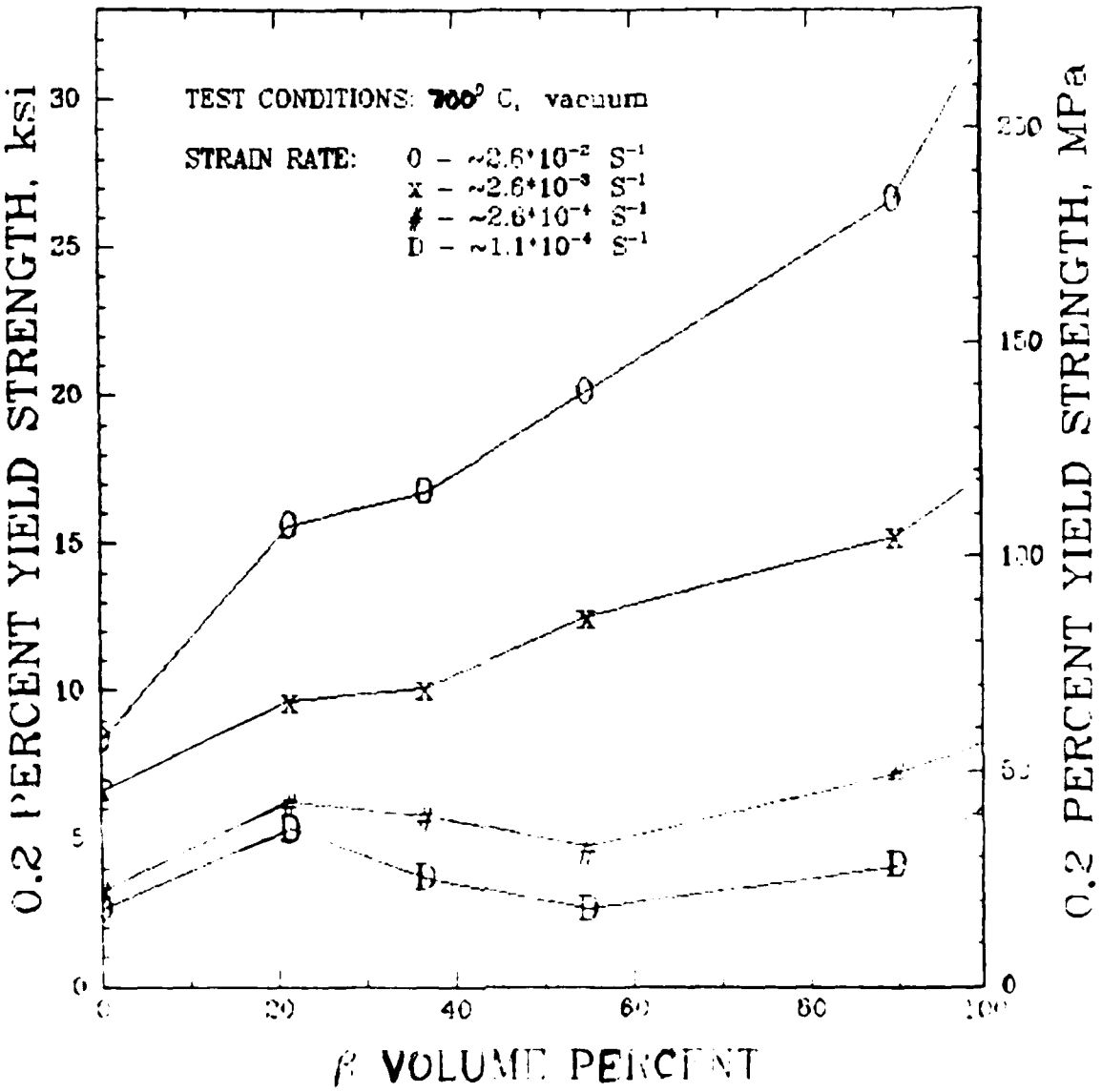

Fig.42: Flow stress vs β volume percent for different α - β Ti—Mn alloys. The flow stress corresponds to 0.2 pct plastic strain offset.

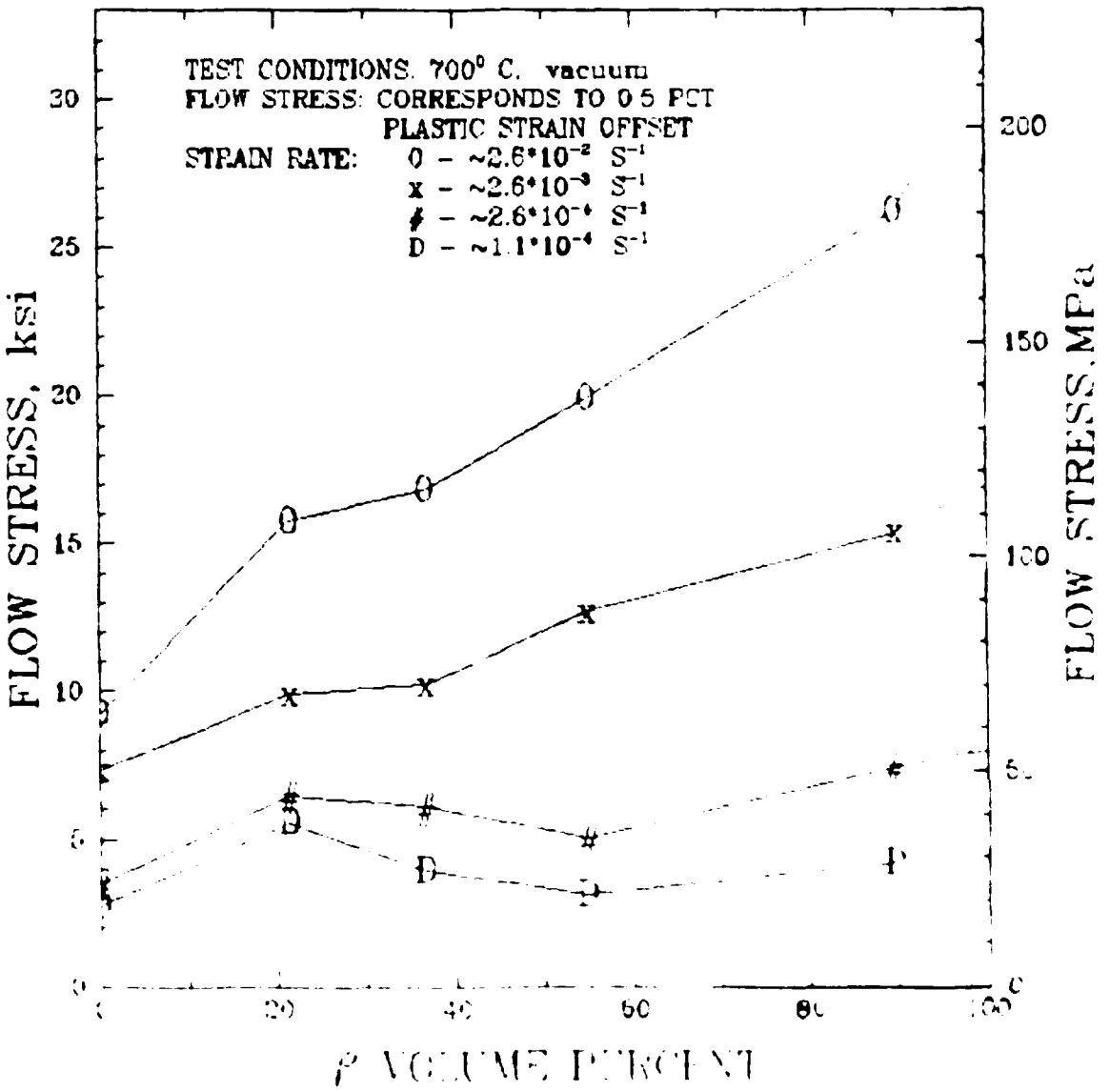

Fig.43: Flow stress vs β volume percent for different α-β Ti—Mn alloys. The flow stress corresponds to 0.5 pct plastic strain offset.

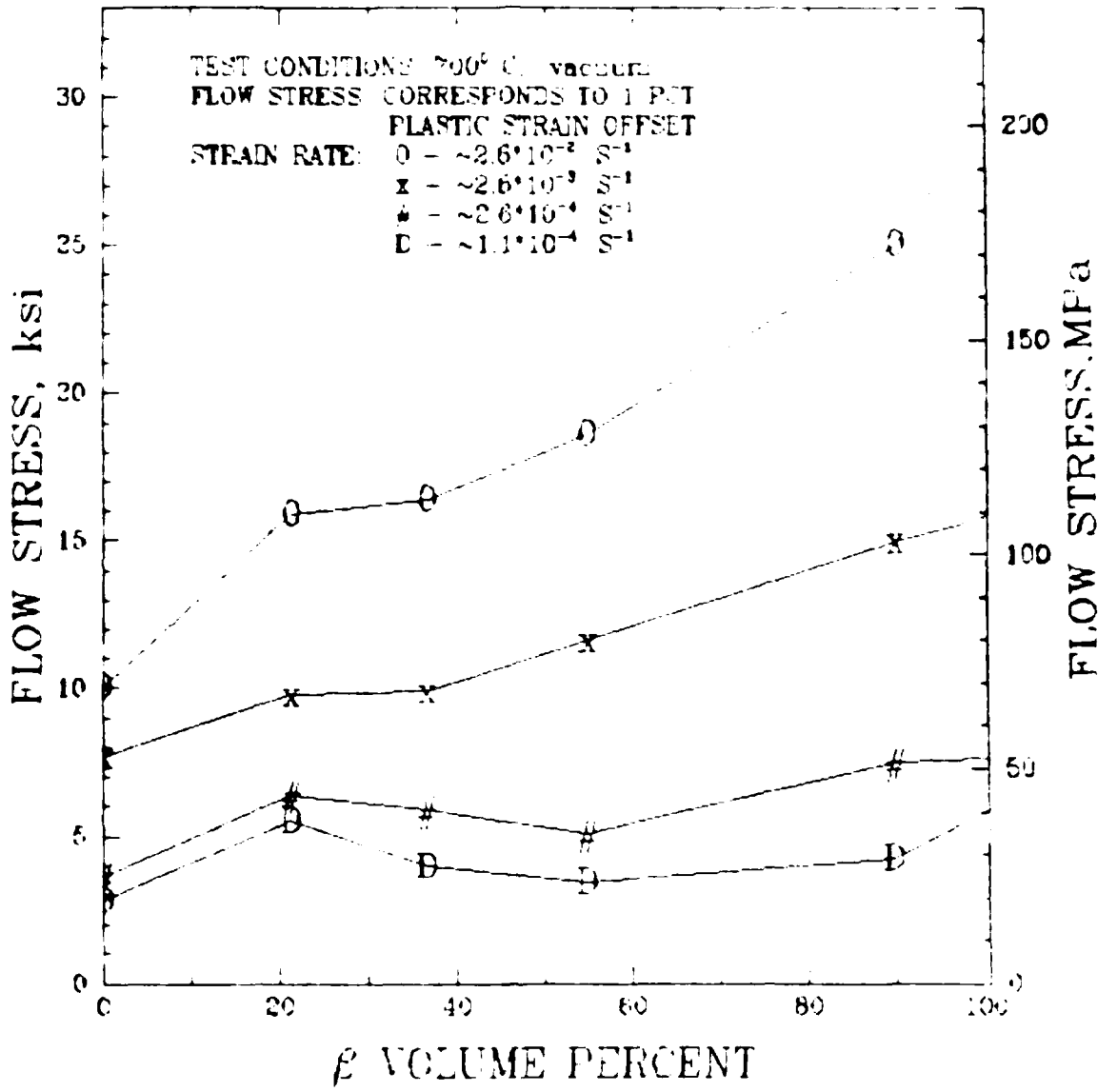

Fig.44: Flow stress vs β volume percent for different α-β Ti—Mn alloys. The flow stress corresponds to 1 pct plastic strain offset.

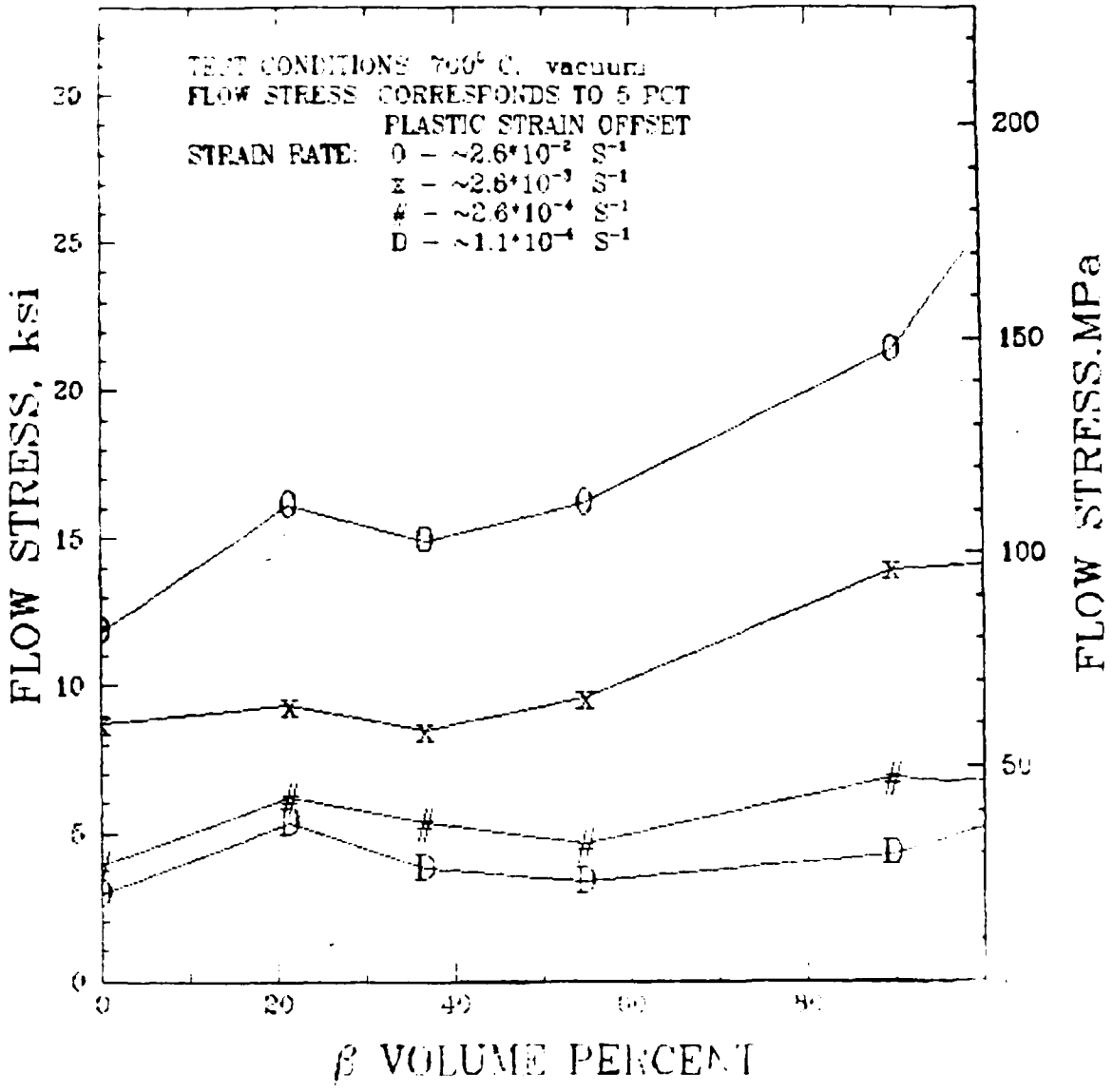

Fig.45: Flow stress vs β volume percent for different [illegible]

The flow stress corresponds to 5 pct plastic strain [illegible]

AD-A179 727 FUNDAMENTAL STUDIES ON HIGH TEMPERATURE DEFORMATION 2/2
RECRYSTALLIZATION AND (U) MARYLAND UNIV COLLEGE PARK
DEPT OF CHEMICAL AND NUCLEAR ENGIN S ANKEM ET AL
UNCLASSIFIED 18 FEB 87 AFOSR-TR-87-0458 AFOSR-85-0367 F/G 11/6 1 NL

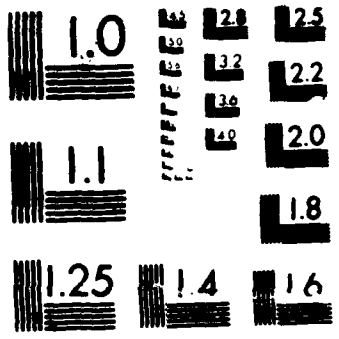

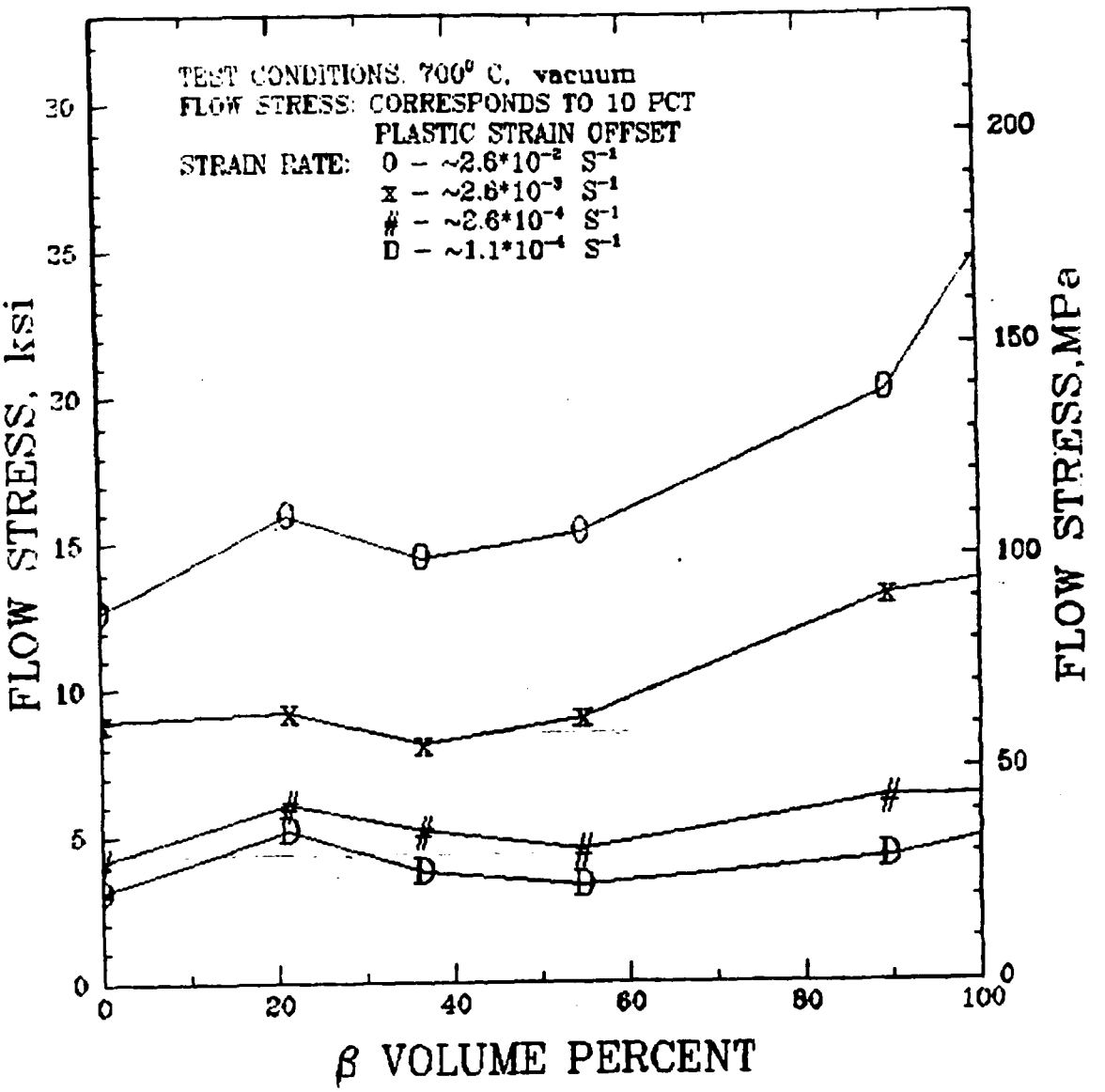

Fig.46: Flow stress vs β volume percent for different α-β Ti—Mn alloys. The flow stress corresponds to 10 pct plastic strain offset.

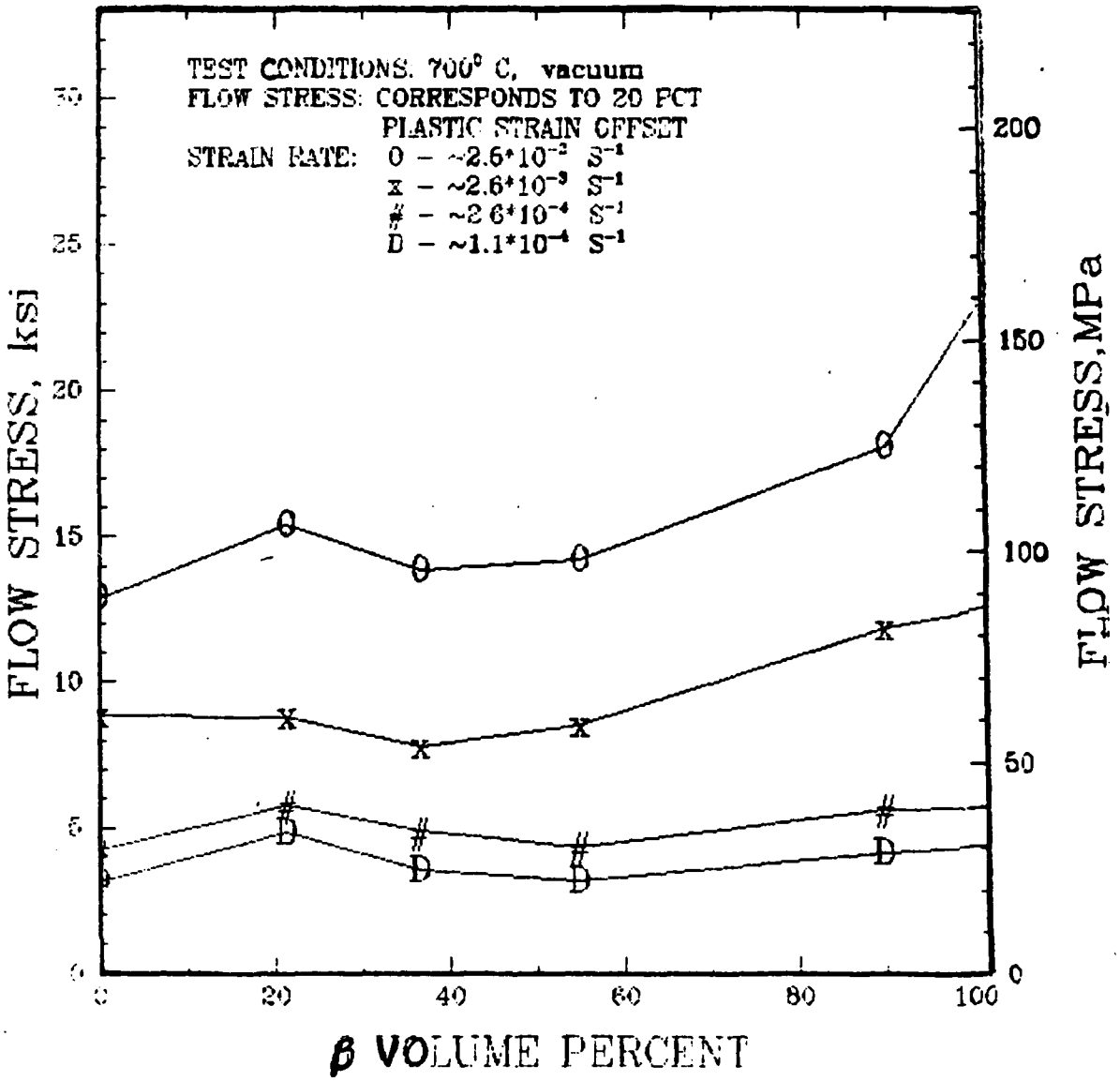

Fig.47: Flow stress vs β volume percent for different α-β Ti—Mn alloys. The flow stress corresponds to 20 pct plastic strain offset.

END

6-87

DTIC